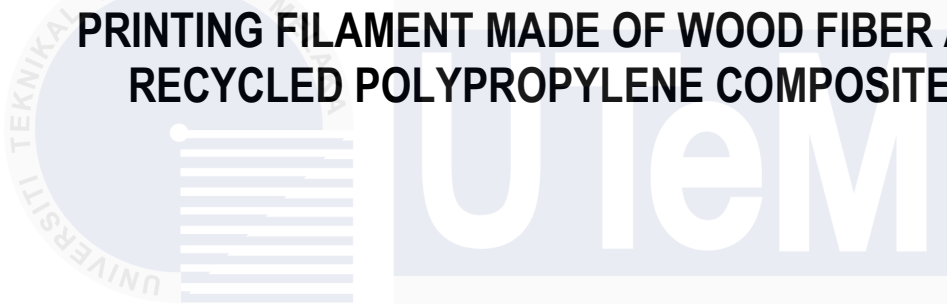




اونيور سيتي تیکنیکل ملیسیا ملاک

UNIVERSITI TEKNIKAL MALAYSIA MELAKA

**THE INFLUENCE OF MAPP COUPLING AGENT ON 3D
PRINTING FILAMENT MADE OF WOOD FIBER AND
RECYCLED POLYPROPYLENE COMPOSITES**



اونيور سيتي تیکنیکل ملیسیا ملاک

UNIVERSITY OF **NUR YASMINN AMIRA BINTI ISMANOR AIZAL**

**BACHELOR OF MANUFACTURING ENGINEERING
TECHNOLOGY WITH HONOURS**

2024



**Faculty of Industrial and Manufacturing Technology and
Engineering**

**THE INFLUENCE OF MAPP COUPLING AGENT ON 3D PRINTING
FILAMENT MADE OF WOOD FIBER AND RECYCLED
POLYPROPYLENE COMPOSITES**

Nur Yasminn Amira Binti Ismanor Aizal

Bachelor of Manufacturing Engineering Technology (BMIW) with Honours

2024

**THE INFLUENCE OF MAPP COUPLING AGENT ON 3D PRINTING FILAMENT
MADE OF WOOD FIBER AND RECYCLED POLYPROPYLENE COMPOSITES**

NUR YASMINN AMIRA BINTI ISMANOR AIZAL



**A thesis submitted
in fulfillment of the requirements for the degree of
Bachelor of Manufacturing Engineering Technology (BMIW) with Honours**

اونيورسيتي تيكنيكل مليسيا ملاك

UNIVERSITI TEKNIKAL MALAYSIA MELAKA

**Faculty of Industrial and Manufacturing Technology and
Engineering**

UNIVERSITI TEKNIKAL MALAYSIA MELAKA

2024

DECLARATION

I declare that this Choose an item. entitled “ THE INFLUENCE OF MAPP COUPLING AGENT ON 3D PRINTING FILAMENT MADE OF WOOD FIBER AND RECYCLED POLYPROPYLENE COMPOSITES” is the result of my own research except as cited in the references. The Choose an item. has not been accepted for any degree and is not concurrently submitted in candidature of any other degree.

Signature

:



Name

:

NUR YASMINN AMIRA BINTI ISMANOR AIZAL

Date


:

10 January 2024

UNIVERSITI TEKNIKAL MALAYSIA MELAKA

APPROVAL

I hereby declare that I have checked this thesis and in my opinion, this thesis is adequate in terms of scope and quality for the award of the Bachelor of Manufacturing Engineering Technology (BMIW) with Honours.

Signature :  _____
Supervisor Name : DR NUZAIMAH BTE MUSTAFA _____
Date : 10 Januari 2024 _____

اونيورسيتي تيكنيكل مليسيا ملاك

UNIVERSITI TEKNIKAL MALAYSIA MELAKA

DEDICATION

Assalamualaikum, first and foremost, I appreciate Allah SWT for allowing me to complete my final project on time. Thank you also to my parents, Ismanor Aizal Bin Ismail and Yuzalinda Binti Mohd Yusoff, for their unwavering support in whatever I accomplish in life. Thank you for assisting me in becoming someone who can achieve anything with effort. Thank you very much for sponsoring my education while I was in year one, semester one. They also spent a lot of money on this last project to realise the product that I designed for it. To my supervisor, Dr. Nuzaimah Bte Mustafa, who has always assisted me in completing this project and ensuring that I am on the correct road and following all of the forms for this report. My supervisor, Dr Nuzaimah, thank you for your patience in waiting for every step forward from me. Thank you for understanding me and constantly encouraging me so that I refuse to give up. I was able to complete my project on time because of Dr.'s encouragement and support.

ABSTRACT

The goal of this research was to investigate the effect of MAPP as a compatibilizer on the surface morphology, mechanical, and physical properties of 3D printing filament made from wood fiber and recycled polypropylene (r-WoPPc). The r-WoPPc filaments with MAPP loadings of 0%, 1%, 3%, and 5% by weight were produced using twin screw extruder and then printed using 3D printing. The printed specimens were tested for tensile and flexural. Morphological of r-WoPPc filament and the 3D-printed tensile fracture surface was examined. Additionally, investigations were conducted on the water absorption, soil burial degradation of r-WoPPc. The results revealed that 5% MAPP addition in r-WoPPc yielded the highest tensile and flexural strength which improved by 110.27% and 89.12% compared to without MAPP. The MAPP strengthened the adhesion between wood fiber and recycled PP matrix, resulting in improved r-WoPPc performance. Better adhesion between wood fiber and PP can be observed from the filament surface morphology of 5% r-WoPPc which wood fiber is adequately adhered to the matrix PP. Additionally, the morphology of the tensile fracture surface shown an even fracture for the specimen with 5% MAPP while the specimens with 0%, 1% and 3% MAPP showed uneven fracture. The enhanced properties of r-WoPPc resulted from MAPP's maleic anhydride functions esterify wood fiber surface hydroxyls. The water absorption results also shows that 5% MAPP adhesion has the lowest percentage of water absorbed for 42.1%. The soil burial result has proven that with the presence of 5% MAPP in the composite makes the soil burial degradation of filament with the highest weight loss of 8.06%.

ABSTRAK

Matlamat penyelidikan ini adalah untuk menyiasat kesan MAPP sebagai penyerasi ke atas morfologi permukaan, mekanikal, dan sifat fizikal filamen cetakan 3D yang diperbuat daripada gentian kayu dan polipropilena kitar semula (r-WoPPc). Filamen r-WoPPc dengan muatan MAPP sebanyak 0%, 1%, 3% dan 5% mengikut berat dihasilkan menggunakan penyemperit skru berkembar dan kemudian dicetak menggunakan cetakan 3D. Spesimen yang dicetak telah diuji untuk tegangan dan lentur. Morfologi filamen r-WoPPc dan permukaan patah tegangan cetakan 3D telah diperiksa. Selain itu, penyiasatan telah dijalankan ke atas penyerapan air, kemerosotan pengebumian tanah r-WoPPc. Keputusan menunjukkan bahawa 5% penambahan MAPP dalam r-WoPPc menghasilkan kekuatan tegangan dan lenturan tertinggi yang meningkat sebanyak 110.27% dan 89.12% berbanding tanpa MAPP. MAPP mengukuhkan lekatan antara gentian kayu dan matriks PP kitar semula, menghasilkan prestasi r-WoPPc yang lebih baik. Lekatan yang lebih baik antara gentian kayu dan PP boleh diperhatikan daripada morfologi permukaan filamen 5% r-WoPPc yang gentian kayu melekat secukupnya pada matriks PP. Selain itu, morfologi permukaan rekahan tegangan menunjukkan keretakan sekata untuk spesimen dengan 5% MAPP manakala spesimen dengan 0%, 1% dan 3% MAPP menunjukkan keretakan tidak sekata. Ciri-ciri dipertingkatkan r-WoPPc terhasil daripada fungsi anhidrida maleik MAPP mengesteri hidroksil permukaan gentian kayu. Keputusan serapan air juga menunjukkan bahawa 5% lekatan MAPP mempunyai peratusan air yang paling rendah diserap sebanyak 42.1%. Hasil pengebumian tanah telah membuktikan bahawa dengan adanya 5% MAPP dalam komposit menyebabkan kemerosotan pengebumian tanah filamen dengan penurunan berat yang paling tinggi iaitu 8.06%.

ACKNOWLEDGEMENTS

In the Name of Allah, the Most Gracious, the Most Merciful

I would want to begin by thanking and praising Allah the Almighty, my Creator and Sustainer, for all I have received from the beginning of my existence. I would like to thank Universiti Teknikal Malaysia Melaka (UTeM) for offering a study platform.

My heartfelt thanks go to my main supervisor, Dr. Nuzaimah Bte Mustafa, for all of her help, advice, and enthusiasm. Dr. Nuzaimah unwavering patience in coaching and sharing vital insights will be remembered for the rest of my life. In addition, I would like to express my gratitude to my co-supervisors, Dr. Yusliza for her continuous support.

Finally, I want to express my appreciation to my parents, Ismanor Aizal Bin Ismail and Yuzalinda Binti Mohd Yusoff, for their persistent support and encouragement throughout my life. My eternal gratitude also goes to my siblings for their moral support. I would also like to thank my family for their unending love, compassion, and prayers. Finally, I would want to express my gratitude to everyone, especially my friends, who have helped, encouraged, and pushed me to finish my studies.

TABLE OF CONTENTS

	PAGE
DECLARATION	
APPROVAL	
DEDICATION	
ABSTRACT	i
ABSTRAK	ii
ACKNOWLEDGEMENTS	iii
TABLE OF CONTENTS	iv
LIST OF TABLES	vii
LIST OF FIGURES	ix
LIST OF SYMBOLS AND ABBREVIATIONS	xvii
LIST OF APPENDICES	xviii
CHAPTER 1 INTRODUCTION	19
1.1 Problem Statement	19
1.2 Research Objective	20
1.3 Scope of Research	21
CHAPTER 2 LITERATURE REVIEW	22
2.1 Background	22
2.2 Introduction	24
2.3 3D-Printing	25
2.3.1 3D-Printing History	25
2.3.2 3D-Printing Process	27
2.4 3D Printing Material	31
2.4.1 Plastics	32
2.5 Natural Fiber	51
2.5.1 Wood Fiber	52
2.6 Chemical Treatment for Wood Fiber	55
2.6.1 Sodium Hydroxide (NaOH) Treatment	55
2.7 Coupling Agent: Maleic anhydride polypropylene (MAPP)	64
2.8 Composites 3D Printing	65
2.8.1 Recycling of Polypropylene (PP)	65
2.8.2 Composite filled with MAPP	69
2.9 Filament	78
2.10 Filament Processing	81

2.10.1	Extrusion	82
2.10.2	Screw	84
2.10.3	Die	88
2.11	Summary	89
CHAPTER 3 METHODOLOGY		94
3.1	Introduction	94
3.2	Raw material	96
3.2.1	Recycled polypropylene (PP)	96
3.2.2	Wood fiber	97
3.2.3	Sodium hydroxide (NaOH)	98
3.2.4	Maleic Anhydride-Grafted Polypropylene (MAPP)	99
3.3	Preparation material	100
3.3.1	Preparation for wood fiber	100
3.3.2	Preparation for recycled polypropylene	101
3.3.3	Preparation for MAPP	101
3.4	Characterization of wood fiber	102
3.5	Wood fiber treatment	103
3.5.1	Preparation of NaOH solution	103
3.5.2	Treatment of fiber with NaOH solution	104
3.6	Preparation of recycled polypropylene/ wood fiber/ MAPP composites	106
3.7	Pellet Fabrication	110
3.8	Preparation of Filament	113
3.8.1	Extrusion Process	113
3.8.2	Characterization of filament	115
3.9	Preparation of specimen	116
3.10	Testing of specimens	118
3.10.1	Tensile test	118
3.10.2	Flexural test	122
3.10.3	Water absorption test	125
3.10.4	Soil burial test	126
3.10.5	Surface morphology	128
3.11	Summary	129
CHAPTER 4 RESULTS AND DISCUSSION		130
4.1	Introduction	130
4.2	Fabrication of r-WoPPc filament	131
4.3	Fabrication of 3D printed r-WoPPc	132
4.4	Characterization of the r-WoPPc filament	133
4.4.1	r-WoPPc filament dimension	133
4.4.2	r-WoPPc filament density	134
4.4.3	r-WoPPc filament surface morphology	135
4.5	Mechanical properties	137
4.5.1	Tensile strength	137
4.5.2	Tensile fracture surface morphology	140
4.5.3	Flexural strength	144
4.6	Physical properties	148
4.6.1	Water absorption test	148

4.6.2	Soil burial test	151
CHAPTER 5		155
5.1	Conclusion	155
5.2	Recommendations	157
5.3	Project Potential	157
REFERENCES		159
APPENDICES		167



اونيورسيتي تيكنيكل مليسيا ملاك

UNIVERSITI TEKNIKAL MALAYSIA MELAKA

LIST OF TABLES

TABLE	TITLE	PAGE
Table 2.1:	SPI classification of plastics with properties and applicability in the construction industry (Kazemi et al., 2021)	35
Table 2.2:	Semi-crystalline and amorphous polymers have similar properties	36
Table 2.3:	Mechanical Properties of ABS Filament (Rezaeian et al., 2022)	43
Table 2.4:	Constant construction parameters are used to create the test specimens (Rezaeian et al., 2022)	43
Table 2.5:	Advantages and Disadvantages of Polypropylene	45
Table 2.6:	Mechanical and Thermal Properties of Polypropylene.	50
Table 2.7:	Coir fiber tensile strength with NaOH treatment (Karthikeyan et al., 2014)	56
Table 2.8:	Effect of fiber length on tensile strength of NaOH-treated coir fiber-reinforced epoxy composites (Karthikeyan et al., 2014)	57
Table 2.9:	Composition of Rpp/mcc Composites (Izzati Zulkifli et al., 2015b)	72
Table 2.10:	Fabricating Materials and Applications in 3D Printing (Pavan Kalyan & Kumar, 2022)	74
Table 2.11:	Designation of composites in relation of the type and quantity of PPMA used (Trombetta et al., 2010)	75
Table 2.12:	Sample formulations of kenaf and PP compositions (Saad, 2018)	76
Table 2.13:	Composition of the PP/GS/MAPP polymer composites formulations (Yağci et al., 2021)	77

Table 2.14: Mechanical properties of the kenaf polypropylene composites using four different MAPP coupling agent types (85 wt% kenaf, 10 wt% PP, 5 wt% MAPP pressed at 345 kPa) (Sanadi & Stelte, 2023b)	77
Table 2.15: Properties of different filaments, moisture content after conditioning, and MOE for 3D-printed specimens after conditioning in various climates (Aguirre-Cortés et al., 2023)	79
Table 2.16: Printing Parameters for rPP, PP and PLA Filaments (Kristiawan et al., 2021)	81
Table 2.17: Extrusion Parameters Relation (Kristiawan et al., 2021)	82
Table 2.18: The summary of the article/journal for composite material.	90
Table 3.1: Specifications of filament materials (Kristiawan et al., 2022)	97
Table 3.2: Specification of sodium hydroxide (Nur Hamzah et al., 2016)	99
Table 3.3: Weight ratio of water and NaOH	104
Table 3.4: Composition of wood fiber, polypropylene and MAPP (wt%).	108
Table 3.5: The filament extrusion processing parameters	115
Table 3.6: Printing Settings.	117
Table 4.1: Weight of r-WoPPc absorption test	149
Table 4.2: Weight loss of r-WoPPc (g)	152
Table 5.1 Gantt Chart PSM 1	167
Table 5.2: Gantt Chart PSM 2	169

LIST OF FIGURES

FIGURE	TITLE	PAGE
Figure 2.1:	3D Printing Techniques	23
Figure 2.2:	The 3D printing process using natural fibres	24
Figure 2.3:	3D printed object life cycle (Rais et al., 2023)	26
Figure 2.4:	3D printing layer by layer (Mpofu et al., 2014)	28
Figure 2.5:	Flowchart of 3D printing operation (Shinde et al., 2020)	29
Figure 2.6:	Diagram of 3D printing process (Geng et al., 2023)	30
Figure 2.7:	Diagram of printing setup (Geng et al., 2023)	31
Figure 2.8:	Difference between thermoplastics and thermosetting polymers (Bobo, 2013)	33
Figure 2.9:	Dynamic Covalent Chemistry (Jin et al., 2019)	34
Figure 2.10:	The Structural Formula of PLA (Ramanadha reddy & Venkatachalapathi, 2023)	38
Figure 2.11:	Production of PLA in schematic diagram (Ramanadha reddy & Venkatachalapathi, 2023)	38
Figure 2.12:	Micro-structure of PLA (Sharma et al., 2022)	39
Figure 2.13:	Structural formula of acrylonitrile butadiene styrene (ABS) (Tsuchikura et al., 2013)	41
Figure 2.14:	Chemical of ABS Formula	41
Figure 2.15:	SEM Images of a) neat ABS, b) ABS/UM, and c) ABS/TM composites (Che Ismail & Akil, 2018)	44
Figure 2.16:	Polypropylene Structure	44

Figure 2.17: Thermal conductivity of injection-molded polypropylene-particle composites with varied fillers and fractions of filler (Weidenfeller et al., 2004).	47
Figure 2.18: Thermal conductivity as a function of BN content for each PP/BN composite (Cheewawuttipong et al., 2013).	48
Figure 2.19: Thermal conductivity coefficient of polypropylene matrix reinforced by CNTs with different distribution patterns versus temperature (3% volume percent, Thickness of interphase = (a) 0, (b) half of SWCNT diameter and (c) SWCNT diameter) (Ansari et al., 2018)	50
Figure 2.20: Fiber Classification (Dimple et al., 2023)	52
Figure 2.21: Multiscale structure of wood (Q. Zuo et al., 2023)	53
Figure 2.22: Diagram of Wood Dust Particle Size (Nafis et al., 2023)	54
Figure 2.23: Typical structure of (i) untreated and (ii) NaOH treated natural fiber (Behera et al., 2018)	55
Figure 2.24: Surface appearance of the coir fiber before alkali treatment (Karthikeyan et al., 2014)	57
Figure 2.25: Surface appearance of the coir fiber after 2% NaOH treatment (Karthikeyan et al., 2014)	58
Figure 2.26: Surface appearance of the coir fiber after 4% NaOH treatment (Karthikeyan et al., 2014)	58
Figure 2.27: SEM Image of Untreated and 1, 3, 5, 7 & 9% NaOH treated banana (Parre et al., 2020)	60
Figure 2.28: Scanning electron microscopy images of the cross-sectional area of the flexural specimens (Serra-Parareda et al., 2020)	61

Figure 2.29: Tensile strength of untreated and alkali treated Bamboo fiber reinforced epoxy composites(Behera et al., 2018)	63
Figure 2.30: Tensile modulus of untreated and alkali treated Bamboo fiber reinforced epoxy composites (Behera et al., 2018)	63
Figure 2.31: MAPP reaction mechanism with a lignocellulosic surface hydroxyl group(Rowell, 2006)	64
Figure 2.32: Recycling process of polypropylene scraps(Ardente et al., 2007)	66
Figure 2.33: Surface observation of T/P and T/P/MA blends as related to post-2nd and post-3rd recycling. (A) Post-2nd-recycling group; (B) post-3rd-recycling group (Lin et al., 2020)	67
Figure 2.34: SEM images of the tensile specimens' side area in the (a) first, (b) second, (c) third, (d) fourth, (e) fifth, and (f) sixth rounds of recycling (Vidakis et al., 2021).	68
Figure 2.35: SEM images of the tensile specimens' fractured surfaces of the (a) first, (b) second, (c) third, (d) fourth, (e) fifth, and (f) sixth rounds of recycling (Vidakis et al., 2021)	68
Figure 2.36: Commonly used plastics and their applications	69
Figure 2.37: Recycled Woodchip Reinforced Polypropylene Composites with MAPP Compatibility (Sanadi & Stelte, 2023a)	70
Figure 2.38: Effect of fiber loading to tensile strength of PP/CF composite with and without MAPP (Sabri et al., 2013)	71
Figure 2.39: Filament manufacturing begins with the separate components (PP and SCF) (Almeshari et al., 2023b)	78

Figure 2.40: OM images of longitudinal section of tensile tested sample for 11%SCF/PP composite (Almeshari et al., 2023b)	80
Figure 2.41: Wellzoom Desktop Extruder Line II.	81
Figure 2.42: Extruder Machine Parts (Kristiawan et al., 2021)	82
Figure 2.43: Filament Work Flow (Kristiawan et al., 2021)	83
Figure 2.44: A schematic of a typical single-screw extruder (Altinkaynak, 2010)	84
Figure 2.45: Schematic representation of twin screw extruder and processing of hot melt extrusion (Reddy et al., 2011)	86
Figure 2.46: Twin screw extruder (Courtesy of American Leistritz Co., Somerville, NJ) (Crowley et al., 2007)	86
Figure 2.47: Cross-section of single- and twin-screw extruders (Patil et al., 2016)	87
Figure 2.48: Diagram of an extruder screw (Crowley et al., 2007)	87
Figure 2.49: Sheet die idea like a coat hanging (Kostic & Reifschneider, 2006)	88
Figure 2.50: Improper extrusion die design causes product faults. The flaws are related to the profile's substantial bending and twisting (Truong et al., 2020)	89
Figure 3.1: Flow chart of methodology	95
Figure 3.2: Granulated pellets of recycled PP	96
Figure 3.3: wood fiber	97
Figure 3.4: NaOH Pellet	98
Figure 3.5: MAPP Pellets	99
Figure 3.6: Wood fiber is washed with distilled water	100
Figure 3.7: Wood fiber is being dried in an oven.	101

Figure 3.8: Sieve process; (a) clean wood fiber, (b) three different sieve sizes, (c) wood fiber is placed in sieve, (d) the machine is switch on for 30 minutes	102
Figure 3.9: Preparation of NaoH solution	104
Figure 3.10: Wood fiber treatment with NaOH solution; (a) Wood fiber and NaOH solution, (b) The solution of sodium hydroxide (NaOH) dissolves the wood fiber, (c) Distilled water used to rinse treated wood fiber, (d) Tray with treated wood fiber, (e) The tray is placed inside the oven, (f) Wood fiber after 24 hours in the oven	105
Figure 3.11: Hot-press machine	106
Figure 3.12: The recycled polypropylene, wood fiber and MAPP are mixed together	107
Figure 3.13: Hot-press process; (a) weighing MAPP, PP and wood fiber, (b) combine the composites into the plastic bag, (c) get the moulds ready, (d) place the composites within the mould, (e) uniformly distribute the composites, (f) insert the mould into the machine, (g) configure the parameter, (h) composites upon completion of hot-pressing	108
Figure 3.14: Hot-press parameter	109
Figure 3.15: Cooling press parameter	110
Figure 3.16: Cheso crusher machine	111
Figure 3.17: Pellet fabrication; (a) composite on the cutting machine, (b) cutting process, (c) insert composite into crusher machine, (d) required size of pellet	112
Figure 3.18: Single Extruder	113
Figure 3.19: Extrusion process of filament; (a) pellets are put into the funnel, (b) parameter is set up, (c) pellet melted and transformed into filament, (d)	

filament travels through tubs of cooling water, (e) the roller pulls the filament while the sensors measures the filament's size, (f) precise filament size required	114
Figure 3.20: FDM 3D printing	118
Figure 3.21: Instron Model 8872	119
Figure 3.22: Tensile test; (a) Place the specimen to the machine, (b) See the tensile data in the computer, (c) The specimen is break into two, (d) Specimens after the testing	120
Figure 3.23: Tensile test specimens	121
Figure 3.24: Tensile test specimens after testing	122
Figure 3.25: Instron Floor Mounted Material Testing System Model 5585	123
Figure 3.26: Flexural testing; (a) The specimen is placed on the machine, (b) The controller is used to adjust the machine's up and down operation, (c) Three-point bending test , (d) Data obtained from the testing.	124
Figure 3.27: Flexural specimens for testing	125
Figure 3.28: Flexural specimens after testing	125
Figure 3.29: Water absorption test	126
Figure 3.30: Soil burial testing process; (a) An electronic balance is being utilised for weighing the filament, (b) 50g of soil are added to the plastic container at first, (c) Wrap the filament with a mesh cloth, (d) Place the wrapped filament on the soil, (e) Buried the wrapped filament in an additional 100g of soil, (f) Repeat the steps to all % of MAPP.	127
Figure 3.31: Digital Microscope Dino-Lite AM4114 / AD4113	128

Figure 4.1: Fabrication of r-WoPPc filament; (a) Wood fiber is prepared, (b) A sieving machine is used to sieve wood fiber, (c) NaOH solution is used to treat wood fiber, (d) Post-oven treatment of wood fiber, (e) The recycled polypropylene, wood fiber and MAPP composite is blended within a plastic bag, (f) The r-WoPPc after being hot-pressed, (g) The composite is crushed to pellet, (h) Filament obtained after extrusion process	131
Figure 4.2: Filament of r-WoPPc; (a) Without MAPP, (b) 1% MAPP, (c) 3% MAPP, (d) 5% MAPP	132
Figure 4.3: Fabrication of 3D printed r-WoPPc	132
Figure 4.4: r-WoPPc filament dimension (mm)	134
Figure 4.5: Density of filament	135
Figure 4.6: High precision micrograph with 250x magnification of r-WoPPc filament surface morphology; (a) without MAPP, (b) 1% MAPP, (c) 3%MAPP, (d) 5% MAPP	136
Figure 4.7: Effect of MAPP content on tensile strength of r-WoPPc.	138
Figure 4.8: Effect of MAPP content on modulus elasticity of tensile of r-WoPPc.	139
Figure 4.9: MAPP reaction mechanism with a lignocellulosic surface hydroxyl	140
Figure 4.10: High precision micrograph with 250x magnification of r-WoPPc tensile fracture specimens; (a) without MAPP, (b) 1% MAPP, (c) 3%MAPP, (d) 5% MAPP	142
Figure 4.11: High precision micrograph with 250x magnification of r-WoPPc filament; (a) without MAPP, (b) 1% MAPP, (c) 3%MAPP, (d) 5% MAPP	144
Figure 4.12: Effect of MAPP content on flexural strength of r-WoPPc.	146

Figure 4.13: Effect of MAPP content on modulus elasticity of flexural of r-WoPPc.	147
Figure 4.14: Water absorption rate of r-WoPPc (%)	150
Figure 4.15: MAPP reaction mechanism with a lignocellulosic surface hydroxyl	151
Figure 4.16: Weight loss of r-WoPPc after buried in soil for 21 days.	154



LIST OF SYMBOLS AND ABBREVIATIONS

D,d	-	Diameter
cm	-	Centimeter
mm	-	Milimeter
Mpa	-	Mega Pascal
%	-	Percent
kN	-	Kilo Newton
g	-	gram
°	-	Degree
μm	-	Micro meter
rpm	-	Revolution per minutes
rPP	-	Recycled Polypropylene
rWD	-	Recycled Wood Dust
PP	-	Polypropylene
WF	-	Wood Fiber
WD	-	Wood Dust
MAPP	-	Maleated Anhydride Grafted Polypropylene
MAPE	-	Maleated Anhydride Grafted Polyethylene

LIST OF APPENDICES

APPENDIX	TITLE	PAGE
APPENDIX A	Gantt Chart for PSM 1 & 2	167
APPENDIX B	Turnitin Report	170



CHAPTER 1

INTRODUCTION

1.1 Problem Statement

The outstanding chemical resistance, superior mechanical qualities, and low density of polypropylene are well recognised (Zulkifli & Noorasikin, 2013). However, using it as a filament for 3D printing might create some difficulties. The tendency of PP to warp while printing is one of the key issues with utilising PP as a filament. This may result in faulty prints because the print may lift off the build plate. It is crucial to print PP at a high temperature on a hot build plate in order to avoid warping. The low melting temperature of PP in comparison to other popular 3D printing materials like ABS or PLA is another problem. In order to avoid the filament from cooling and hardening before it can adequately attach to the preceding layer, printing at faster rates may be necessary to achieve excellent layer adhesion. Besides, PP is more likely than certain other filaments to thread and ooze while printing (Awogbemi & Kallon, 2023). Unwanted material accumulation between pieces or on the print surface may occur from this. With that, composites made of wood fibre and recycled polypropylene fibre have gained significant attention in recent years due to their eco-friendliness, renewability, and potential for replacing traditional materials such as plastics and metals.

Wood-Plastic Composite (WPC) filament is what is created when polypropylene (PP) and wood fibers are combined as a 3D printing filament. But there are still problems occur such as the wood fibers in WPC filament tend to clog the nozzle more frequently, especially if the nozzle is too tiny or the fibers are not finely ground. Failure to print as a

result might necessitate periodic printer maintenance. Then, WPC filament may be more brittle and more likely to break while printing if there are wood fibers present. The printing procedure may be interrupted as a result, producing unsuccessful prints. These composites' poor mechanical qualities, however, prevent them from being used widely. The weak interfacial bonding between the wood fiber and recycled polypropylene fiber is one of the key causes of the lower mechanical performance. When a compatibilizer is not used, the bond between the wood and the polymer is significantly weaker (Mohebbi & Kazemi, 2011). The use of coupling agents like MAPP has demonstrated potential for strengthening the mechanical characteristics of composites by increasing interfacial bonding (Rajendran Royan et al., 2021). For WPCs, MAPP can result in a 30–100% increase in mechanical characteristics (Hao et al., 2021).

1.2 Research Objective

The objective of studying the influence of MAPP coupling agent on 3D printing filament made of wood fiber and recycled polypropylene composites can be several, but some of the possible objectives are:

1. To produce 3D-printing filament with the material made of wood fiber, PP with the different ratios of MAPP.
2. To investigate the mechanical properties of 3D printed sample from the filament made of wood fiber and recycled polypropylene with and without the use of MAPP coupling agent.

Overall, the goal of this research is to look into the potential of MAPP coupling agents to improve the mechanical properties of composites made of wood fiber and recycled polypropylene fiber, which could have significant implications for the development of sustainable and eco-friendly materials for a variety of applications.

1.3 Scope of Research

The scope of this research are as follows:

- Testing and analyse physical, morphological, and mechanical of filament.
- Develop alternative material for 3D printing filament based on combination of Polypropylene (PP) and wood fiber.
- Material that used in this study are wood fiber and recycled polypropylene (PP) with MAPP 0%, 1%, 3% and 5%.



CHAPTER 2

LITERATURE REVIEW

2.1 Background

These days, boosting production was important for purposes involving global marketing. This manufacturing procedure was in line with the advancement of new, innovative technologies. One of the most advanced manufacturing techniques, known as additive manufacturing or 3D printing, was created by individuals working mostly in the design and manufacturing industries. Since it is economical and simple, fused deposition modelling (FDM) is one of the most extensively utilised 3D printing technologies (Almeshari et al., 2023a). The 3D printing technique employs thermoplastic filaments, which are plastics (also known as polymers) that melt rather than burn when heated, allow for moulding and sculpting, and solidify when cooled. However, when filament is utilised for printing, higher printing temperatures (between 210 and 260 °C) are employed, which releases toxic fumes and is not environmentally beneficial (Musa et al., 2022).

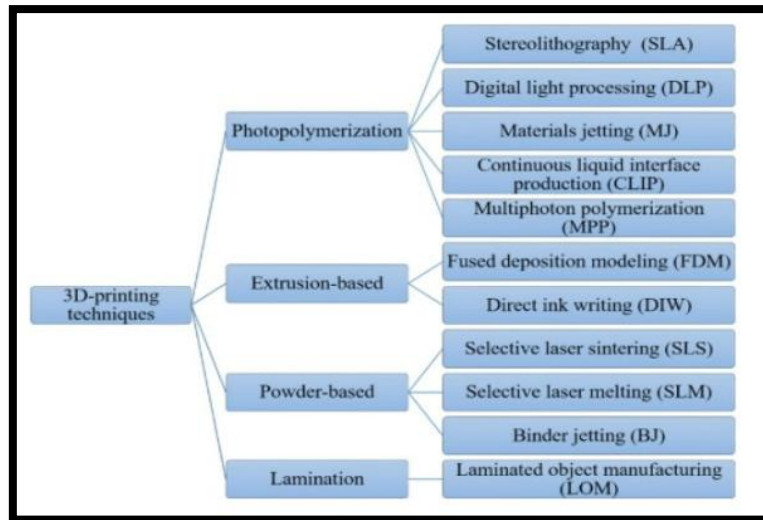


Figure 2.1: 3D Printing Techniques

In today's culture, reducing environmental deterioration is a major public issue. The primary focus of this research is natural fiber reinforced polymer matrix composites. Composites are fiber-reinforced polymer resin-based hybrid materials that combine the excellent mechanical and physical performance of fibers with the attractive appearance and physical properties of polymers. As the fiber content rises, it has been seen that natural fiber composites perform better (Mohammed et al., 2022). Hence, this study is to implement a combination of recycling waste which is Wood Fiber with the recycled plastic material (Polypropylene), the utilisation of a brand-new class of high-quality, inexpensive recycling filaments will be presented.

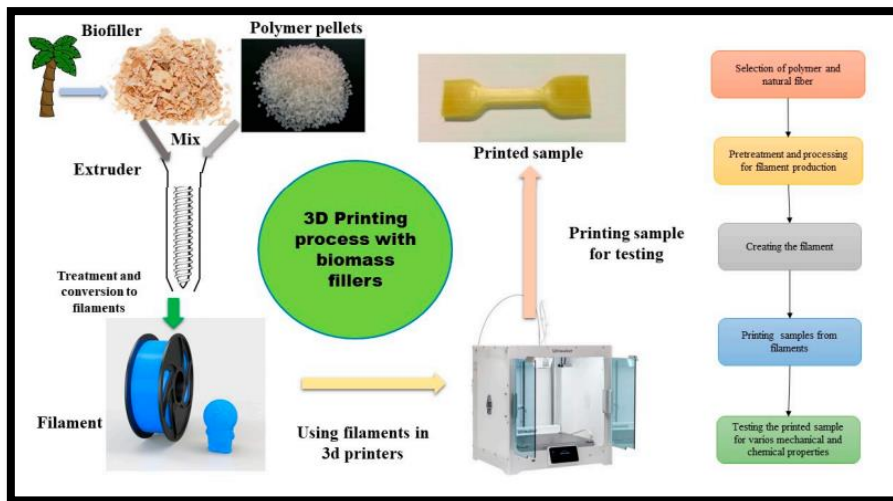


Figure 2.2: The 3D printing process using natural fibres

In this project, the composites of Wood Fiber and Recycled Polypropylene give a lot of advantages but the connection between wood fiber and polymer is quite weak since polyolefin is a hydrophobic substance and wood fiber is a hydrophilic material. Then, MAPP, a coupling agent, was added to the WPCs to strengthen the contact bonding. Since different melt-used polymer matrices have variable mechanical characteristics for MAPP, the polymer mix PP/MAPP was studied as a benchmark. In contrast, due to the high interface bonding strength of WPCs with coupling, the tensile strength and impact strength were greatly increased with the addition of the coupling agent (Yuan et al., 2008a).

Physical, mechanical, and morphological sample testing will be done for this investigation. This wood fiber reinforced with matrix Polypropylene will be tested for its tensile and flexural capabilities, water absorption, and microscopic characteristics.

2.2 Introduction

A literature review is a thorough analysis of certain works on a given subject. The literature review, in the context of a research thesis, is a critical synthesis of earlier research.

The most crucial stage in finding information about the subject is a literature study. Literature can be found in journals, books, newspapers, magazines, the internet, theses and dissertations, conference proceedings, reports, and films. The information on the materials and preparations utilised in composites is examined in this chapter.

2.3 3D-Printing

2.3.1 3D-Printing History

In recent years, additive manufacturing (AM) methods have evolved substantially. Because of the availability of several types of AM technologies as well as numerous consumable materials, the area of this technology is rapidly increasing. The key advantages of the AM method are as follows: No need to create tools and fixtures, cost-effectiveness of manufacturing for a limited number of items, waste material reduction, developing and producing tailored products, and cost-effectiveness of customised production. It is also crucial to choose the appropriate printing settings. If thorough judgements are made, the outcome will be proper and sustainable. Furthermore, correct material selection for a given application is crucial in AM operations. An extrusion-based 3D printer is a type of additive manufacturing technology that is used for prototyping, modelling, and the production of functional parts. (Akhoundi & Sousani, 2023).

AM, often known as 3D printing, is a manufacturing technology that builds an object from the ground up by adding material in the form of thin layers. The graphic displays a 3D printed item's life cycle. The CAD file is converted into an outer surface geometry representation, which is frequently in stereolithography (STL) format, in order to print an item. Using the STL file and the user-defined design parameters, a slicer application creates a printer-specific sequence of instructions (G-code). G-code commands are sent to the

printer, where the firmware sequentially executes them to print the object. There are supporting procedures that revolve around this essential action, such as procurement and job provisioning (Rais et al., 2023).

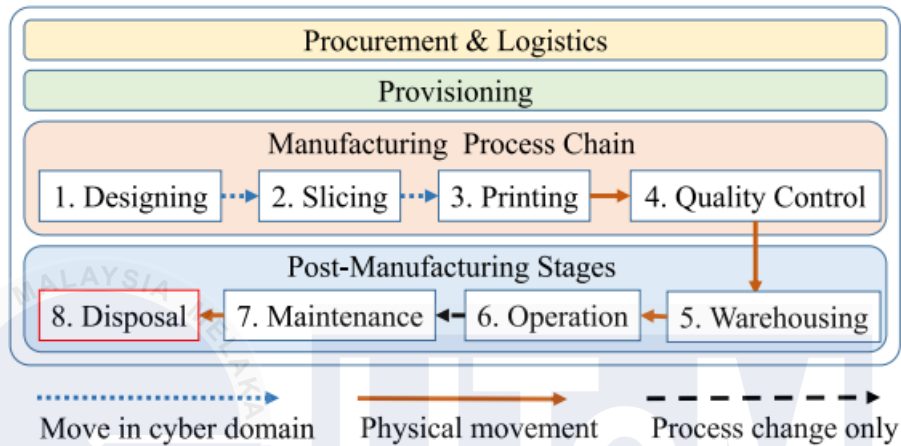


Figure 2.3: 3D printed object life cycle (Rais et al., 2023)

In the 1980s, the first 3D printers were utilised, using a computer tracing a pattern immersed in a liquid polymer. The sketched pattern was hardened into a layer by the laser, and this was how you manufactured a plastic item. Since then, much progress has been made in additive manufacturing, and material extrusion is now used. This procedure produces an item by pushing materials from a mechanical head, similar to how inkjet printers extrude ink onto paper. Surprisingly, the cost of getting 3D printers has been lowering as technology has advanced. Domestic use of 3D printers is increasing, with the average cost rising to a few hundreds of dollars. However, one significant disadvantage is that printing 3D items takes competence; in fact, both the digital file and the final printing require a qualified individual. 3D printing is changing the way industries work, prompting some observers to coin the term "Second Industrial Revolution." (Mpfu et al., 2014).

To summarise, in the recent years 3D printing technology has grown into a flexible and powerful tool in the advanced manufacturing industry. 3D printing technology is gaining popularity in the industrial sectors and offers several benefits to consumers, corporations, and governments. As a result, more information is needed to go forward with efforts to increase 3D printing technology utilisation. More understanding of 3D printing technology will help businesses and governments upgrade and improve 3D printing infrastructure. Thus, the goal of this article is to offer an overview of the many types of 3D printing technologies, the materials used for 3D printing technology in the manufacturing industry, and, lastly, 3D printing technology applications. Researchers can perform further study on the many types of 3D printing machines and the materials that can be used by each type of machine. (Shahrubudin et al., 2019).

2.3.2 3D-Printing Process

It is said by (Pavan Kalyan & Kumar, 2022) that the 3D printing begins with the creation of a virtual model of the thing to be manufactured. The virtual design is utilised to produce a template for the real product. This virtual design may be created from scratch using a 3D modelling programme such as CAD (Computer Aided Design). A 3D scanner may also be used to scan an existing object. This scanner creates a 3D digital duplicate of an object that is then imported into a 3D modelling programme. In preparation for printing, the model is subsequently cut into hundreds or thousands of horizontal layers. This prepared file is then uploaded to the 3D printer, which will create the item layer by layer as illustrated in the image below. Every slice (2D picture) is read by the printer, and the item is created layer by layer, with no trace of layering apparent, but with a 3-dimensional structure (Aguirre-Cortés et al., 2023).

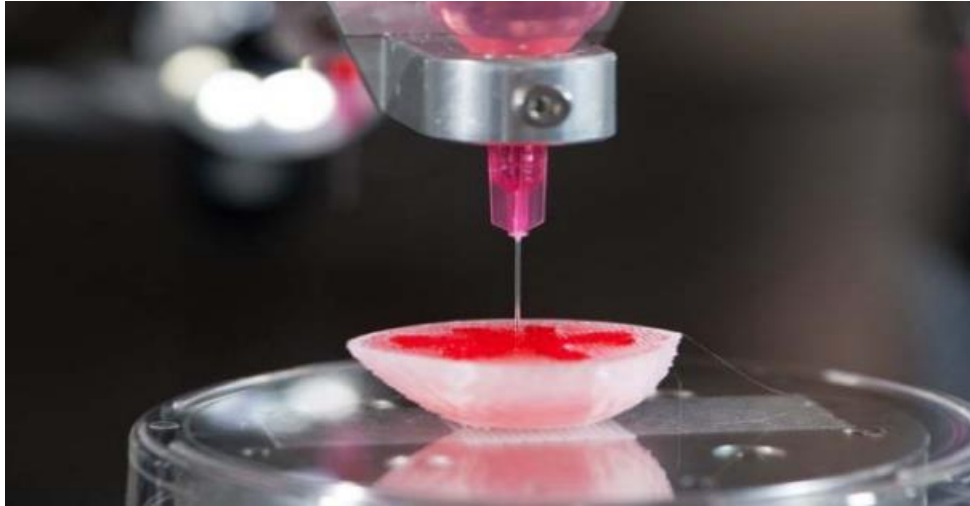


Figure 2.4: 3D printing layer by layer (Mpofu et al., 2014)

The procedure of 3D printing includes the drawing of 3D objects to be printed in CAD software. However, the 3D objects file cannot be used as is. These files must be converted to STL format. There is a wide range of software available on the market that may be used for drawing and modelling. Fusion360, Solid Works, and Auto CAD are a few examples. In addition, 3D scanners are now accessible for creating programming files (Le Duigou et al., 2016). This programme transfers data to the printer's main board via PCs as well as pen drives or memory cards. When the programme is sent to the printer, the material begins to heat up in the extruder and the filament begins to melt. This melting material was put on the print bed as programmed, and the item was created by depositing components layer by layer on top of one another. The layers are horizontal, cross, and zigzag with each other, as well as hexagonal or honey comb in structure (Shinde et al., 2020).

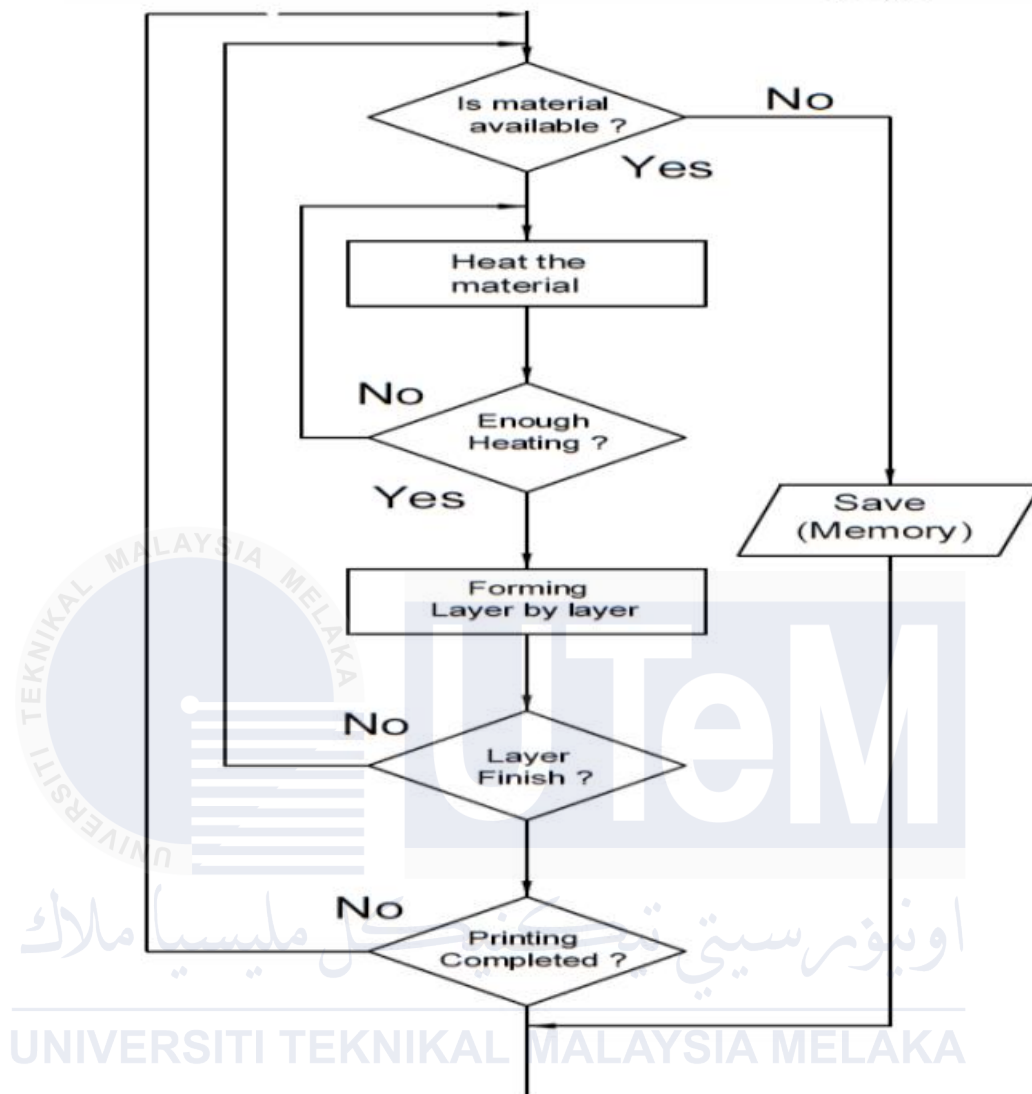


Figure 2.5: Flowchart of 3D printing operation (Shinde et al., 2020)

Initially, 3D modelling software is used to construct the appropriate geometry. After that, the modelled object is split in two dimensions with slicing software, and the print path is designed and produced as a print file. Prior to printing, this file is loaded into the printer's control system. When printing begins, the printer will uniformly extrude the cementitious material, and layers will be stacked into the contours of the modelled design based on the print file's programmed settings; the specific technique is represented in Figure 2.4. Based

on the unique qualities of 3D printing, both extrudability and buildability must be fulfilled for efficient 3D printing of cementitious materials (Geng et al., 2023).

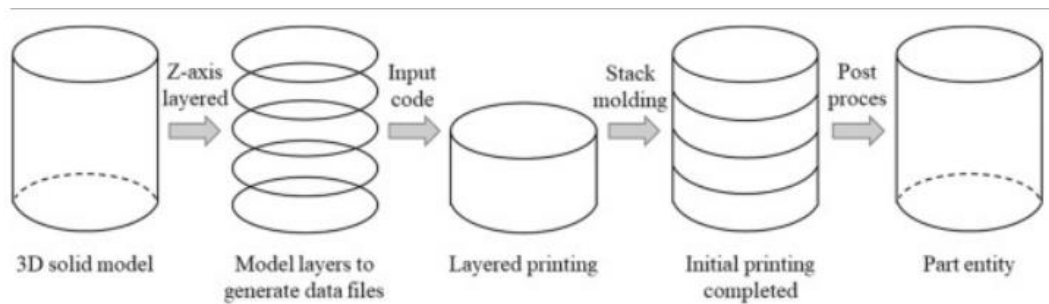


Figure 2.6: Diagram of 3D printing process (Geng et al., 2023)

Extrudability refers to the ability of new material to travel through the print pipeline and print nozzle. Buildability refers to the printing layer's ability to endure deformation caused by shear stresses generated by its own weight and the weight of successive layers. Only once the material has passed through the "liquid" phase (satisfactory extrudability) and the "solidification" phase (satisfactory buildability) can 3D printing be called successful (BG et al., 2023). Furthermore, because 3D printing extruded concrete filaments are formed in stacks, the material distribution inside the building is less uniform than with traditionally poured and vibrated concrete, as seen in Fig. 3. Non-homogeneity can have an immediate influence on engineered materials' macroscopic mechanical behaviour. And cavities will undoubtedly emerge between adjacent concrete filaments and layers, resulting in a weak bond surface (Geng et al., 2023).

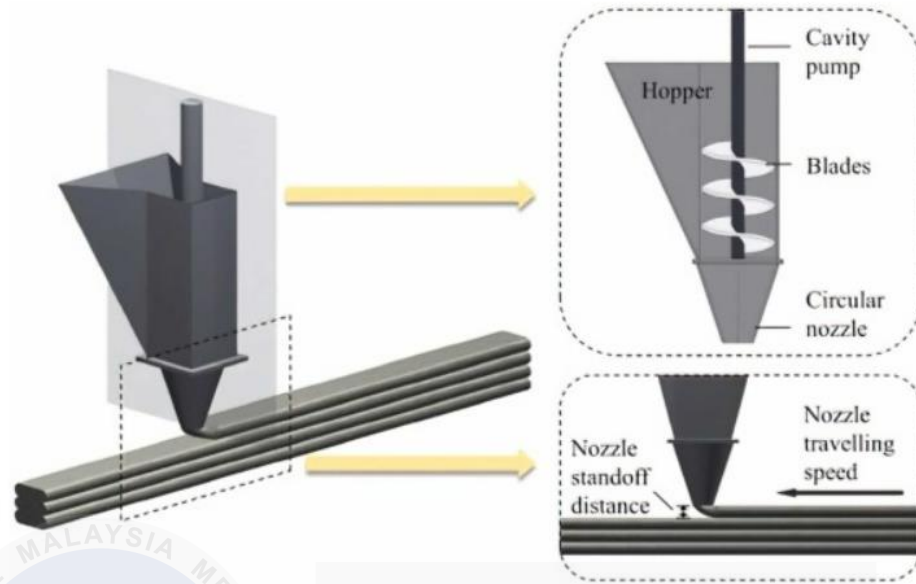


Figure 2.7: Diagram of printing setup (Geng et al., 2023)

2.4 3D Printing Material

Like any other manufacturing process, 3D printing needs high-quality materials that meet certain standards in order to produce items of consistently high quality. For that reason, the suppliers, purchasers, and end-users of the material establish material control procedures, standards, and agreements. A wide range of materials, including ceramic, metals, polymers, and their combinations in the form of hybrids, composites, or functionally graded materials (FGMs), may be used in 3D printing to generate fully functional components (Shahrubudin et al., 2019).

Plastics are the most often used material for 3D printing. This is the most adaptable material for 3D printed toys and home accessories. This is available in clear, as well as green, red, and yellow. Plastic is lightweight and resilient, with a high surface smoothness. This method's polymers are often composed of one of the following materials: PLA, ABS, and PP are a few examples (Shinde et al., 2020). According to (Sharma et al., 2022), PLA and

ABS are the two most commonly used polymer filament types in FDM printing. Biodegradable Polyvinyl Alcohol (PVA) and High Impact Polystyrene (HIPS), as well as sturdy and flexible Polyethylene Terephthalate (PET) and nylon (PA), are other common forms of plastic used for commercial 3D printer filament. A more extensive theory involving plastic materials, namely two major ones, PP and Recycle PP, is set in the next chapter for the sake of relevancy to this research.

2.4.1 Plastics

Plastics, which are widely used in building, housing, toys, medical, and other industries, have recently become a critical commodity in human existence. Plastics have significantly increased white pollution while making life simpler. In China, more than 40 million tonnes of waste plastics must be recycled each year, and the figure is increasing year after year. Plastics are desirable due to characteristics such as versatility, low cost, and light weight (Kazemi et al., 2021). They have generated a varied assortment of things in nearly every sector during the last 50 years. Polyethene terephthalate (PET), polyvinyl chloride (PVC), high-density polyethylene (HDPE), low-density polyethylene (LDPE), polystyrene (PS), and polypropylene (PP) have all been discovered since the discovery of polystyrene in 1839. (Oyinlola et al., 2023). PVC plastics are extensively used in a range of applications, including construction PVC pipes, advertising and interior design PVC foam boards, and so on (Li et al., 2023).

Polymers are divided into two types: thermoplastic polymers and thermosetting polymers (Figure 2.6). Unlike thermoplastics, thermosetting polymers create a chemically connected 3D network and so cannot melt. Thermosetting polymers offer several benefits over thermoplastic polymers, including strong temperature stability, little solvent interaction, and relatively steady behaviour over time (Bobo, 2013). Thermoplastics are

reprocessable and completely recyclable polymeric materials composed of linear polymer chains with no crosslinks. Thermo-processing decreases intermolecular interactions between polymer chains but does not result in chemical bonding. As a result, thermoplastics may be reshaped repeatedly by heating without affecting their physical properties. However, as compared to thermosets, they frequently have weaker chemical resistance and mechanical high-temperature characteristics (Jin et al., 2019).

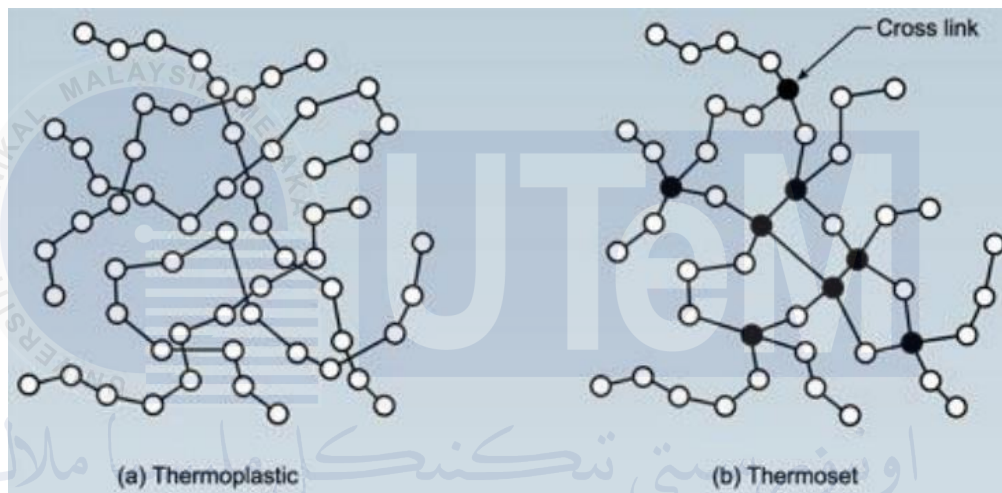


Figure 2.8: Difference between thermoplastics and thermosetting polymers (Bobo, 2013)

Malleable thermosets are crosslinked polymers having dynamic covalent bonds that may be broken and rebuilt reversibly. They have garnered a lot of attention in recent years since they combine the advantages of thermosets and thermoplastics. They have good mechanical properties, thermal and chemical stability, and are reprocessable and recyclable, just like thermoplastics. (Lin et al., 2020). Thermosets are highly crosslinked covalent network polymers with outstanding tensile properties, chemical and heat resistance, and dimensional stability. Thermosets have several applications, ranging from kettle handles to surface coatings to automobile bodywork. However, thermosets cannot be reused or regenerated after failure because they cure via the formation of irreversible chemical

linkages 1, 2. Furthermore, any shape change produced by reversible bond-exchange events (for example, disulfide crosslinks) has been referred to as "creep" and is seen as a drawback of polymeric materials. As a result, thermoset networks are designed to be irreversible and nearly unrecyclable (Jin et al., 2019).

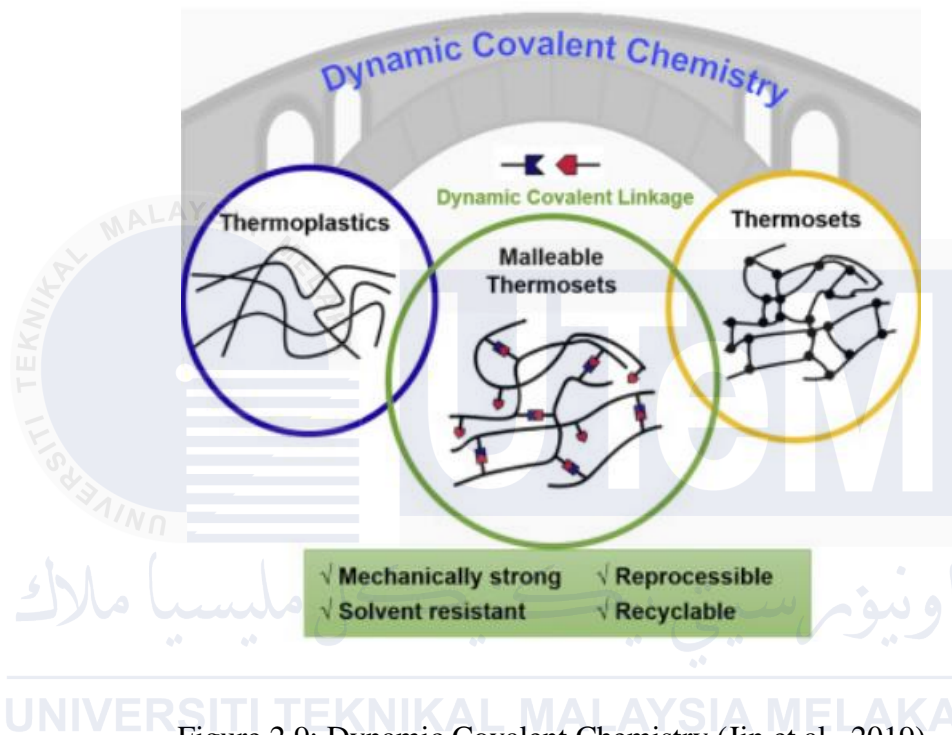


Figure 2.9: Dynamic Covalent Chemistry (Jin et al., 2019)

As (Kazemi et al., 2021) previously stated, thermoplastics may go through melting and hardening cycles when heated, and they are recycled using all three recycling techniques (mechanical, chemical, and incineration). Because the mechanical technique and incineration have simple and rather set procedures, we will concentrate on improvements in chemical recycling technologies in this section. Not all plastics manufactured are recyclable, according to the Society of the Plastics Industry (SPI) categorization. The SPI divides available plastics into seven groups based on polymer type, and each category is allocated a number code indicating its kind (44). Table 2.1 shows this categorization as well as its use in the building sector.

Table 2.1: SPI classification of plastics with properties and applicability in the construction industry (Kazemi et al., 2021)


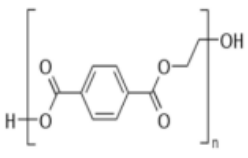

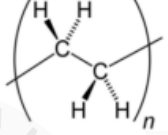

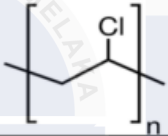

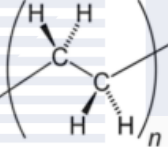

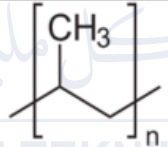

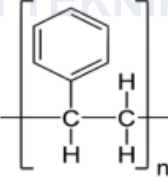

Polymer name Symbol	Chemical structure	Uses	Can be recycled	Construction material applicability
polyethylene terephthalate  PET		soda bottles, water bottles, medicine jars, and salad dressing bottles	yes	asphalt modification(45), porous concrete(46, 47), soil stabilization(48), producing glass fiber reinforced polymer (GFRP) rebar(49)
high-density polyethylene  HDPE		soap bottles, detergent, and bleach containers, and trash bags	yes	asphalt modification(50), concrete structural components(51), soil stabilization(52)
polyvinyl chloride  PVC		plumbing pipes, cables, and fencing	limited	asphalt modification(53), durable concretes(54)
low-density polyethylene  LDPE		cling wrap, sandwich bags, and grocery bags	limited	asphalt modification(55), cement bricks(56)
Polypropylene  PP		reusable food containers, prescription bottles, and bottle caps	limited	asphalt modification(57), lightweight concrete(58), gypsum plasters(59)
Polystyrene  PS		plastic utensils, packaging peanuts, and Styrofoam	no	asphalt modification(60), lightweight cement mortars(61)
other plastics (e.g., acrylic, polycarbonate, etc.)  Other	-	water cooler bottles, baby cups and fiberglass	no	gypsum plasters(62), recycled concrete(63)

Table 2.2: Semi-crystalline and amorphous polymers have similar properties

Semi-crystalline polymers (PP, PLA, nylon, etc.)	Amorphous polymers (ABS, PC, PS, etc.)
Predominantly opaque	Predominantly transparent
Better chemical resistance and resistance to stress-cracking and fatigue	Prone to stress-cracking and poor fatigue resistance
Difficult to bond	Easier to bond
Average impact resistance	Better impact resistance
Sharper melting point	Soften over a range of temperatures
More challenging to process due to higher shrinkage upon cooling	Lower shrinkage upon cooling, easier to process

2.4.1.1 PLA

PLA is one of the most imaginative materials that has been developed in a wide range of applications. This polymer is thermoplastic as well as biodegradable. Because of its biocompatibility and absence of metabolic toxicity, PLA can be employed in therapeutic applications (Kristiawan et al., 2021). PLA surpasses poly (hydroxyl alkanooates), poly (ethylene glycol), and polycaprolactone (PCL). PLA has higher thermal processability and is easier to manufacture in standard manufacturing processes than other biopolymers. PLA is useful for food packaging and biological applications because to its transmission, nonreactive nature, and hydrophobic nature (Ramanadha reddy & Venkatachalapathi, 2023).

PLA is useful for food packaging and biological applications because to its transmission, nonreactive nature, and hydrophobic nature. PLAs are lactic acid aliphatic polyesters that are frequently used in the biomedical sector as tissue scaffolds, internal sutures, and implant devices. PLA is also used to cover high tunnel shields. They have a cheaper manufacturing cost, are more abundant in nature, and have a lower molecular weight than petro polymers (Jin et al., 2019). This PLA has just a few features in common with

other polymers such as polyethylene. The production methods for fibers, films, sheets, and containers are also straightforward and consistent. This study focused on the most recent advances, groundbreaking discoveries, and research in the field of PLA-based composite sciences. (Ramanadha reddy & Venkatachalapathi, 2023).

When the poly-L-lactic acid (PLLA) concentration is greater than 90%, PLA is crystalline; when it is less than that, PLA is amorphous. The melting point and glass transition temperatures rise with increasing PLLA content (Maddah, 2016a). From (Ramanadha reddy & Venkatachalapathi, 2023), Amorphous PLA has a density range of 1.248 g/ml to 1.290 g/ml, while crystalline PLA has a density range of 1.210-1.430 gcm³. PLA's soluble nature varies according on the conditions; for example, at boiling temperatures, it is completely soluble, while at typical room temperature, it is moderately soluble in acetone and toluene.

Lactic acid comes in two varieties: L-lactic acid and D-lactic acid. PLA-poly-lactic acid belongs to the PLLA-Poly-L-lactic acid, PDLA-Poly-D-lactic acid, and PDLLA-Poly-DL-lactic acid families. PLLA-Poly-L-lactic acid has garnered considerable interest from researchers due to its unique properties in nature, such as physical appearance, high strength, low weight, biocompatibility, and biodegradability (Awogbemi & Kallon, 2023).

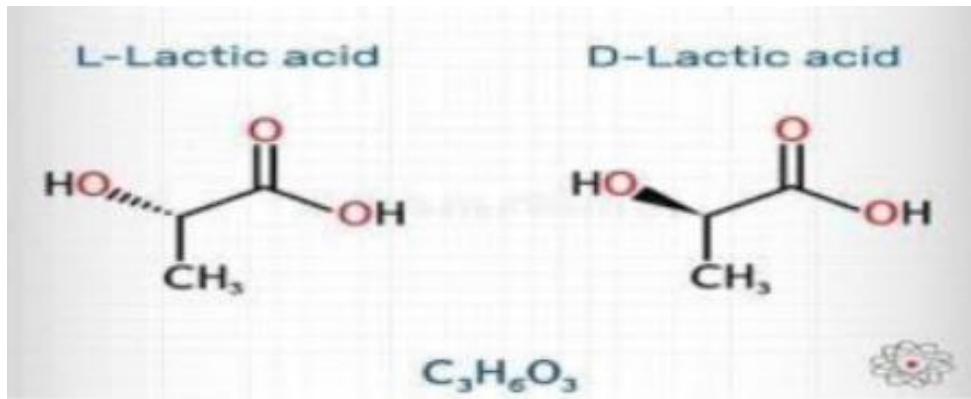


Figure 2.10: The Structural Formula of PLA (Ramanadha reddy & Venkatachalapathi, 2023)

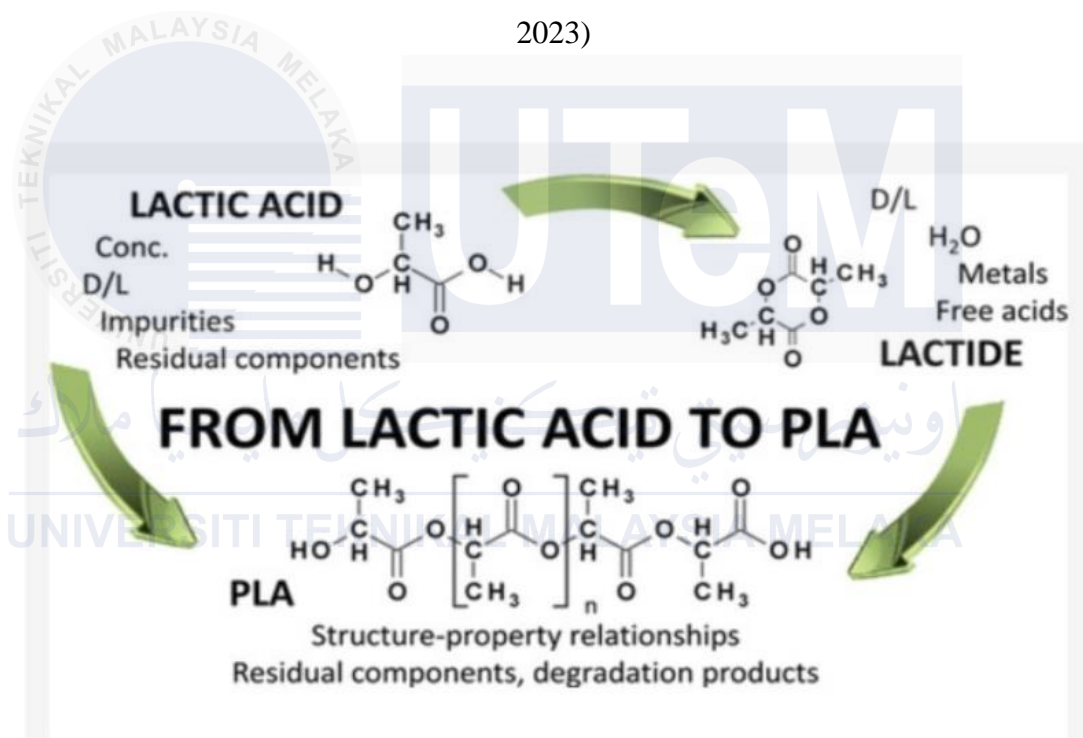


Figure 2.11: Production of PLA in schematic diagram (Ramanadha reddy & Venkatachalapathi, 2023)

Because PLA has a stunning transparent property, it broadens its range of applicability to various sectors such as aerospace industries, remote control vehicles, automobile industries, quick prototyping (3D printing), and other industrial applications. Furthermore, PLAs are environmentally benign since they are frequently produced by the

fermentation of natural plant materials such as starch, leaves, and grains, and they are readily reclaimable, ecological, and decomposable. PLA has emerged as the most eco-friendly biopolymer material (Jin et al., 2019). Then, there is the fact that PLAs may be manufactured utilising a number of traditional processing processes. PLAs can also be manufactured industrially by the use of an innovative and cost-effective polymerization technique. Some common manufacturing techniques include screw extrusion, blow extrusion compound moulding, blow moulding, casting and dipping, foamed thermo sets, joining, fiber reinforcing, and finishing (Ramanadha reddy & Venkatachalapathi, 2023).

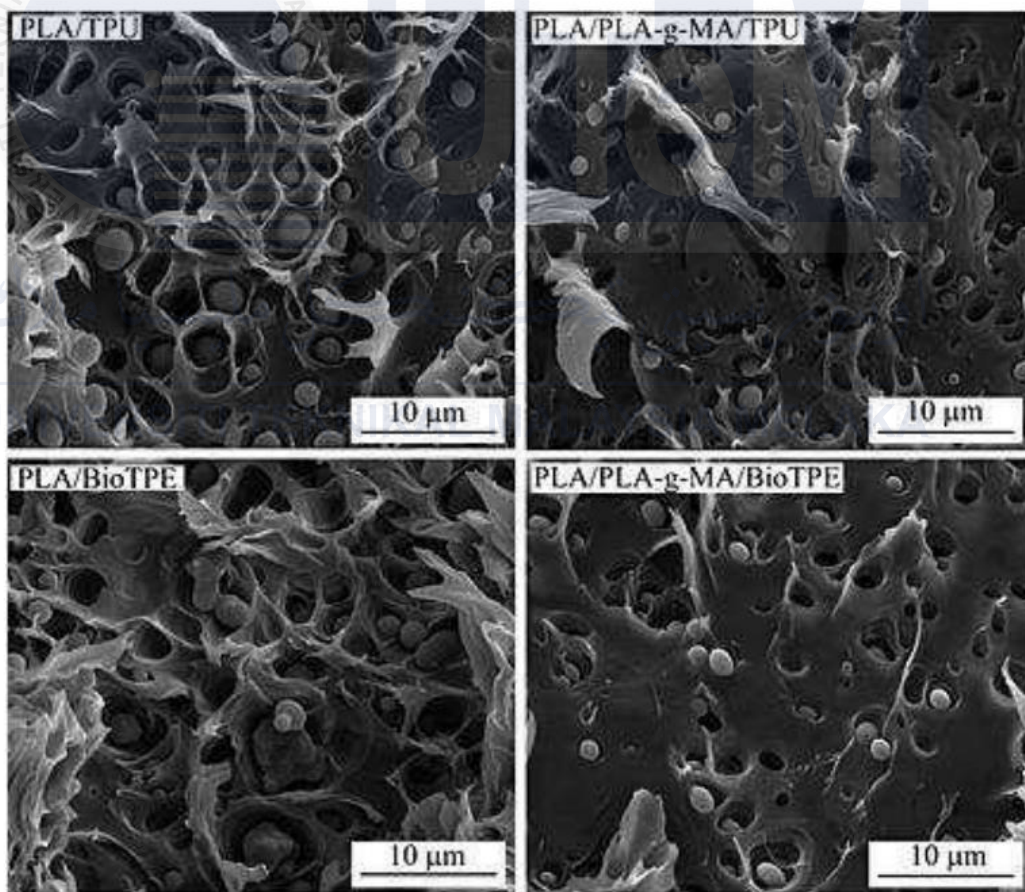


Figure 2.12: Micro-structure of PLA (Sharma et al., 2022)

2.4.1.2 ABS

ABS is a copolymer composed of three components: butadiene, styrene, and acrylonitrile. Butadiene-styrene copolymers improve impact resistance, but acrylonitrile is prone to forming chemical connections with external components. The composition of these three components has a significant influence on the qualities of ABS copolymer. ABS is a thermoplastic engineering material that comprises a butadiene component that is equally distributed throughout the acrylonitrile and styrene matrix (Che Ismail & Akil, 2018). When utilised for applications, ABS possesses exceptional mechanical strength, high dimensional stability, toughness, ease of processing, chemical inertness, cheap cost, and global availability. ABS was introduced in the 1950s as a more rigorous substitute for SAN copolymers (Singh et al., 2023).

ABS was originally a combination of SAN, commonly known as nitrile rubber. Nitrile is a natural rubber, whereas SAN is a synthetic rubber. Because of the ambient temperature, this structure is amorphous, glassy, robust, and impact-resistant (Kristiawan et al., 2021). ABS is an excellent material for home 3D printers. It is known for its strength and safety. ABS is available in a range of hues. As a result, the material is ideal for things like stickers and toys. ABS is also utilised in the manufacture of jewellery and vases (Shinde et al., 2020). ABS is the material of choice for FDM printing when a product with high durability and temperature tolerance is required due to its structural strength and ability to endure high temperatures. ABS 3D printed products may be painted whatever colour you like because ABS spools come in a number of hues.

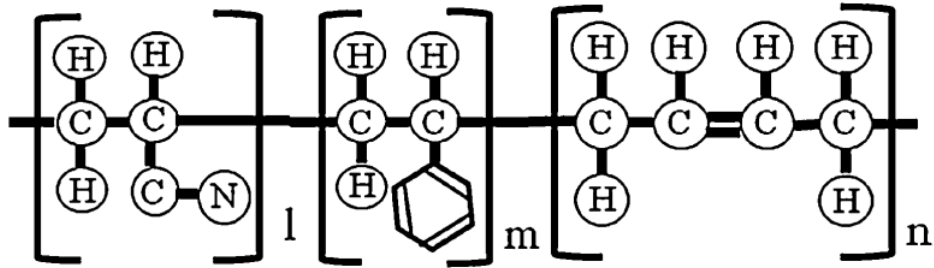


Figure 2.13: Structural formula of acrylonitrile butadiene styrene (ABS) (Tsuchikura et al., 2013)

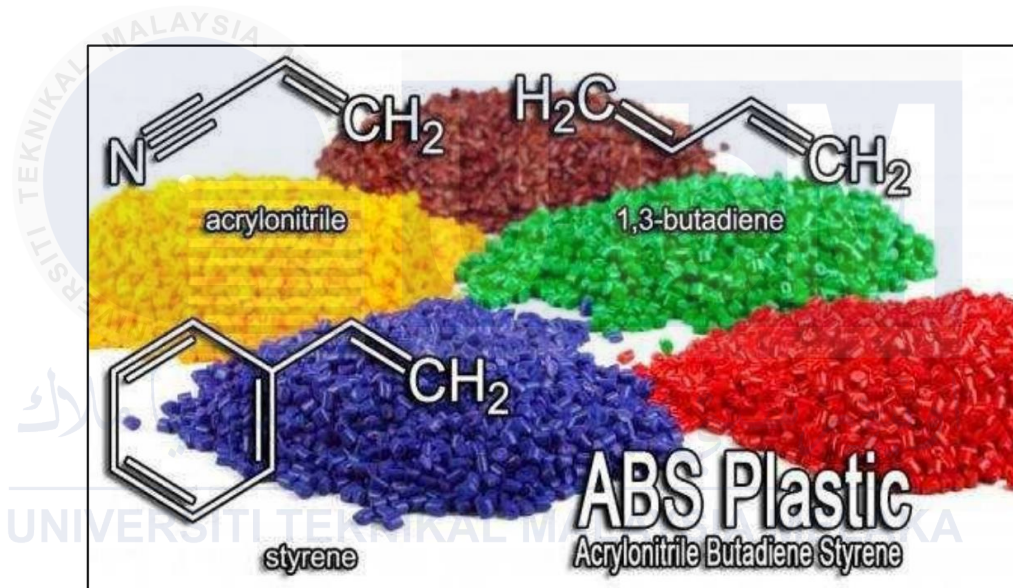


Figure 2.14: Chemical of ABS Formula

It does, however, have certain inherent shortcomings in terms of mechanical strength and weather resistance, limiting its ability to be a versatile thermoplastic. ABS may be combined with any polymer to increase tensile strength, structural integrity, durability, and heat resistance. Because of its chemical composition, which includes a copolymer of three different monomers and a functional group consisting of styrene and nitrile, ABS is recognised as the most blending-friendly polymer (Sabri et al., 2013). ABS, a kind of industrial polymer, is widely used in the production of a wide range of technological

structures, automobiles, machine components, and household products. ABS and its derivatives are used in the automotive industry to manufacture bumpers, seats, dashboard fuel systems, body (including panels), interior trim, electrical components, exterior trim, lighting, upholstery liquid reservoirs, and underhood components. In theory, blending ABS terpolymer with PP enhances the blend's physical and thermal properties only if the components are miscible. Styrene ethylene butadiene styrene (SEBS) copolymer is frequently grafted with ABS to provide a compatibilizer for mixing with numerous inert polymers. When SEBS is added to ABS, it loses its chemical inertness and facilitates the creation of contacts with other polymer chains (Singh et al., 2023).

The FDM-ABS specimens were created using an Umbriel 3D Printer 300x (ZPrinter Co., Iran). The printing machine was set to a resolution of 300 μ m to produce the highest quality samples with the fewest manufacturing flaws. The mechanical properties of the ABS thermoplastic filament are shown in Table 2.3. The consistent building parameters for creating test specimens for tensile and fracture studies are then shown in Table 2.4. It has been stated by (Rezaeian et al., 2022) that a raster angle of 45°/-45° for ABS-FDM components might result in increased mechanical and fracture resistance; hence, this raster orientation was chosen for the current work. The nozzle and bed temperatures were calculated using the ABS filament datasheet. All of the printed specimens were created through the thickness at printing rates of 10, 30, 50, and 70 mm/s. The reasoning behind selecting these printing speeds is addressed in the final paragraph of the introduction. For the tensile and fracture experiments, dog-bone and Semi-Circular Bending (SCB) specimens were created.

Table 2.3: Mechanical Properties of ABS Filament (Rezaeian et al., 2022)

Tensile modulus (GPa)	1.00–2.65
Yield stress (MPa)	13.0–65.0
Ultimate tensile strength (MPa)	22.1–57.0
Maximum elongation (%)	3.0 – 19.0

Table 2.4: Constant construction parameters are used to create the test specimens

(Rezaeian et al., 2022)

Building parameters	Value
Filament diameter	1.75 mm
Infill density	100%
Nozzle diameter	0.4 mm
Nozzle temperature	235 °C
Bed temperature	140 °C
Raster angle	45/-45°
Layer orientation	Printed layers are parallel to the printer bed.

From (Che Ismail & Akil, 2018), it shows that Figure 2.13 depicts the fracture surface of neat ABS and ABS composites including 5% filler. Figure (2.13a) shows that the fracture surface of clean ABS was smooth. When muscovite was implanted in the ABS matrix vs the ABS/UM composite, the micrograph revealed a little increase in surface roughness. Because portion of the filler was detected detached from the ABS matrix, this most likely implies inhomogeneity and non-filler dispersion. The existence of extra voids and cavities is visible, resulting in fracture initiation sites and localised stress concentration. A gap implies weak and poor interfacial adhesion between the filler and the matrix, which has a detrimental influence on flexural properties. The micrograph of ABS/TM, on the other hand, showed a more homogenous filler dispersion with less particle agglomeration inside the matrix, as illustrated in Figure (2.13c). In this situation, the TM is in close contact with the matrix,

Polypropylene is extremely resistant to organic solvents and electrolysis. This polymer has a lower impact strength than polyethylene but a greater working temperature and tensile strength. Furthermore, this polymer is resistant to acids and alkalis but not to aromatic, aliphatic, or chlorinated solvents. Polypropylene is a lightweight polymer with a density of 0.90 g/cm³ that may be used in a variety of industrial applications. Polypropylene, on the other hand, should not be used at temperatures below 0°C (Maddah, 2016b).

Table 2.5: Advantages and Disadvantages of Polypropylene

Advantages of PP		Disadvantages of PP
Homo-polymer	Copolymer	Degraded by UV (Ultraviolet)
Process ability, Good	Process ability, High	Flammable, but retarded grades available
Impact resistance, Good	Impact resistance, High	Attacked by chlorinated solvents and aromatics
Stiffness, Good	Stiffness, High	Difficult to bond
Food contact, Acceptable	Food contact, Not preferable	Several metals accelerate oxidative degrading
		Low temperature impact strength is poor

Experiments revealed that polypropylene has good and desirable physical, mechanical, and thermal properties when used in room temperature applications. It has a somewhat stiff structure, a high melting point, a low density, and a moderately high impact resistance. The crystallinity of PP ranges between 40% and 60% (Maddah, 2016b).

2.4.1.4 Thermal Properties of Polypropylene (PP)

Plastics that are often utilised, such as polypropylene (PP) or polyamide, are electrical insulators with low heat conductivity. novel applications, such as heat sinks in electronic packaging, need the development of novel composites with better thermal conductivity. The thermal behaviour of polymers may be considerably improved by adding fillers to plastics. Because of the wide range of applications, such filled polymers with higher thermal conductivities than unfilled ones are becoming an increasingly important area of study, such as in electronic packaging in applications with decreasing geometric dimensions and increasing power output, such as in computer chips or electronic packaging (Weidenfeller et al., 2004).

Figure 2.15 from (Weidenfeller et al., 2004) demonstrates that the thermal conductivity of glass fibre and barite filled polypropylene composites develops relatively slowly, but magnetite and strontium ferrite considerably improve the thermal conductivity of the PP. The use of magnetite or strontium ferrite to improve polymer thermal conductivity is comparable to the use of common fillers such as aluminium oxide (Al_2O_3) or aluminium nitride (AlN) to increase polymer thermal conductivity.

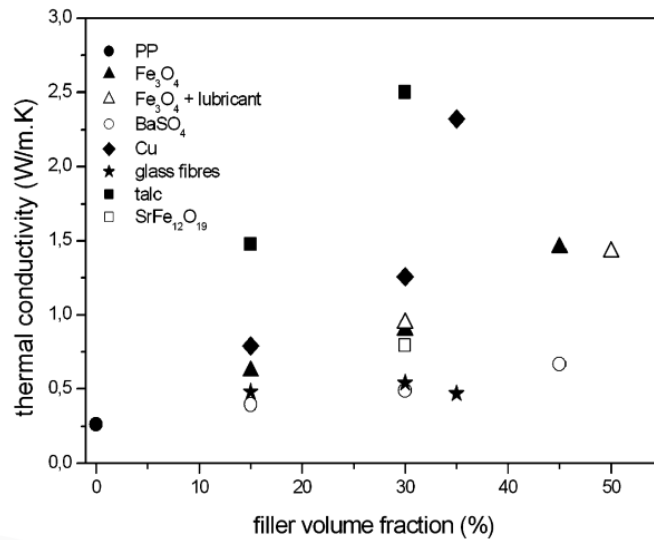


Figure 2.17: Thermal conductivity of injection-molded polypropylene-particle composites with varied fillers and fractions of filler (Weidenfeller et al., 2004).

Figure 2.16 displays the thermal conductivity of composites as a function of BN concentration. Obviously, when the BN concentration grew, so did the thermal conductivity. The thermal conductivity of a PP/BN composite is virtually independent of the PP melt viscosity at different BN concentrations. The thermal conductivity of the PP/BN-l composite was larger than that of the PP/BN-s composite at the same BN concentration. This is a preserved result. Furthermore, when using big size BN (BN-l), the increasing rate of thermal conductivity as a function of BN concentration became substantial at high BN levels (Cheewawuttipong et al., 2013).

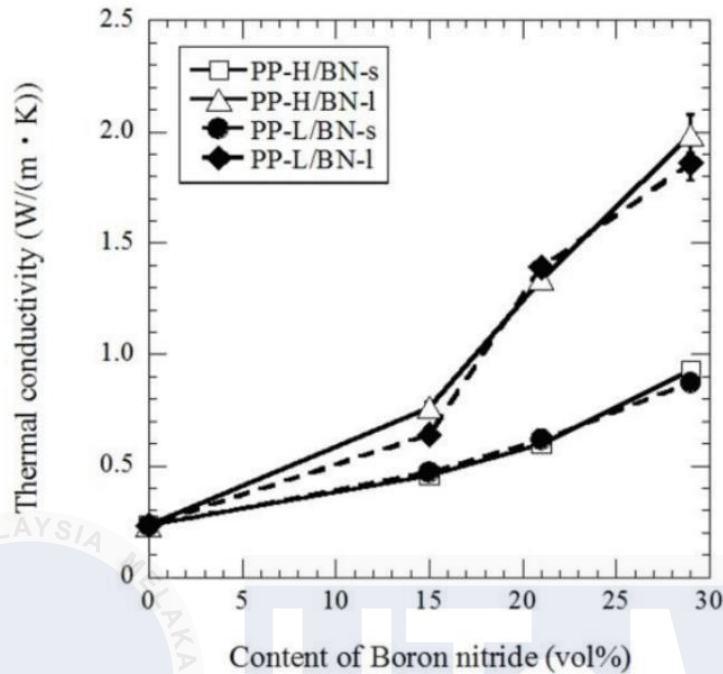
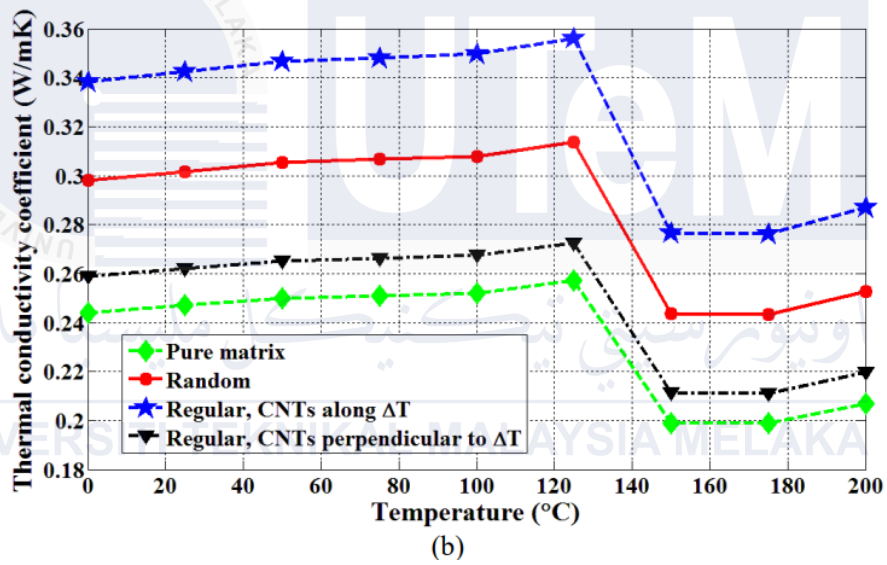
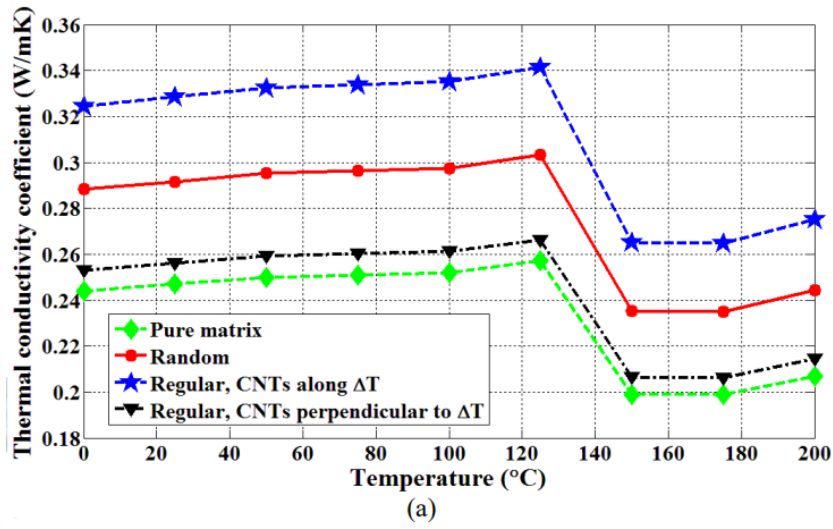


Figure 2.18: Thermal conductivity as a function of BN content for each PP/BN composite (Cheewawuttipong et al., 2013).

CNT reinforced polypropylene has curves that are parallel to those of pure polypropylene. In other words, as the temperature rises, the thermal conductivity coefficient of the nanocomposites increases until it reaches 200°C. The curves subsequently rapidly decline, and the thermal conductivity coefficients once again increase with temperature. As a result, the thermal behaviour of CNT reinforced polypropylene is dictated by the polymer matrix's thermal behaviour (Ansari et al., 2018).



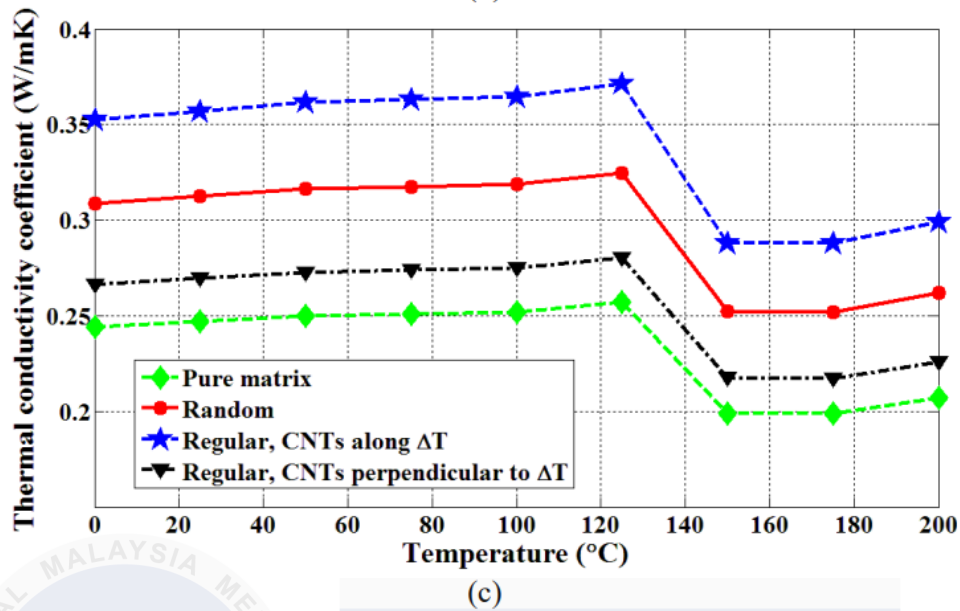


Figure 2.19: Thermal conductivity coefficient of polypropylene matrix reinforced by CNTs with different distribution patterns versus temperature (3% volume percent, Thickness of interphase = (a) 0, (b) half of SWCNT diameter and (c) SWCNT diameter) (Ansari et al., 2018)

Table 2.6: Mechanical and Thermal Properties of Polypropylene.

Property	Homopolymer			Copolymer	
	3	0.7	0.2	3	0.2
Melt flow index	3	0.7	0.2	3	0.2
Tensile strength (MPa)	34	30	29	29	25
Elongation at break (%)	350	115	175	40	240
Flexural modulus (MPa)	1310	1170	1100	1290	1030
Brittleness temp. (°C)	+15	0	0	-15	-20
Vicat softening point (°C)	154-150	148	148	148	147
Rockwell hardness (R-scale)	95	90	90	95	88.5
Impact strength (ft Ib)	10	25	34	34	42.5

2.5 Natural Fiber

Natural fibers are seen to be superior to synthetic fibers owing to their eco-friendliness materials research in the twenty-first century. Indeed, sustainable building materials that make optimal use of renewable resources are gaining popularity. Although synthetic fibers such as steel and polypropylene are still commonly utilised to improve the mechanical properties of cementitious composites due to their established efficacy, they are expensive and may raise building costs and pollutants (Abedi et al., 2023).

Natural fibre reinforcement in polymers demonstrates high strength and stiffness in natural fibre reinforced composites. The most common natural fibres produced across the world include banana, bamboo, sugarcane, jute, kenaf, flax, palm, sisal, hemp, coir, ramie, and abaca (Faruk et al., 2012). In nature, these natural fibres are less costly, lighter, biodegradable, recyclable, and non-toxic. Aside from that, natural fibre offers excellent mechanical and insulating properties, as well as low machine wear (Sahu et al., 2023).

Tensile, hardness, density, flexural, impact, and water absorption tests are the most common examinations performed to determine the physico-mechanical properties of natural fibre filled polymer composites. When choosing fibre for diverse uses, the strength of natural fibre should be taken into account. Matrix selection, strength at the polymer interface, dispersion, orientation, processing method, and porosity are all factors that impact the mechanical characteristics of NFC (Sahu et al., 2023).

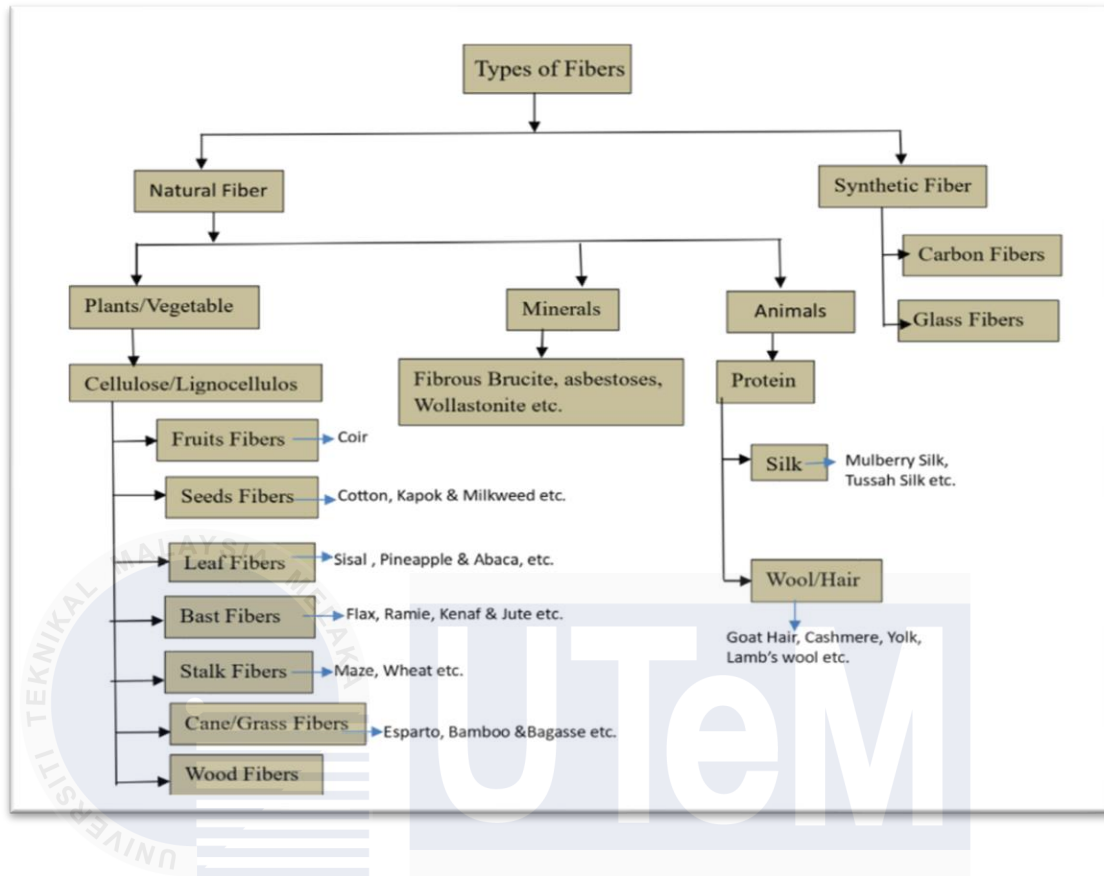


Figure 2.20: Fiber Classification (Dimple et al., 2023)

2.5.1 Wood Fiber

Wood, a renewable, ecologically benign, and biodegradable biomass resource, is widely employed in modern culture (Y. Zuo et al., 2023). Rather than developing adhesive formulations, the properties of wood composites might be improved by directly modifying various wood forms such as veneer, strands, chips, and fibres. Wood attributes like as mechanical, thermal, and physical capabilities, compatibility, dimensional stability, and surface energy have all been influenced by chemical alterations in reactive groups (Sarioğlu et al., 2023).

Creating a chemically active wood surface, rather than just an adhesive-wood interface, will increase the bonding efficacy and durability of wood-based composites.

Acetylation of hydroxyl groups on wood, for example, has been widely utilised to minimise hydrophilicity and water absorption while enhancing dimensional stability and resistance to biological metabolism in solid wood and wood fibers (Y. Zuo et al., 2023). A detailed analysis found that when the WPF size was 80 mesh and the fibre mass fraction was 5%, the best optical, thermal, and mechanical properties were obtained (Gao et al., 2023).

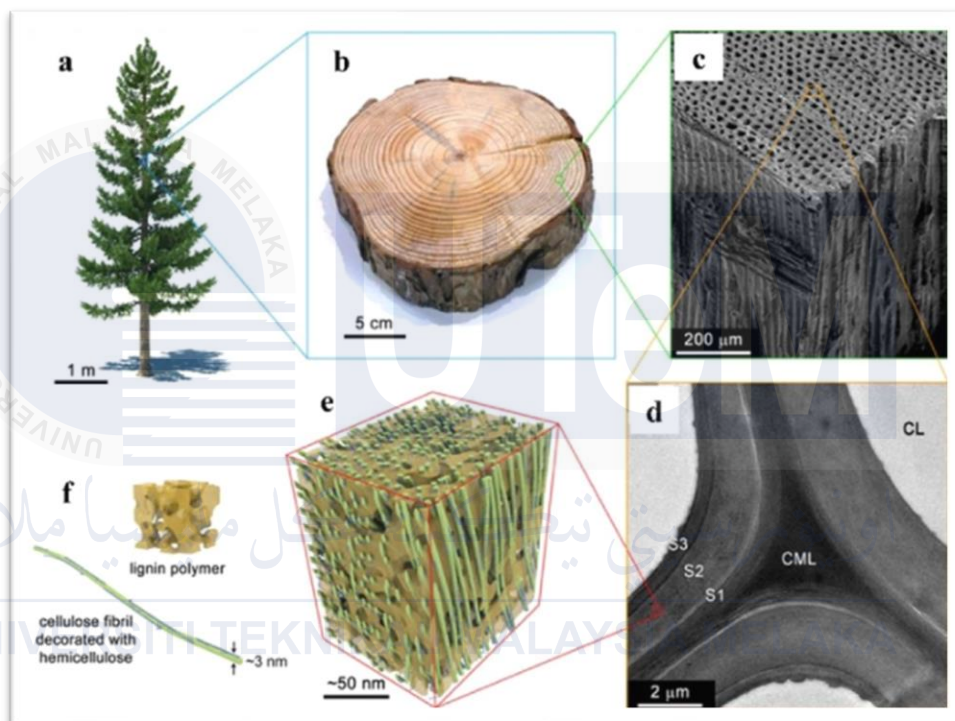


Figure 2.21: Multiscale structure of wood (Q. Zuo et al., 2023)

The figure above shows the Coniferous tree (a). (b) A pine tree in cross section. (c) SEM view shows channels running parallel to the development direction of the wood. (d) A transmission electron microscope (TEM) picture of the ultrastructure of the wood cell wall. CL stands for cell lumen; CML is for compound middle lamella; and S1, S2, and S3 stand for secondary cell wall layers. (e) Diagram of the lignocellulose nanoscale architecture. (f) Amorphous lignin polymer with cellulose fibril with hemicellulose schematic (Y. Zuo et al., 2023).

The sieve mesh sizes used ranged from 300 μm to 200 μm , and finally to 125 μm . The particle size analyser equipment was utilised in the dry measurement mode, and a random 150 g sample of wood dust was obtained to analyse the size content of the wood dust used. It is quite difficult to clean wood filler with a mix of dirt particles, grease, and microscopic metal pieces. The sieved particles are washed several times in distilled water to remove dust and other pollutants before drying for 24 hours in a hot air oven at 60 $^{\circ}\text{C}$ on a portion of an untreated wood fiber sample (Nafis et al., 2023).

From (Nafis et al., 2023) also stated that the particle size analysis is recorded by the Malvern Mastersizer 3000 Aero S dry powder disperser. The sample is dispersed by accelerating the dry powder particles via a venturi with compressed air and utilising a mesh size of 125m with high volume distribution rather than a different mesh size, saying that there is no more than 1% volume distribution with a mesh size of 125-200 m. The total quantity investigated from a 200 g sieve of wood dust with a mesh size of 100-125 m resulted in 90% detection during the examination. The remainder of the study at mesh size 75-100 m is 50% detectable, 50-75 m is 10% detectable, 25-50 m is 5% detectable, and less than 25 m is just 3% detectable.

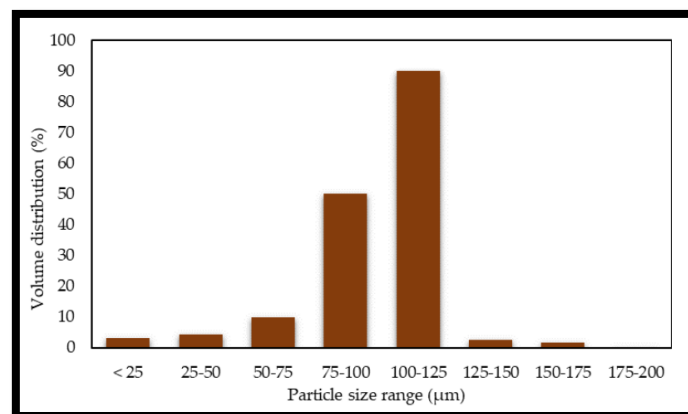


Figure 2.22: Diagram of Wood Dust Particle Size (Nafis et al., 2023)

2.6 Chemical Treatment for Wood Fiber

2.6.1 Sodium Hydroxide (NaOH) Treatment

There are several methods of treatment that (Serra-Parareda et al., 2020) have employed in supplying fiber prior to conducting trials or testing. Several stages, such as wood fiber treatment, should be considered. Silane coupling agents have been widely employed as efficient coupling agents in a wide range of industrial sectors to increase fiber-matrix adhesion strength due to their simplicity of application, durability, and diversity, as well as their inexpensive cost.

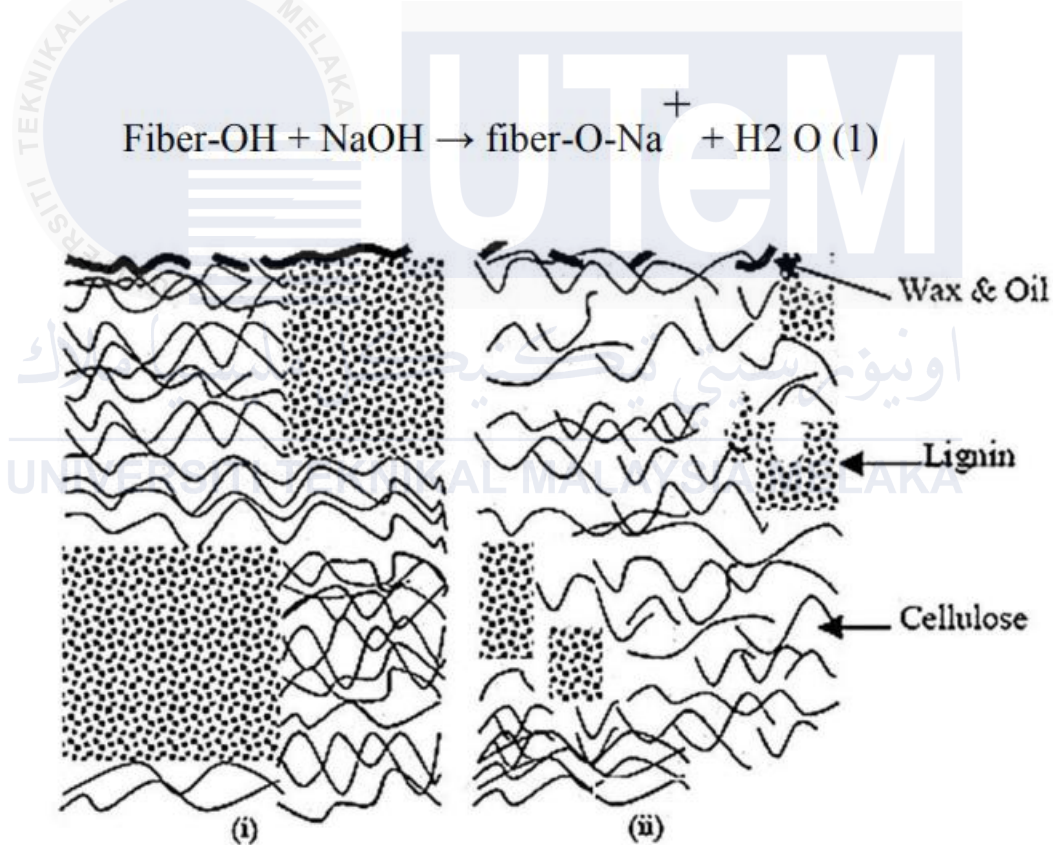


Figure 2.23: Typical structure of (i) untreated and (ii) NaOH treated natural fiber (Behera et al., 2018)

Poor matrix-fiber adhesion is a common problem in natural fiber-reinforced composites. To overcome this issue, researchers suggested specific physical and chemical procedures for fiber surface modification. Alkali treatment, a rapid and easy surface modification procedure, is often used in natural fiber composites. The alkali treatment is shown to successfully increase the tensile and flexural properties, however it reduces the impact strength. Water's capacity to absorb compounds decreases after alkali treatment. However, the concentration of the NaOH solution and the length of time the fiber is immersed in it dictate how mechanical characteristics fluctuate (Loganathan et al., 2020).

From (Karthikeyan et al., 2014), at room temperature (27–29°C), the coir fibers were exposed to various concentrations of 2%, 4%, 6%, 8%, and 10% NaOH solution. The findings showed that rising alkali density is associated with a decreasing trend in fiber tensile strength. Each group's tensile strength was found to vary significantly from the others. Lignin and pectin leach out more readily at higher alkali concentrations, which is bad for the strength of the fiber. Table 2.7 below shows the tensile strength of fibers treated with NaOH. Tensile strength does not change much between 4% and 6% NaOH concentrations. For budgetary considerations, a NaOH content of 4% may be advised to generate a stronger composite.

Table 2.7: Coir fiber tensile strength with NaOH treatment (Karthikeyan et al., 2014)

Fiber	Tensile strength (MPa)	Elongation (%)
Original fiber	617.6	18.8
2% NaOH	582.6	28.0
4% NaOH	568.7	27.1
6% NaOH	553.3	23.1
8% NaOH	544	23.9
10% NaOH	527.7	22.9

Table 2.8: Effect of fiber length on tensile strength of NaOH-treated coir fiber-reinforced epoxy composites (Karthikeyan et al., 2014)

Fiber length (mm)	NaOH concentration				
	2%	4%	6%	8%	10%
	Tensile strength (MPa)				
10	8.567	12.845	12.807	9.908	8.455
20	9.242	13.380	13.327	10.098	8.659
30	13.171	13.782	13.702	10.498	8.941
	Elongation (%)				
10	0.882	0.3	1.01	0.743	0.72
20	0.9	0.5	1.067	0.766	0.733
30	0.92	0.525	1.0	0.797	0.755

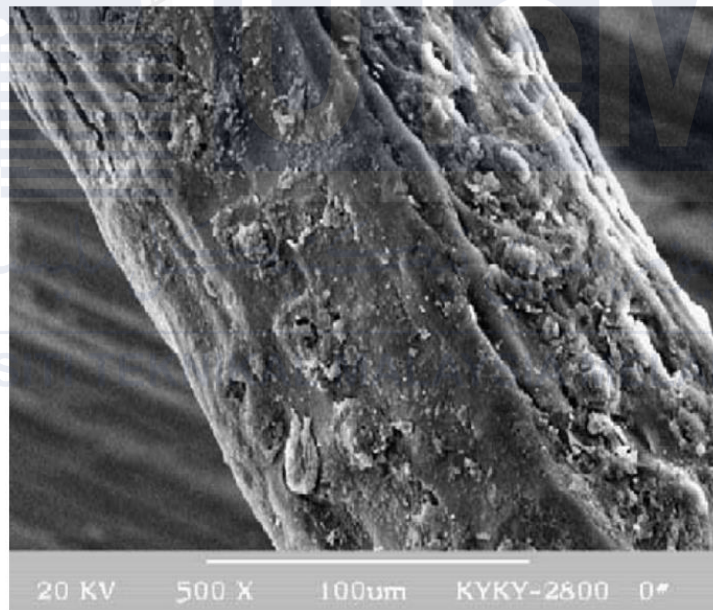


Figure 2.24: Surface appearance of the coir fiber before alkali treatment (Karthikeyan et al., 2014)

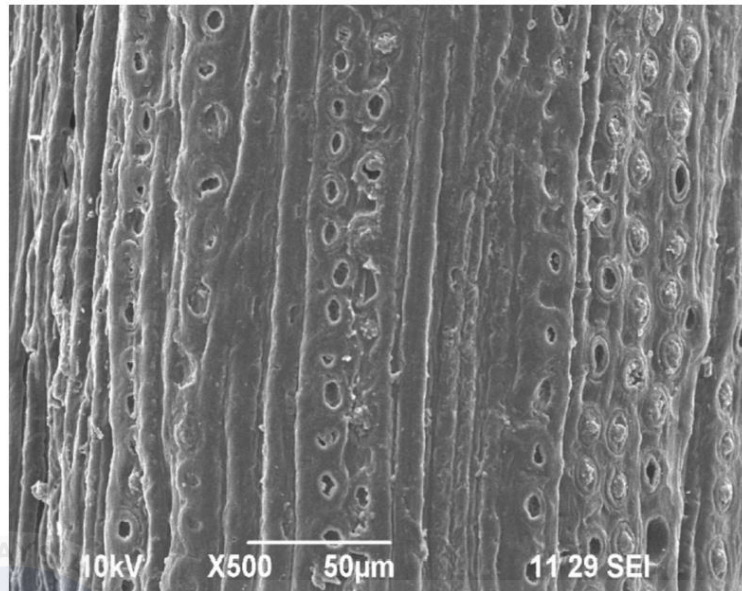


Figure 2.25: Surface appearance of the coir fiber after 2% NaOH treatment (Karthikeyan et al., 2014)

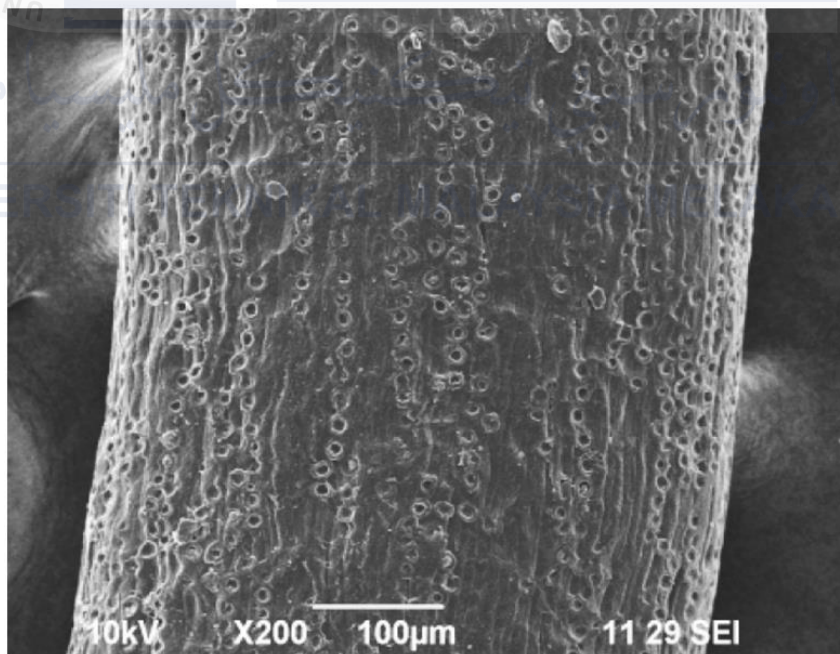
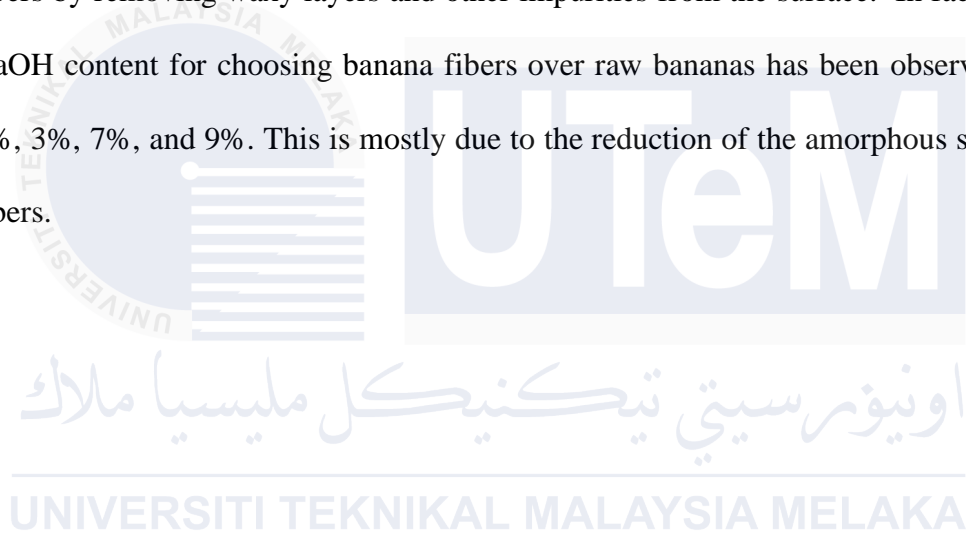


Figure 2.26: Surface appearance of the coir fiber after 4% NaOH treatment (Karthikeyan et al., 2014)

On the other hand, (Parre et al., 2020) have separate immersions in 1, 3, 5, 7, and 9% NaOH (relative to banana fiber weight%) were made with the dried banana leaf fibers for a 24-hour period at room temperature. The untreated banana fibers illustrated in Fig. 2.26(a) have a characteristic form due to the presence of chemical elements such as lignin, cellulose, hemicelluloses, and wax, which give the bio-composite its mechanical and thermal robustness. The additional layers of banana fibers may be due to a change on the outer (Fig. 2.26(b-f)). It clearly demonstrates that NaOH treatment boosts the heat resistance of banana fibers by removing waxy layers and other impurities from the surface. In fact, the optimal NaOH content for choosing banana fibers over raw bananas has been observed to be 5%, 1%, 3%, 7%, and 9%. This is mostly due to the reduction of the amorphous sections of the fibers.



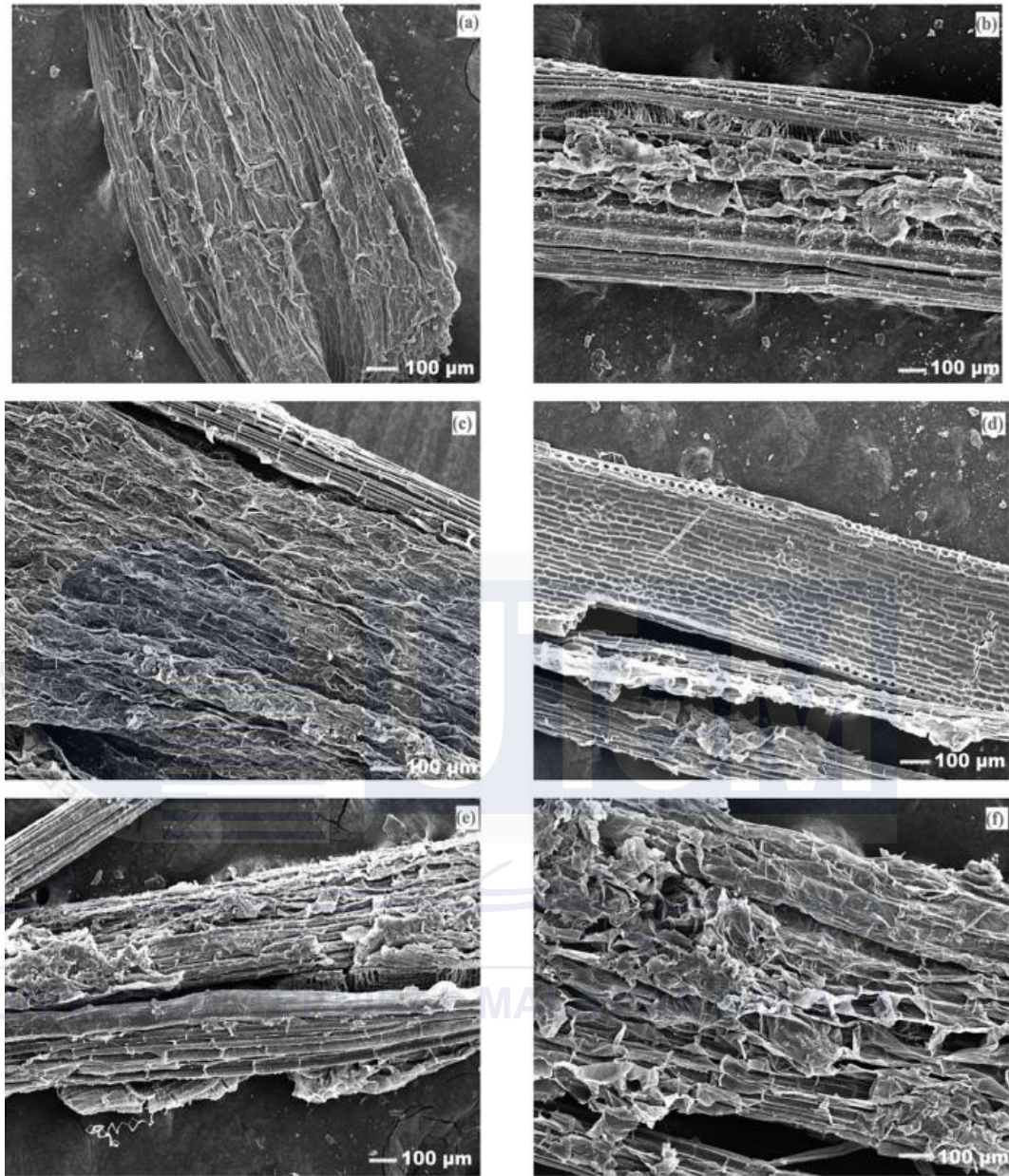


Figure 2.27: SEM Image of Untreated and 1, 3, 5, 7 & 9% NaOH treated banana (Parre et al., 2020)

The Hemp core fibers were used as reinforcement in the composite materials, and polypropylene was used as the polymer matrix. Then, for the chemical treatment, sodium hydroxide (NaOH) and anthraquinone (AQ) were used. To determine how the strength of the treatment impacted the fibers' capacity to stiffen, three distinct digestions comprising 5, 7.5, and 10 weight percent of NaOH, respectively, were created (Serra-Parareda et al., 2020).

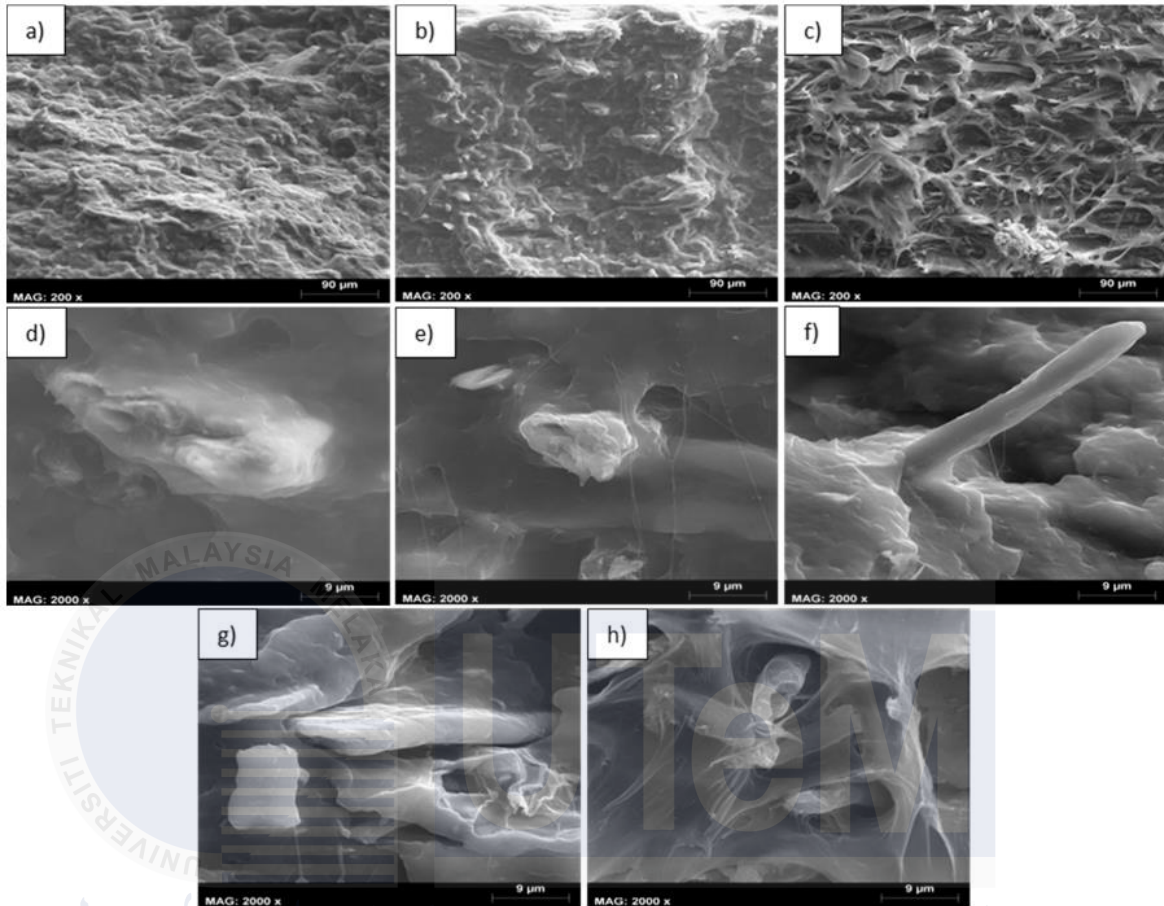


Figure 2.28: Scanning electron microscopy images of the cross-sectional area of the flexural specimens (Serra-Parareda et al., 2020)

From figure 2.26 above, (a) PP+20% hemp—5% NaOH (200×), (b) PP+20% hemp—7.5% NaOH (200×), (c) PP+20% hemp—10% NaOH (200×), (d) PP+20% hemp—5% NaOH (2000×), (e) PP+20% hemp—7.5% NaOH (2000×), (f) PP+20% hemp—10% NaOH (2000×), (g) PP+50% hemp—5% NaOH (2000×) and (h) PP+50% hemp—10% NaOH (2000×) (Serra-Parareda et al., 2020).

(Serra-Parareda et al., 2020) state that the cross-sectional area of the flexural specimens grew more erratic (Figure 2.26c) and more voids could be seen as the NaOH treatment intensity was raised. In specimens charged with fibers and treated at lower NaOH

concentrations, the structure was smoother and better preserved (Figure 2.26a, b). At greater magnifications, it is possible to see that the fibers treated with 5% NaOH (Figure 2.26d) bind more to the matrix (2000). Furthermore, as seen in Figures 2.26e, f, the dispersion and adhesion to the matrix significantly reduced under more intensive NaOH treatments. Variations in fiber loading (20 and 50 wt%) and fibers treated at the same NaOH concentration of 5% were seen in the composite (Figure 2.26d, g). Higher NaOH concentrations (10% NaOH) and fiber compositions of 20 and 50% wt exhibited comparable behaviour (Figure 2.26f, h). Figure 2.26g, h compares composites with high fiber levels (50 wt%) and NaOH concentrations ranging from 5 to 10%. It demonstrates that fibers treated with greater NaOH had reduced matrix adherence and dispersion.

From (Behera et al., 2018), it demonstrates that Alkali-treated Bamboo fiber reinforced epoxy composites outperformed untreated fiber reinforced composites in terms of mechanical properties. With increasing alkali content, bamboo fiber reinforced composites demonstrated increased tensile strength and tensile modulus. The composite containing 4% NaOH improved the greatest.

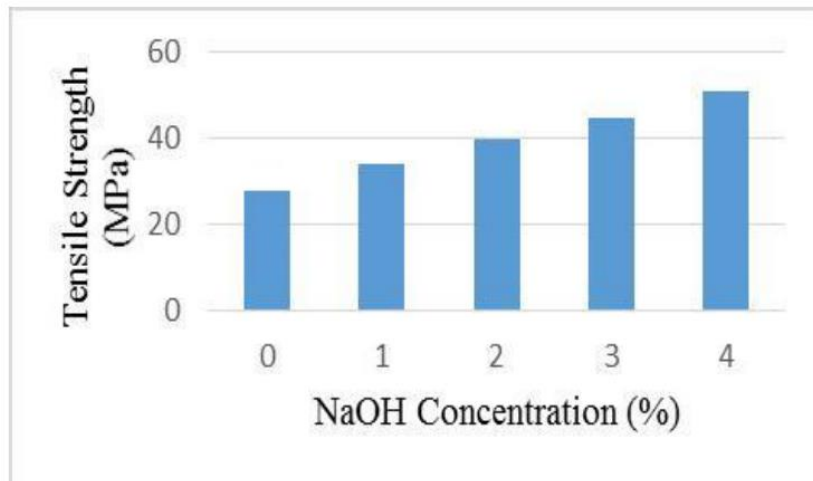


Figure 2.29: Tensile strength of untreated and alkali treated Bamboo fiber reinforced epoxy composites (Behera et al., 2018)

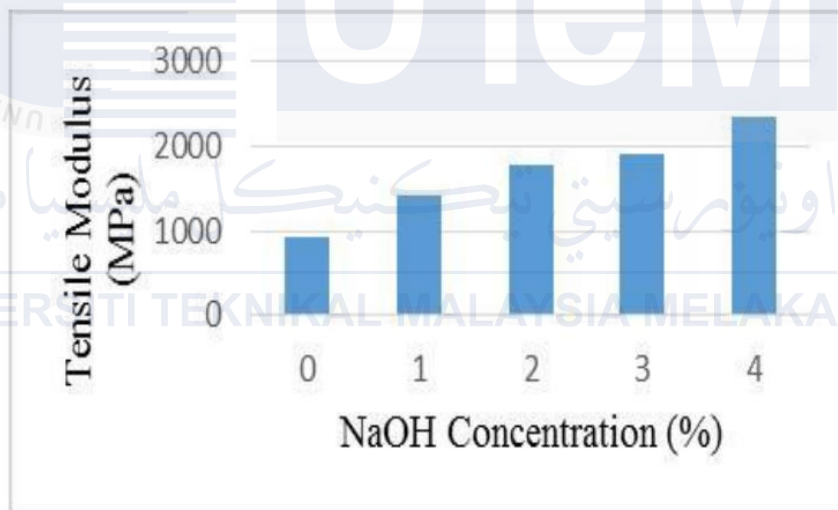


Figure 2.30: Tensile modulus of untreated and alkali treated Bamboo fiber reinforced epoxy composites (Behera et al., 2018)

2.7 Coupling Agent: Maleic anhydride polypropylene (MAPP)

The most widely used technique for increasing interfacial adhesion has been the use of MAPP, which is a very effective compatibilizer for bio-filler and matrix at the interface. The addition of a coupling agent had the largest effect on strength and modulus. This is owing to the thermodynamic segregation of the MAPP towards the interface, which leads in the formation of covalent bonding to the fiber surface's -OH groups (Ramli et al., 2012). MAPP-containing composites are also more thermally stable.

MAPP has low surface energy and is intended to improve wood-polymer compatibility by forming stronger connections at interfaces and lowering WPC surface tension (Mohebbi & Kazemi, 2011). The mechanism....The presence of 3 wt% MAPP with PP appeared to have consistently impregnated the reinforcing fibers, which should have boosted the reinforcing fibers-matrix compatibility (Mohebbi & Kazemi, 2011). The thermal stability of treated wood fiber-based composites with a matrix of 3% MAPP and polypropylene is shown to be greater than that of the polypropylene matrix alone.

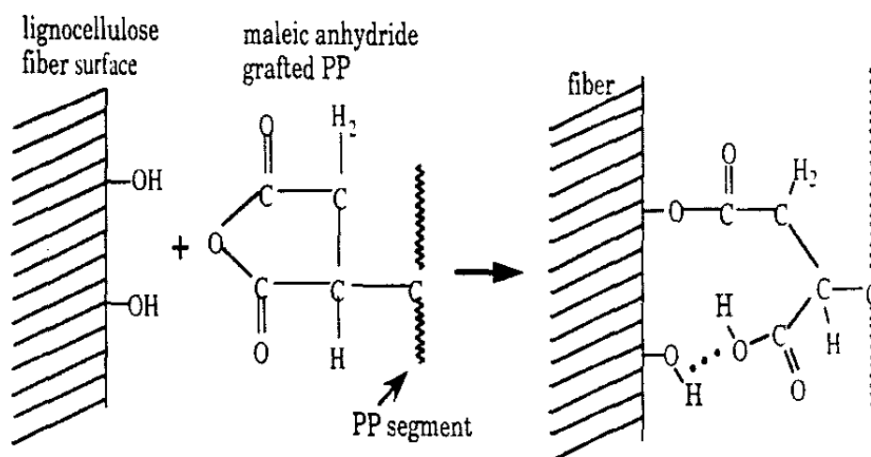


Figure 2.31: MAPP reaction mechanism with a lignocellulosic surface hydroxyl group (Rowell, 2006)

2.8 Composites 3D Printing

2.8.1 Recycling of Polypropylene (PP)

Polypropylene is a thermoplastic that is commonly used in plastic mouldings, stationery folders, packaging materials, plastic tubs, non-absorbable sutures, and diapers. It may be harmed by UV radiation from the sun and oxidised at high temperatures. The capacity of microbes to breakdown PP has also been studied. Because of the abundance of ingredients, low cost, ease of manufacturing, and huge diversity, plastic items have been widely used in many nations in recent decades. Plastics production in the globe has reached 300 million tonnes per year, with global growth in plastic items predicted to reach 400 million tonnes by 2020. (Lin et al., 2020).

The massive number of plastic derivatives and their disposal have become a worldwide and critical concern, causing issues for the ocean and the ecology (Rocha & Rosa, 2019). They are classified into thermoset plastic and thermoplastic based on their intrinsic properties, with the latter exhibiting reversibility and hence being appropriate for reclamation. Despite its remarkable reversibility, thermoplastic may exhibit degraded performance and lose its initial benefits due to poor processing conditions or errors (Lin et al., 2020).

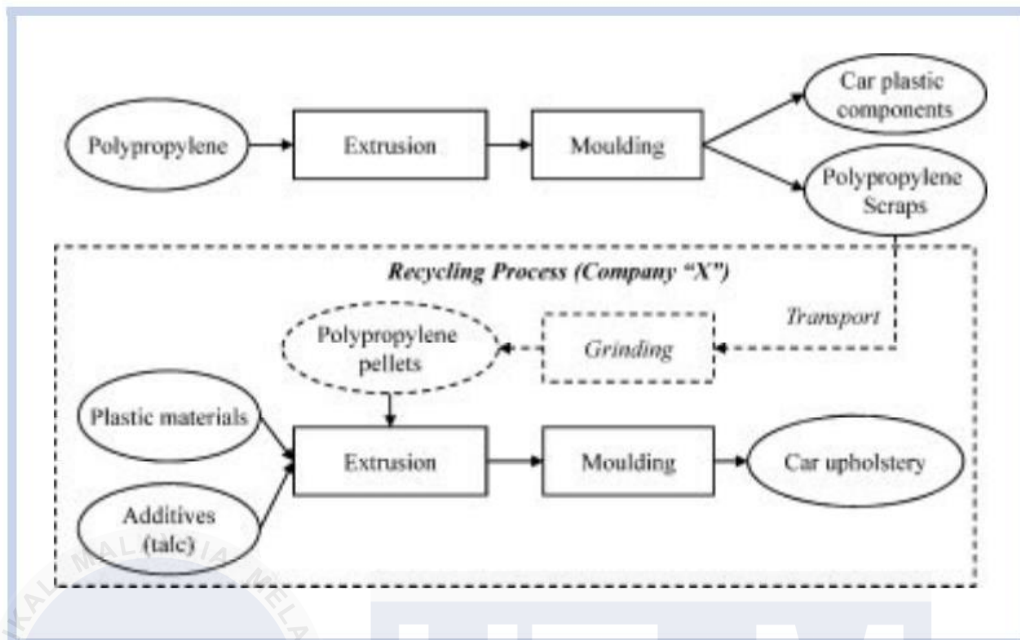


Figure 2.32: Recycling process of polypropylene scraps(Ardente et al., 2007)

Instead of separate thermoplastic polyurethane and polypropylene ingredients, recycled thermoplastic T/P waste compounds were utilised. Because thermoplastic polyurethane (T) and polypropylene (PP) have distinct inherent qualities, PP is widely utilised to improve the mechanical and thermal properties of T. The distinguishing property of thermoplastic materials is their ability to be reshaped at the appropriate temperature. Because of their diverse inherent qualities, thermoplastic waste compounds are difficult to recycle (Kristiawan et al., 2022). This research focuses on how to repurpose polymer waste components and investigates the reshaped materials in terms of morphological observation, thermal characteristics, and tensile capabilities. Furthermore, the impact of the presence of a compatibilizer on the different characteristics of T/P and T/P/MA waste blends will be explored following numerous melting-recycling cycles (Lin et al., 2020).

According to the comparison of the photos of T90 and T70, blends with a higher T content appear in dark yellow, whereas blends with a higher P content appear in lighter

yellow in Figure 2.32. Figure 2.32B shows that P100 and T100 waste-blended samples do not show distinct defects in the post-3rd-recycling process and still maintain good formability. It is a good piece of evidence that the thermoplastic materials can be well reformed within an appropriate treatment. At the same time, the MA-containing blends also have stable formability and can be hot-pressed efficiently. With a greater number of melting–recycling cycles, MA provides T/P matrices with significant compatibility and stability (Lin et al., 2020).

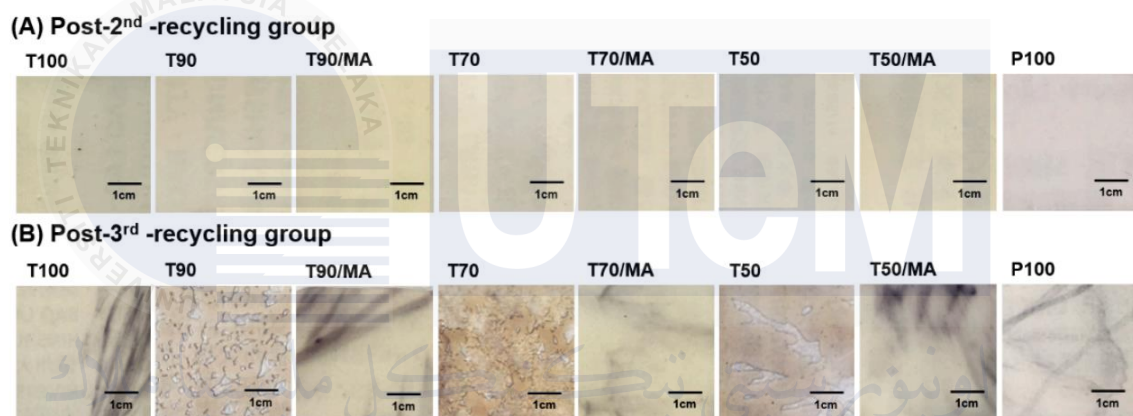


Figure 2.33: Surface observation of T/P and T/P/MA blends as related to post-2nd and post-3rd recycling. (A) Post-2nd-recycling group; (B) post-3rd-recycling group (Lin et al., 2020)

Then, figure 2.32 depicts SEM pictures of the tensile specimens' side portions in order to find any flaws in the specimen laying and to study the layering interfusion of the specimens in each round of recycling. Figure 2.33 shows SEM images of cracked surfaces of tensile specimens, one for each round of recycling, to explore fracture mechanisms and expose any probable association with mechanical property results (Vidakis et al., 2021).

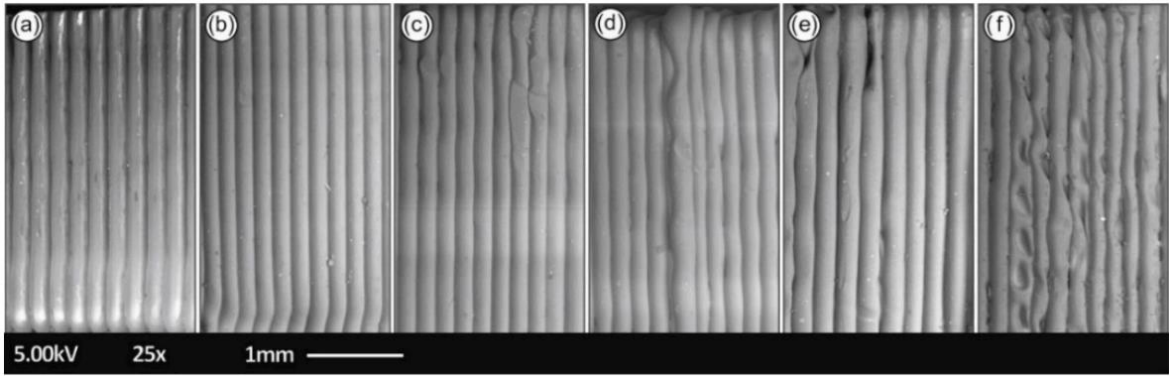


Figure 2.34: SEM images of the tensile specimens' side area in the (a) first, (b) second, (c) third, (d) fourth, (e) fifth, and (f) sixth rounds of recycling (Vidakis et al., 2021).

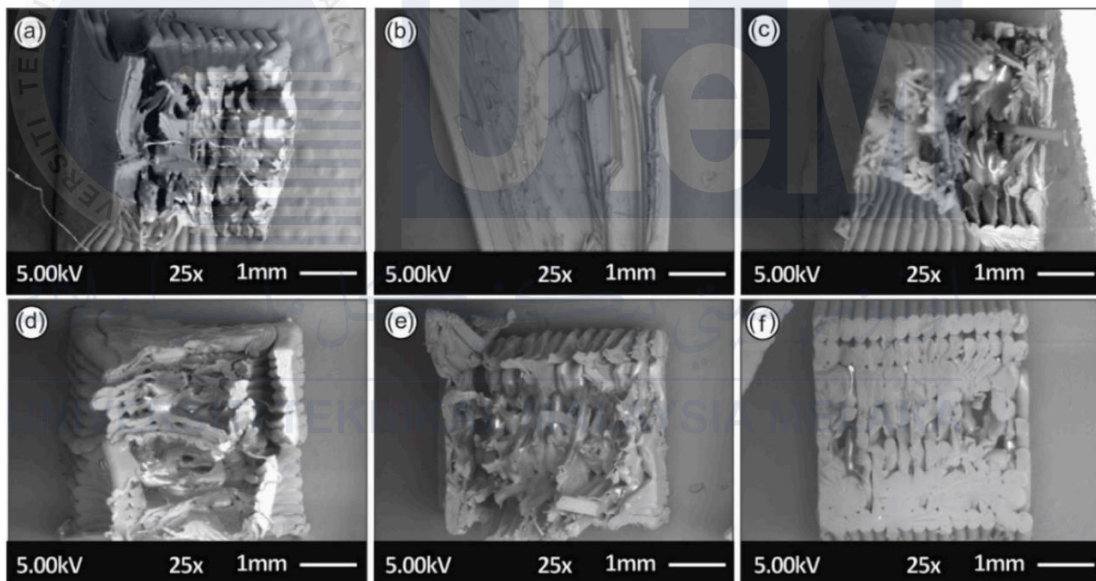









Figure 2.35: SEM images of the tensile specimens' fractured surfaces of the (a) first, (b) second, (c) third, (d) fourth, (e) fifth, and (f) sixth rounds of recycling (Vidakis et al., 2021)

Plastics are generally inexpensive, long-lasting, and simple to make. The following table (Figure 2.34) describes some of the most regularly used polymers and their uses.

Plastic Recycling Symbol	Plastic Name	Where to Find This Plastic in Your Home	This Plastic is Valued For
 PETE	Polyethylene Terephthalate	water and soda bottles	clarity strength impermeability to gas and moisture
 HDPE	High Density Polyethylene	milk jugs, grocery bags and toiletry bottles	stiffness strength resistance to moisture permeability to gas
 v	Polyvinyl Chloride	water pipes, blister packaging for non-food items	strength ease of blending with other materials versatility
 LDPE	Low-density Polyethylene	food bags, squeezable bottles, cling films, disposable cups	flexibility ease of processing ease of sealing barrier to moisture
 PP	Polypropylene	microwaveable containers, yogurt cups, disposable plates / cups	strength resistance to heat, chemicals, oils and moisture
 PS	Polystyrene	disposable plates, cups, cutlery, containers and packing peanuts	clarity versatility molding ease
 OTHER	Other (often Polycarbonate or ABS)	beverage bottles, CD's, lenses for glasses, riot shields	properties dependent upon the mixture of polymers may contain BPA

www.leftbraincraftbrain.com

Figure 2.36: Commonly used plastics and their applications

2.8.2 Composite filled with MAPP

Coupling agents are used to enhance the interactions between polymers and wood fibers, and hence the bonding between them, by modifying their surfaces. Surfactants, bonding agents, dispersion agents, and compatibilizers are some of the various types of

coupling agents. Pre-processing treatments are used to WPC components to improve the interface characteristics of WF and polymer and to counteract the hydrophilic tendency of WFs. There are three types of treatment methods: chemical, mechanical, and thermal. Chemical treatment is widely utilised, although it has major environmental consequences. As a result, mechanical and thermal treatment procedures have been offered as less harmful alternatives to chemical treatment (Elsheikh et al., 2022).

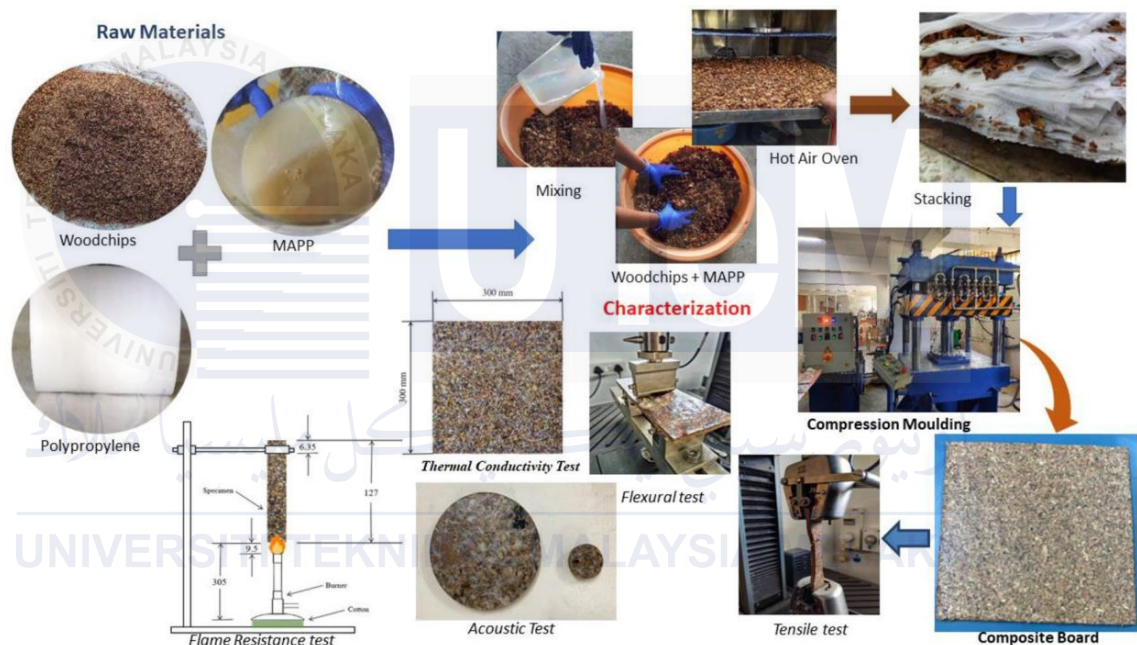


Figure 2.37: Recycled Woodchip Reinforced Polypropylene Composites with MAPP Compatibility (Sanadi & Stelte, 2023a)

From (Sabri et al., 2013), MAPP has been used as a compatibilizer to improve the mechanical properties of polypropylene/coconut fiber (PP/CF) composites while decreasing their hydrophilicity. The tensile strength of PP/CF composites with and without MAPP under various fiber loading circumstances is shown in Figure 2.36. Tensile strength may be increased by increasing fiber loading. The interfacial area between the fiber and the matrix grew weak as the fiber loading increased.

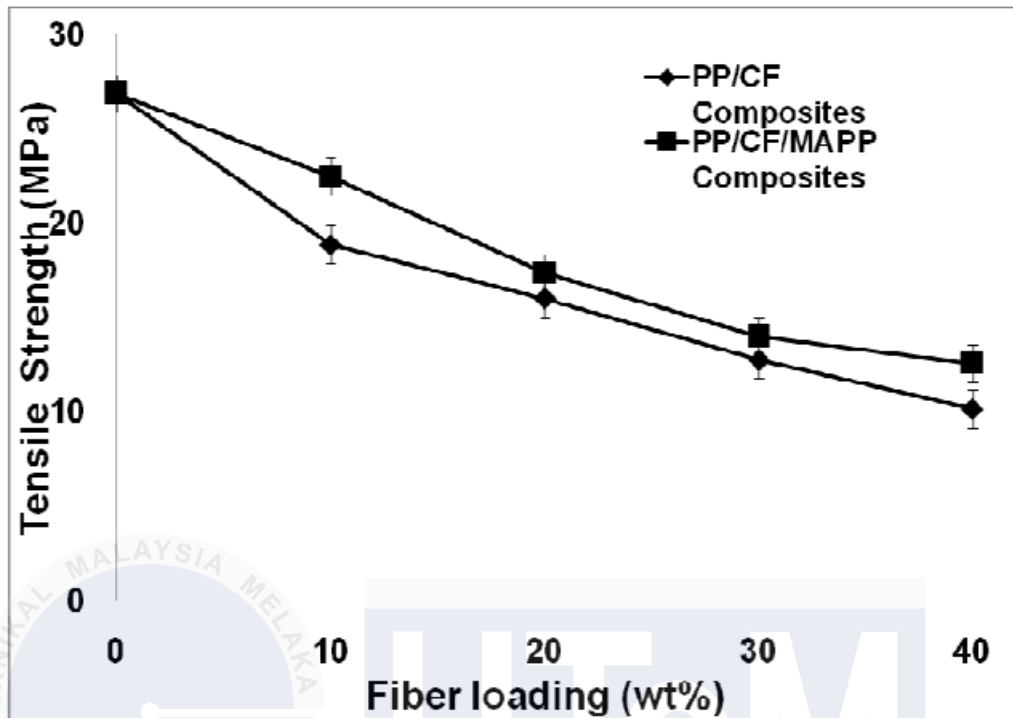


Figure 2.38: Effect of fiber loading to tensile strength of PP/CF composite with and without MAPP (Sabri et al., 2013)

2.8.2.1 Fabrication of Composite

The incredible physical and mechanical qualities of composite materials have raised their demand in recent years. The fabrication process is a critical aspect in the creation of a new product. The greatest issue in composite material is to maintain the low cost and high production rate process due to the mixed usage of metal, ceramic, and polymer (Ravinder Kumar, 2019). According to the literature research, there are numerous procedures for fabricating the composite.

From (Liu et al., 2022), the WFs were dried at 120 °C using an impulse-cyclone drying treatment apparatus until the moisture content was less than 3%. A high-speed mixer was then used to blend the PP, WF, and MAPP at varied mass fraction ratios. The mixtures were pelletized and pulverised into minute granules using a co-rotating twin-screw extruder.

Another single-screw extruder was used to extrude the granules into 4 mm thick and 100 mm wide WF/PP composite boards.

Following that, according to another study by (Izzati Zulkifli et al., 2015a) shows that to reduce moisture content, all raw materials (rPP, MCC fiber, and MAPP) were dried in an oven at 80°C for 24 hours. After then, the rPP, MCC fiber, and MAPP were mixed in the quantities stated in Table 2.9. The mixtures were created using a twin-screw extruder with barrel temperatures ranging from 160 to 175 degrees Celsius and die temperatures of 180 degrees Celsius. The screw speed was set at 100 revolutions per minute. Before being injection moulded using a Battenfield HM 600/850 injection moulding machine, the extruded composites were crushed to produce small pellets. Temperatures were held between 180 and 190 degrees Celsius. In contrast, the nozzle temperature was held constant at 200oC. According to ASTM D638 and D790, the final samples were created in dumbbell type IV and rectangular shapes.

Table 2.9: Composition of Rpp/mcc Composites (Izzati Zulkifli et al., 2015b)

Sample	rPP (wt%)	MCC (wt%)	MAPP (wt%)
rPP/2MCC	98	2	–
rPP/5MCC	95	5	–
rPP/10MCC	90	10	–
rPP/20MCC	80	20	–
rPP/40MCC	60	40	–
rPP/50MCC	40	60	–
rPP/2MCC/3MAPP	95	2	3
rPP/5MCC/3MAPP	92	5	3
rPP/10MCC/3MAPP	87	10	3
rPP-20MCC-3MAPP	77	20	3
rPP/40MCC/3MAPP	57	40	3
rPP/50MCC/3MAPP	37	60	3

Aside from that, the sawdust was treated with a rotary mill prior to sample processing. After sieving to pass mesh +60/-40, it was oven dried for 24 hours at 1032 °C. To reduce PP melting, the oven dried wood flour, polypropylene (PP), MAPP, and glass fibers were dry mixed at room temperature for 20 minutes in a typical laboratory mixer (1,500 rpm). They were then extruded with a twin-screw extruder, yielding sample bars with a cross section of 1 cm (thickness) and 7 cm (width). The screw rotation rate was set at 90 rpm, and the barrel zones (1-6) were set to 173, 175, 180, 183, 185, and 187°C, with two die zones set to 144 and 109°C (Mohebbi & Kazemi, 2011).

A HAAKE twin-screw extruder (model 557-5052) was used to combine the wood fiber and polymer matrix (Črešnar et al., 2021). The screws had a diameter of 25 mm and a length-to-diameter ratio of 36. WF/PP compounding temperatures were set at 150 and 180°C, respectively. The screw speed was set at 80 revolutions per minute (Yuan et al., 2008a). Prior to compounding, the wood fiber was dried in an oven at 110°C for 12 hours. Two different hoppers feed the wood fiber and polymer into the extruder. For wood fiber, a vibrating hopper was employed to smooth the feeding process. After cooling in a water bath, the extruded composites were chopped with a blender. The mechanical property test sample was created using an injection-molding machine (Battenfeld type 800/315 CDC) after the compounded composites were dried at 70°C for 12 hours.

Table 2.10: Fabricating Materials and Applications in 3D Printing (Pavan Kalyan & Kumar, 2022)

S. no.	Fabricating materials	Subclass	Examples	Applications
1.	Polymers	Thermoplastics	Polycaprolactone (PCA) Poly(lactic-co-glycolic acid) (PLGA) Polylactic acid (PLA) p-hydroxybenzoic acid (PHBA)	Tissue engineering (Trachea, stem cell model) Drug modelling for cancer therapy
2.	Hydrogels	Thermosets Biopolymers	Urethane Resin Chitosan Fibrin Collagen Agar Gelatin Alginate	Tissue engineering (bone, cartilage) Drug delivery (nanomedicine)
3.	Composites	Matrix Fillers	Carbon fiber Silicon carbide Hydroxyapatite Calcium phosphates Ceramics precursors Metal precursors	Prostheses, implants

2.8.2.2 Ratio of Composites

Various researches had been done and a lot of experiment with different type of ratio are used by the authors. The table below shows the ratio of the composite implemented by different journalists.

The ratio of MAPP, PP and Fibers are shows in the Table 2.11. The synthesis of maleated polypropylene (MAPP) through reactive extrusion with varying concentrations of peroxides and maleic anhydride, as well as the characterisation of the obtained MAPP. The author also used data from the fabrication of PP/saw dust composites with and without MAPP coating, as well as the assessment of these composites for mechanical characteristics, water absorption, Izod impact strength, and flexural modulus (Trombetta et al., 2010).

Table 2.11: Designation of composites in relation of the type and quantity of PPMA used

(Trombetta et al., 2010)

Composites	Type/quantity of MAPP	PP(% p/p)	MAPP(% p/p)	Fibers (% p/p)
FOC1	Non-treatment	80	---	20
F2R2E5C1	2.7% MAPP	77.3	2.7	20
F1E1C1	2.7% Comercial MAPP	77.3	2.7	20
F2R2E8C1	5% MAPP	75	5	20
F1E3C3	5% Comercial MAPP	75	5	20
F2R2E7C1	10% MAPP	70	10	20
F1E2C2	10% Comercial MAPP	70	10	20

Then, the author (Saad, 2018) conducted a study on kenaf core fibre - polypropylene (PP) composites using treated and untreated maleated polypropylene (MAPP). The ratio is shown in Table 2.12 below. The results show that maleated polypropylene has gained a lot of interest as a coupling agent because of its efficiency in increasing the mechanical characteristics of wood fiber-polypropylene composites.

Table 2.12: Sample formulations of kenaf and PP compositions (Saad, 2018)

Compositions (%)			
Sample code	PP	Kenaf	Epolene 43 ^a
K10	90	10	-
K10/1	90	10	1
K10/3	90	10	3
K10/5	90	10	5
K30	70	30	-
K30/1	70	30	1
K30/3	70	30	3
K30/5	70	30	5
K50	50	50	-
K50/1	50	50	1
K50/3	50	50	3
K50/5	50	50	5

Besides, (Yağci et al., 2021) shows the composition of PP/GS/MAPP in the research. It shows that the majority of the microspheres were found immersed in the PP matrix, with a significant interface adhesion. This finding supports MAPP's ability to increase the interfacial compatibility of PP/HGS composites. The inclusion of MAPP had no effect on the crystal structure, according to XRD measurements.

Table 2.13: Composition of the PP/GS/MAPP polymer composites formulations (Yağci et al., 2021)

Groups	Polypropylene (wt%)	Glass spheres (wt%)	Maleic Anhydride-g-PP
1	80	20	–
2	79	20	1
3	75	20	5
4	70	20	10
5	65	20	15

From (Sanadi & Stelte, 2023a), it shows that the ratio of 85wt% of kenaf fiber, 10wt% of PP and 5wt% of MAPP to demonstrate that using MAPP as a coupling agent improves the mechanical characteristics of kenaf-polypropylene composites considerably.

Table 2.14: Mechanical properties of the kenaf polypropylene composites using four different MAPP coupling agent types (85 wt% kenaf, 10 wt% PP, 5 wt% MAPP pressed at 345 kPa) (Sanadi & Stelte, 2023b)

MAPP Type	Melt Flow of MAPP 230 °C (10g/min)	Melt Flow of MAPP 190 °C (10g/min)	Anhydride (%)	MOR (MPa)	MOE (GPa)	Deflection at max load (mm)
PB3002	7	---	0.2	17.48 ± 4.95	2.60 ± 0.58	3.04 ± 0.28
PB3150	50	---	0.5	22.43 ± 3.56	2.89 ± 0.34	3.42 ± 0.30
PB3200	250	110	1.0	19.64 ± 5.91	2.39 ± 0.75	3.71 ± 0.25
PB3000	1000	400	1.2	24.38 ± 2.38	3.50 ± 0.28	3.11 ± 0.36

2.9 Filament

The usage of filaments for 3D printing is known as fused filament or filament freedom fabrication (FFF), which is a trademark of fused deposition modelling (FDM) (Das et al., 2021). A control model, which incorporates numerous factors, such as structural, processing, and extruder-related characteristics, supports the functioning concept of the whole system in the FDM printing process. Previous research has found that process factors have a major impact on quality. In addition, the printing orientation, layer thickness, feed rate, infill density and pattern, printing speed, and extrusion temperature of FDM-printed items are also variables to consider. Several investigations from (Yang & Yeh, 2020) have demonstrated that the printing orientation significantly modifies the structures of printed items, resulting in variances in mechanical properties. Furthermore, the printing orientation influences features of printed items such as dimensional accuracy, surface roughness, printing time and cost. (Almeshari et al., 2023b), shows the Figure of the filament process of PP and SCF.

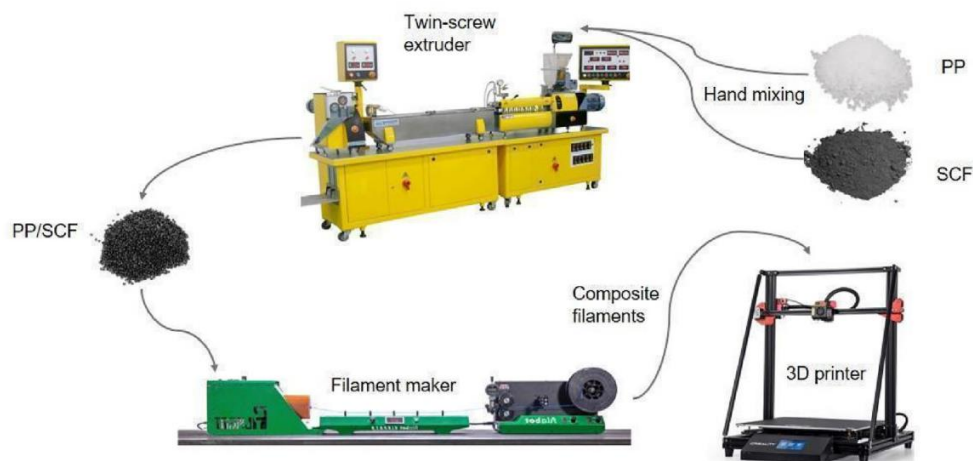


Figure 2.39: Filament manufacturing begins with the separate components (PP and SCF)

(Almeshari et al., 2023b)

A filament's diameter should be uniform throughout the spool in an ideal world. The diameter of a spool of filament is typically 1.75 or 3 mm. The bigger of the two is 1.75mm in diameter, which allows for greater extrusion and plastic flow (Yang & Yeh, 2020). A test has been conducted by (Aguirre-Cortés et al., 2023) to test the specimens using 3D printer (Zortrax, Poland) with a 0.4 mm nozzle, 0.19 mm printing layer thickness, a heated bed, 30 mm. s-1 printing speed, and printing temperatures of 275°C (for ABS) and 230°C (for PLA). Given that all filaments (with varying wood/polymer ratios) were produced under the same conditions (extruder speed and temperature), the diameter deviation was caused by the increasing viscosity of wood-PLA mixtures with higher wood content and thus higher extrusion forces required, which changes similar to Wood Plastic Composites (WPC) production with wood polymer composite formulation, such as wood/polymer ratio, wood particles aspect ratio, and additives.

Table 2.15: Properties of different filaments, moisture content after conditioning, and MOE for 3D-printed specimens after conditioning in various climates (Aguirre-Cortés et al., 2023)

	Filament diameter (mm)	Dry climate (T 20°C, RH 33 %)		Standard climate (T 20°C, RH 65 %)		Humid climate (T 20°C, RH 87%)	
		Moisture content (%)	MOE (N·mm ⁻²) *	Moisture content (%)	MOE (N·mm ⁻²) *	Moisture content (%)	MOE (N·mm ⁻²) *
ABS	1.73	0.4	1313 (70)	0.4	1383 (51)	1.1	1343 (50)
PLA	1.72	0.3	1568 (146)	1.3	1563 (71)	0.8	1477 (38)
Wood PLA 0%	1.61	0.5	1393 (17)	0.6	1442 (39)	1.0	1483 (109)
Wood PLA 10%	1.45	0.9	844 (97)	1.4	768 (75)	2.3	791 (165)
Wood PLA 20%	1.44	0.7	809 (238)	1.4	846 (245)	3.1	542 (255)
Wood PLA 30%	1.47	1.6	771 (36)	2.3	735 (106)	4.0	681 (131)
Wood PLA 40%	1.48	0.8	790 (78)	2.2	798 (75)	3.6	623 (50)
Wood PLA 50%	1.51	1.3	350 (407)	3.0	475 (339)	5.2	469 (155)

The spool that carries SCF/PP filaments is tested by (Almeshari et al., 2023b) in SEM microstructural pictures (at various magnifications) of composites containing 8 and 22 wt% SCF are shown in Figure 2.39. The SCF and PP matrix appear to have good adhesion in the figure because the matrix completely covered the SCF. Because of the good adhesion between the SCF and the PP matrix, the composites demonstrated higher tensile strength, and the strength of the composite improved with increasing SCF concentration. The presence of holes on the composites' fractured surfaces suggests that the SCF were dragged out of the PP matrix rather than shattering, thus the failure of the composite is due to fiber pull out.

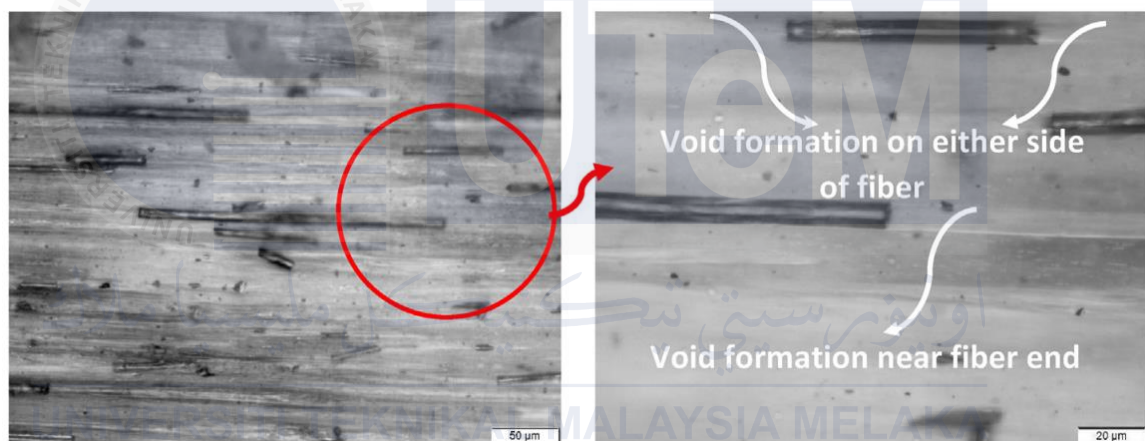


Figure 2.40: OM images of longitudinal section of tensile tested sample for 11%SCF/PP composite (Almeshari et al., 2023b)

From (Kristiawan et al., 2022), a test is performed in which the temperature is regulated to 175-185 °C during the extrusion process, with a screw rotation speed of 24 RPM and the plastic composite is extruded via a 1 mm nozzle. Following printing is done on a hot glass printing platform using a 1 mm thick polypropylene sheet. The filament is produced at temperatures ranging from 180 to 220 degrees Celsius in the nozzle and 80 degrees Celsius in the bed. The molten filament is pushed through a 1 mm nozzle at a rate of 20 mm per

minute with a layer thickness of 0.32 mm. Table 2.16 illustrates the printing settings for each type of filament.

Table 2.16: Printing Parameters for rPP, PP and PLA Filaments (Kristiawan et al., 2021)

Parameters	Values
Nozzle diameter	1.0 mm
Layer thickness	0.32 mm
Infill degree	100%
Printing speed	20 mm/s
Bed temperature	80 °C with an insulating layer (rPP and PP)
Nozzle temperature	210 °C (rPP)
	220 °C (rPP + Glass Powder)
	210 °C (PP)

2.10 Filament Processing

In this part, key filament processing and testing theory is discussed. Figure 2.39 shows the extruder line process.

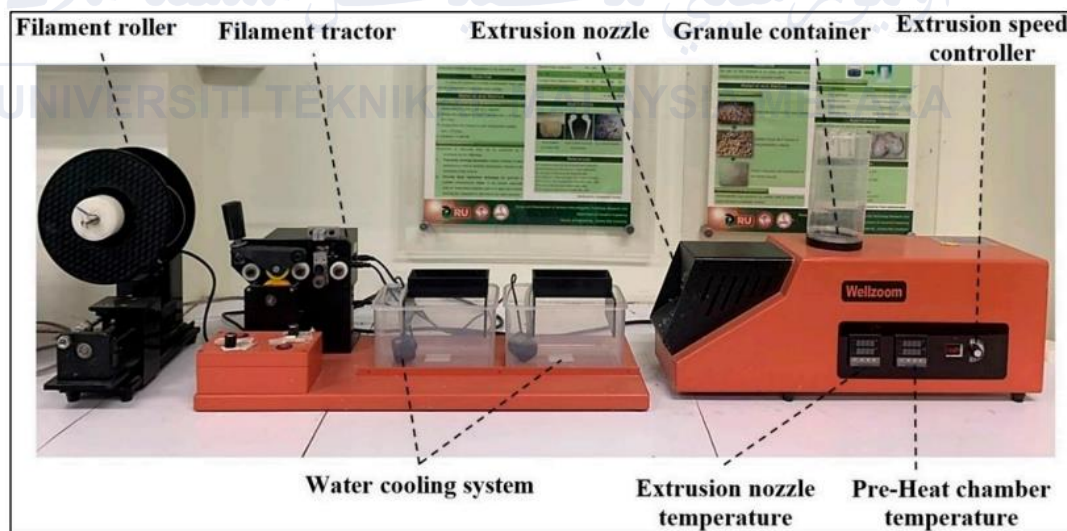


Figure 2.41: Wellzoom Desktop Extruder Line II.

2.10.1 Extrusion

Several suggestions are involved in the filament extrusion process of pure polymers (Kristiawan et al., 2021) investigated filament extrusion outcomes with as minimal distortion as feasible while remaining ordered and smooth. Based on the findings of the interaction of the extrusion parameters, they perform experiments to identify the relationship between extrusion temperature, extrusion speed, and issue solution. The findings are summarised in Table 2.17. For example, the top row shows that if the temperature is lower, the pellets in the extruder do not reach the melting point of the polymer. In that instance, the pellet does not sufficiently melt, resulting in a screw rotation blockage and, as a result, not operating as expected since it is stuck and the rotation slows. Sluggish thrust and high viscosity lead the extrudate diameter to grow big, causing these problems. Their findings may be utilised to compute projected filament output by accounting for the interaction of components.

Table 2.17: Extrusion Parameters Relation (Kristiawan et al., 2021)

Extrusion temperature	Extrusion speed	Result	Solutions
165°C	Very slow	High diameter	Increasing temperature
170°C	Slow	High diameter	Increasing temperature
175°C	Good	—	—
180°C	Good	—	—
185°C	Fast	Filament blister and small diameter	Decreasing temperature
190°C	Too fast	Filament blister and small diameter	Decreasing temperature

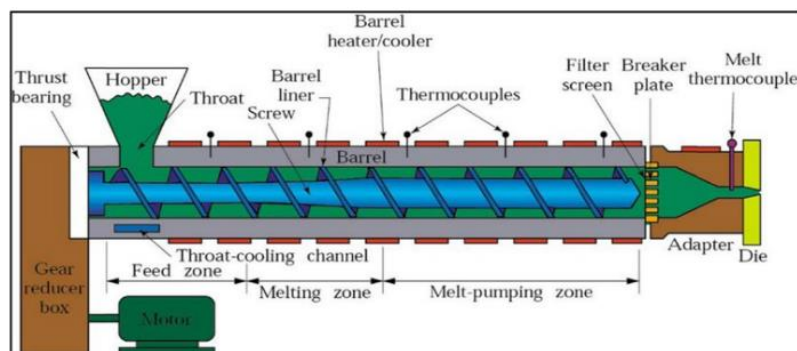


Figure 2.42: Extruder Machine Parts (Kristiawan et al., 2021)

Commercial filaments made from pure polymers may be directly processed as FDM material. However, because each reinforcement in a composite polymer results in a different set of characteristics, the process of producing composite filaments must be approached with caution. Pure polymer filament for FDM goods may be created by extruding pellets or raw ingredients from polymers (Kostic & Reifschneider, 2006). In this procedure, extruders are utilised to push or press the material through holes in the die to form the extrudate (Crowley et al., 2007). An extrusion machine produces filament through a series of stages. The procedure starts with determining the diameter of the filament to be produced, then establishing the extrusion parameters, adding the material in the form of a pellet, and extruding from the nozzle die hole until it is wrapped around the roller machine. Figure 2.41 displays the processes involved in the filament manufacturing process.

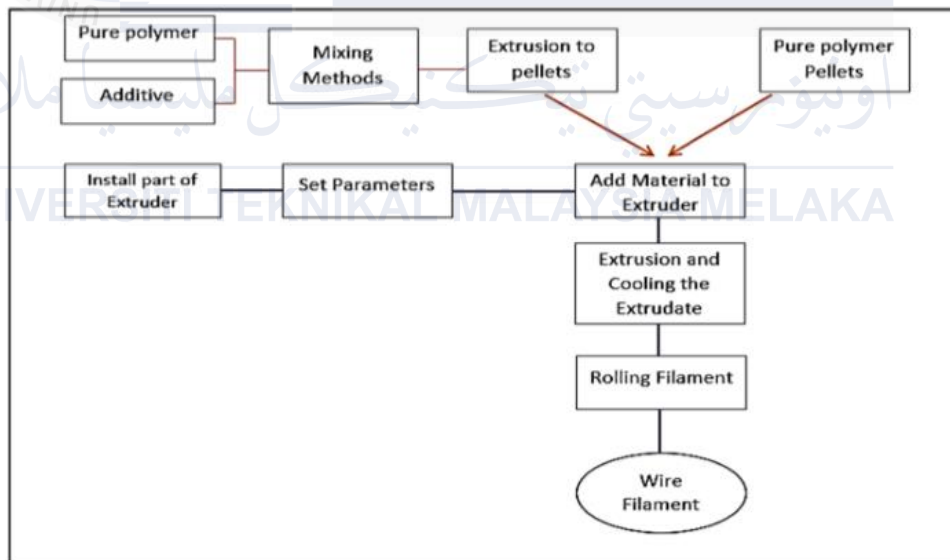


Figure 2.43: Filament Work Flow (Kristiawan et al., 2021)

2.10.2 Screw

Screw extruders are commonly used in extrusion processes such as food processing, injection moulding, and plastic manufacture. It is employed because of its simple geometry, good product quality control, and wider application (Siregar et al., 2014).

According to (Reddy et al., 2011), screw extruders are classified into two categories:

i) Single-Screw Extruder

The most popular extrusion technique on the globe is the single screw extruder. One screw spins inside the barrel and is used for feeding, melting, devolatilizing, and pumping. Mixing is occasionally used for less demanding purposes. Single screw extruders are continuous high-pressure pumps for viscous materials that may generate thousands of pounds of pressure while melting and mixing. The hopper end drives the bulk of extruder screws. When screws are reduced to less than 18 mm in length, they become weak and solids conveyance becomes much less reliable (Crowley et al., 2007).

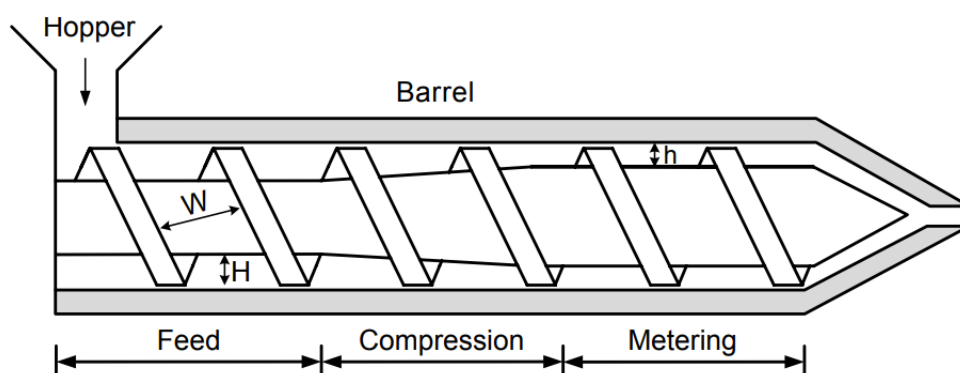


Figure 2.44: A schematic of a typical single-screw extruder (Altinkaynak, 2010)

Nowadays, most single-screw extruders feature three separate functioning zones (Altinkaynak, 2010):

- a. The solid conveying (feed) segment next to the hopper features a deep channel. This section's purpose is to condense and transmit the solid polymer down the helical screw channel.
- b. The channel depth constantly drops during the compression (melting or transition) period. The heat created by the mechanical effort of screw spinning and the heat transferred from the heated barrel melt the polymer in this region.
- c. The metering (melt conveying or pumping) segment at the extruder's delivery end is always shallow. This part is used to homogenise the polymer melt and create the pressure needed to force the molten polymer through a die.

ii) Extruders with Two Screws

The use of two screws allows for a wide range of designs and places different demands on all zones of the extruder, from material transfer from the hopper to the screw to the metered pumping zone. A twin-screw extruder's screws can rotate in either the same (co-rotating extruder) or opposite (counterrotating extruder) direction. Counter-rotating designs are employed when very high shear regions are required because they subject materials to very high shear pressures when the material is driven through the space between the two screws when they come together (Reddy et al., 2011).

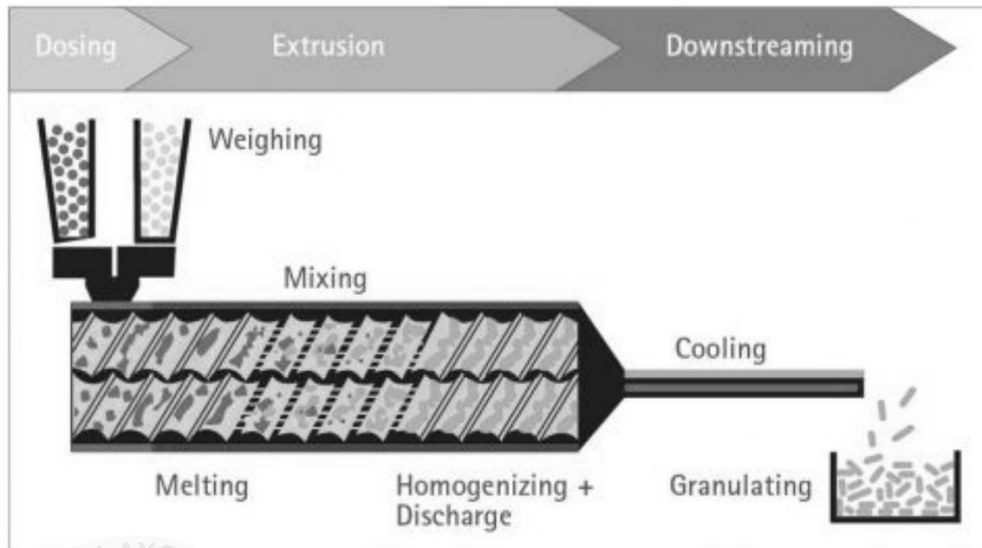


Figure 2.45: Schematic representation of twin screw extruder and processing of hot melt extrusion (Reddy et al., 2011)



Figure 2.46: Twin screw extruder (Courtesy of American Leistrizt Co., Somerville, NJ)

(Crowley et al., 2007)

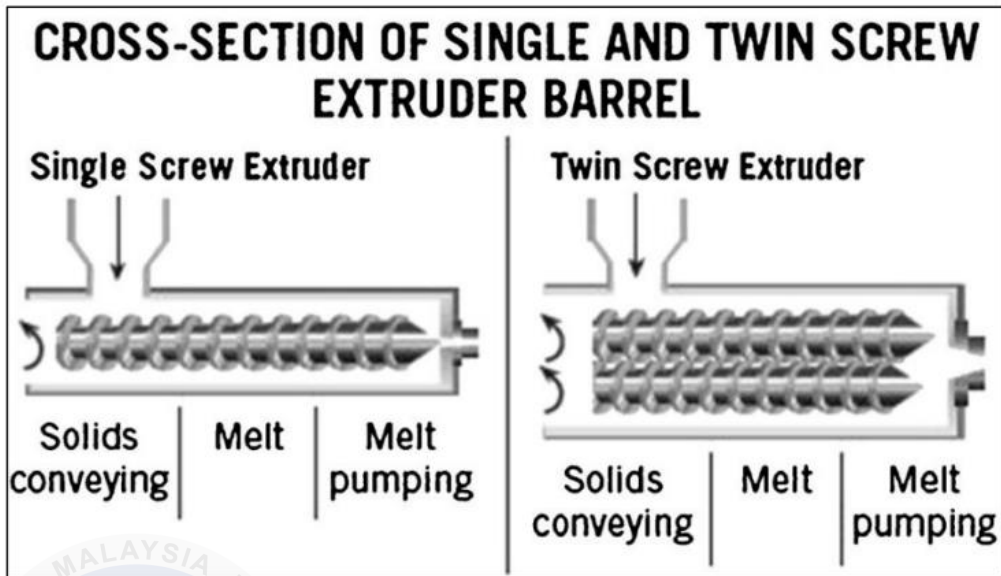


Figure 2.47: Cross-section of single- and twin-screw extruders (Patil et al., 2016)

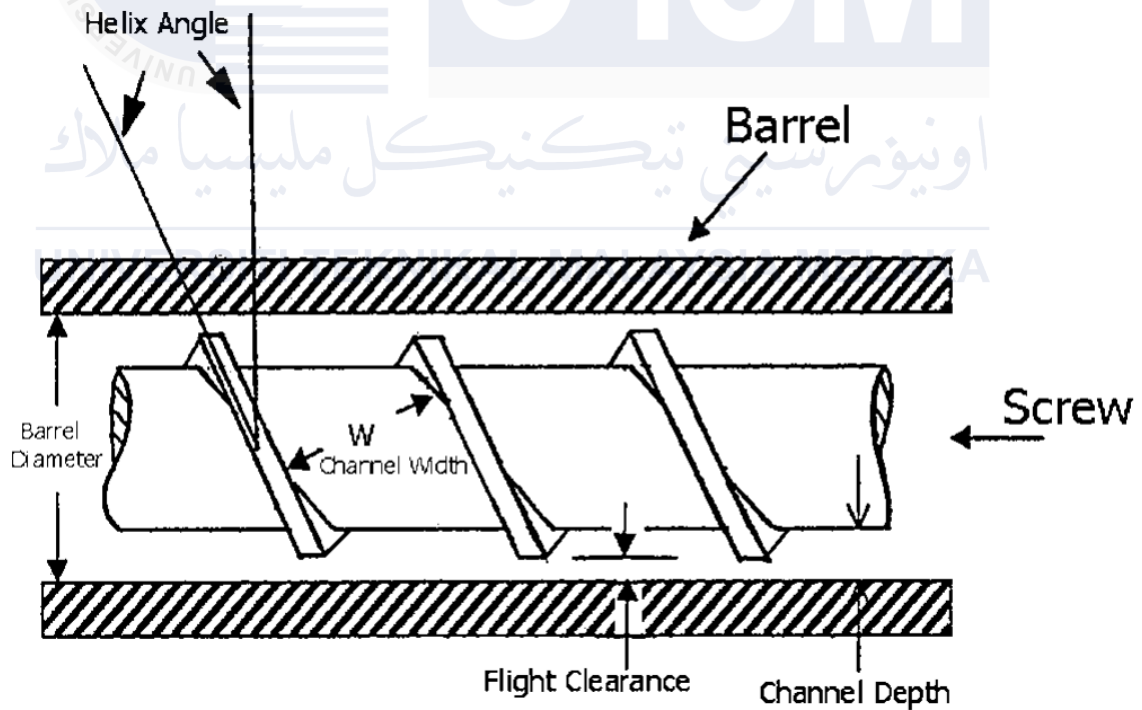


Figure 2.48: Diagram of an extruder screw (Crowley et al., 2007)

2.10.3 Die

From (Truong et al., 2020), extrusion die design has traditionally relied on engineer skill and costly die testing techniques. As a result, die design remains a difficult undertaking. Furthermore, the transverse weld generated between fresh billet material and old material in the cavity of the die is one of the most critical aspects of the current extrusion process.

Extrusion die design is crucial for getting the desired form and dimensions of the extruded product. The job of an extrusion die is to shape the molten plastic exiting an extruder into the appropriate cross section dependent on the product being made. The die links the extrusion barrel's circular exit to the more difficult, and typically more thinner and broader, die exit. Figure 2.47A displays a schematic of a typical die known as a sheet die to explain this point (Kostic & Reifschneider, 2006).

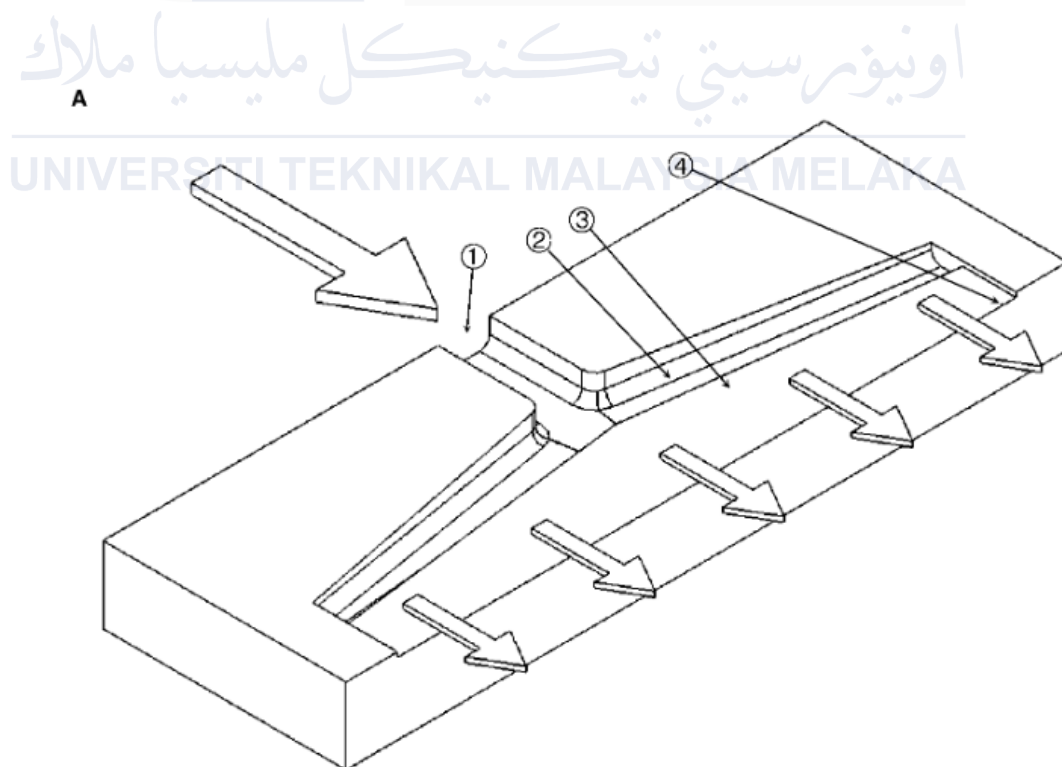


Figure 2.49: Sheet die idea like a coat hanging (Kostic & Reifschneider, 2006)

To ensure the quality of extruded goods, the extrusion die must be constructed to deliver the required pressure for the transverse weld producing aperture while also maintaining extrusion continuity. Because of the extrusion process's complexity, numerical simulation is widely used to estimate process performance, which aids in the design of extrusion dies (Truong et al., 2020).



Figure 2.50: Improper extrusion die design causes product faults. The flaws are related to the profile's substantial bending and twisting (Truong et al., 2020)

2.11 Summary

To summarise, there is an abundance of relevant information gained from prior studies on the MAPP effect on (r-WoPPC) filament in 3D printing. This literature review's findings cover the history and procedure of the FDM 3D printer, 3D printing material, natural fiber 3D printing material, chemical treatment for natural fiber, kind of composite 3D printing filament, and how the filament is processed.

All of this information was acquired and will help with this research, which is a study of the influence of MAPP on the 3D printing filament qualities created from (r-WoPPC). By simply preserving the ratio of wood dust loading, all of the literature review research is critical to the success of this study. According to the literature, the inclusion of the agent coupling or compatibilizer of MAPP has been found to improve bonding conditions.

Table 2.18: The summary of the article/journal for composite material.

No.	Composites	Method of Preparation	References
1)	PP/Kenaf Fiber/MAPP	The mixer was set to 5000 rpm, which corresponded to a blade velocity of 30 m/s at the blade tip. When the temperature hit 190 oC (after about two to three minutes), the material was automatically discharged into a collection tank. The mixture was immediately compression-molded in an 18 x 18 cm mould using a laboratory-scale hot press. The temperature of the hot press plates was between 180 and 190 degrees Celsius.	(Sanadi & Stelte, 2023a)
2)	WF/PP/MAPP	The WFs were dried at 120 °C using an impulse-cyclone drying treatment apparatus until the moisture content was less than 3%. The PP, WF, and MAPP were then	(Liu et al., 2022)

		<p>combined at various mass fraction ratios with a high-speed mixer. The mixes were pelletized using a co-rotating twin-screw extruder and pulverised into minute granules. Using another single-screw extruder, the granules were extruded in WF/PP composite boards with thicknesses of 4 mm and widths of 100 mm.</p>	
3)	PP/GS/MAPP	<p>Prior to melt mixing, polypropylene, glass spheres, and maleic anhydride were dried overnight in a vacuum oven at 105 °C for 24 hours. For 20 minutes, solid compositions were mechanically premixed using a brand batch blender. At 190 to 210 °C at 15 bar pressure and a rotation rate of 20 rpm, samples with varying mixes of PP/HGS/MAPP composites were generated.</p>	(Yağci et al., 2021)
4)	PP/Kenaf Fiber/Epolene 43/MAPP	<p>35 rpm is set for the propeller speed with temperature of 180°C. During the compounding procedure, the epolene 43 was loaded. The epolene 43 concentrations used were 1%, 3%, and 5% (w/w). After 20 minutes of compounding, the compounds</p>	(Saad, 2018)

		were unloaded and chopped into pellets with a crusher machine. The pellets were placed in a mould that measured 17 cm × 17 cm x 0.3 cm.	
5)	RPP/Pinewood Flour/MAPP	The co-rotating twin-screw extruder compounding operating settings, including extruder barrel temperature at distinct extruding zones, melt pressure, and screw speed used for the compounding of both fiber and matrix (PP). Extruder zones Z1, Z2, Z3, Z4, Z5 and die were set to 150°C, 170°C, 180°C, 190°C, 200°C, and 190°C at 276 screw rpm, respectively. PWF + PP + MAPP (0-2-4-6-8%) are supplied into the extruder through feeders. The extruded strand exiting the die head is then pelletized after passing through a water bath.	(Sigdel & Giri, 2016)
6)	PP/CF/MAPP	Polypropylene was discharged into the mixer chamber together with MAPP at a rate of 3 wt% of filler weight. After 12 minutes, the coconut fibre was released into the mixer chamber, and mixing was continued for another 5 minutes. For each mix, the mixing	(Sabri et al., 2013)

		<p>time was 17 minutes. The composite mixes are then squeezed in a Hot-Press Machine to produce a 1.0 mm sheet of composites with dumbbell shape conformity. The hot press processes include 6 minutes of preheating at 180°C, 4 minutes of compression at the same temperature, and 4 minutes of cooling under pressure.</p>	
7)	OPB/PP/MAPP	<p>After drying, the OPB was compounded into polypropylene using a twin-screw compounder with barrel temperatures ranging from 170°C to 190°C from the feeding zone to the die zone. Prior to compounding, the OPB were oven-dried at 105°C for 24 hours to produce a moisture content of less than 5%. 4 levels of loadings are being prepared for all composites.</p>	(Ramli et al., 2012)
8)	HDPE/PP/MAPP	<p>The compounding temperature for WF/PP is set to 180°C. 80 rpm is set to the screw rotation speed. The oven is set to 110°C for drying the wood fiber and for 12 h prior to compounding.</p>	(Yuan et al., 2008b)

CHAPTER 3

METHODOLOGY

3.1 Introduction

With the aid of a flow chart to illustrate the entire project, this chapter goes into great detail about how it will progress. The flow chart acts as a roadmap to ensure that every step of the project's operations goes according to plan. The procedures to be employed, together with the tools and equipment needed for the entire project, were decided throughout this chapter. The research methods given in this chapter were used to achieve the study's objectives.

From the flow chart in Figure 3.1, the very first thing to do is to characterize wood fiber and recycled polypropylene. The wood fiber is sieved to the 125 μ m particle size and if the size is greater than 125 μ m, the sieve procedure is repeated. Next, the wood fiber is treated with a 6% NaOH solution. The MAPP is blended with wood fiber and recycled polypropylene using a hot press machine. If the weight of the composites is less than 500g, repeat the hot press procedure. The composite is then crushed into small pellets for the extrusion process and if the pellet size is large, this procedure is repeated. The pellet is then extruded into filament using a single extruder. The process is repeated if the filament size is less than 1.6mm or greater than 1.9mm. The filament is then used to print specimens for testing, which include morphological, mechanical, and physical tests. Lastly, data analysis is being carried out.

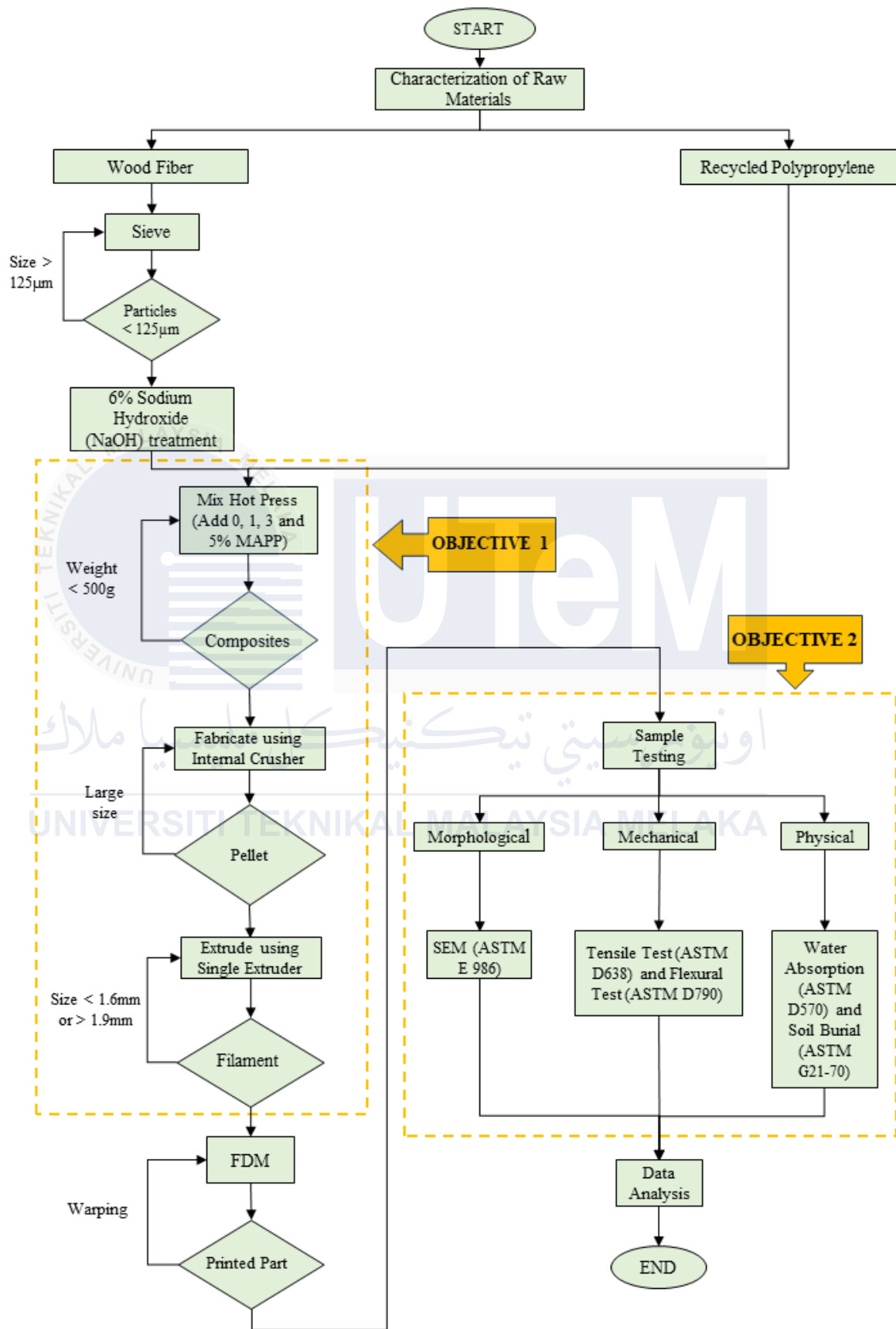


Figure 3.1: Flow chart of methodology

3.2 Raw material

In this project, four basic raw materials will be combined to form a composite: Recycled Polypropylene, wood fiber, Sodium Hydroxide (NaOH), and Maleic Anhydride-Grafted Polypropylene (MAPP). This material was gathered under a variety of conditions.

3.2.1 Recycled polypropylene (PP)

Figure 3.2 shows granulated pellets of recycled PP purchased from Lotte Chemical, with a melt flow rate of 33.8 g/10 min (with 5000 g weight at 230°C). Table 3.1 summarize the specifications for the materials used in the project provided by the vendors.



Figure 3.2: Granulated pellets of recycled PP

Table 3.1: Specifications of filament materials (Kristiawan et al., 2022)

Material	Density (g/cm ³)	Tensile Strength (MPa)	Young's Modulus (GPa)	Pellet Diameter
Recycled PP	0.574	22.5	1.24	5.04

3.2.2 Wood fiber

Wood fiber was bought online through Shopee. Figure 3.3 shows the raw material of the wood fiber.



Figure 3.3: Wood fiber

3.2.3 Sodium hydroxide (NaOH)

For the alkaline treatment in this investigation, NaOH in the shape of a pellet, as illustrated in Figure 3.4, was employed. Table 3.2 provided the material specifications for NaOH.



Figure 3.4: NaOH Pellet

Table 3.2: Specification of sodium hydroxide (Nur Hamzah et al., 2016)

Items	Specification
Physical Form	Pellets
Colour	White
NaOH Content	More than 99%
Water Solubility	100%
Molecular Weight	40 g/mol

3.2.4 Maleic Anhydride-Grafted Polypropylene (MAPP)

MAPP acts as a coupling agent and it is in pellet form. Figure 3.5 shows the MAPP.



Figure 3.5: MAPP Pellets

3.3 Preparation material

3.3.1 Preparation for wood fiber

The wood fiber used in this study was cleaned with distilled water to remove surface dust before being dried in an oven at 80°C for 24 hours to guarantee a moisture content of less than 3 wt.%. The sieve technique is used to determine the particle size of wood fiber. Wood fiber with particle sizes of 125 μm or smaller was used in this experiment. Figure 3.6 shows wood fiber is being washed with distilled water.



Figure 3.6: Wood fiber is washed with distilled water



Figure 3.7: Wood fiber is being dried in an oven.

3.3.2 Preparation for recycled polypropylene

The recycled polypropylene (rPP) pellets were created in the lab. The quantity used was a composite loading of 500 g per sample. This rPP was bought from a vendor specifically for this project and is in fine working order.

3.3.3 Preparation for MAPP

The additive MAPP will be weighed using a scale in line with the set ratio. Since it is in the pellet form, it must be prepared with greater care.

3.4 Characterization of wood fiber

The wood fiber that was characterized in the early stages was in chip form. The particle size was generally large. In the sieving process, the size of the wood fiber was able to be reduced in particle size and it also removed all the unwanted substances. Every layer of the sieve machine has different filters in different sizes. After that, the wood fiber was sieved to 125 μm in size. The 125 μm size of wood fiber is utilized because, in the analysis, 90% of the total quantity studied from the sieve of wood fiber with a mesh size of 100–125 μm is easy to be detected (Nafis et al., 2023). Figure 3.8 shows the process of the characterization of wood fiber using the sieve machine.



Figure 3.8: Sieve process; (a) clean wood fiber, (b) three different sieve sizes, (c) wood fiber is placed in sieve, (d) the machine is switch on for 30 minutes

In Figure 3.8, the sieve procedure will employ clean wood fiber. Once that is done, sieve machine is placed appropriately. The sieving process makes use of three different sieve sizes. The wood fiber is passed through three sieves: 0.3mm, 0.2mm and 0.125mm. This configuration will be used in the sieve method to acquire the exact particle size. Subsequently, activate the siver machine and set the timer for 30 minutes and this process should be repeated until the necessary weight of wood fiber is obtained. At last, the 125 μ m-sized wood fiber will be prepared for the treatment.

3.5 Wood fiber treatment

3.5.1 Preparation of NaOH solution

In this study, the preparation of the NaOH solution consists of adding together 6% of the NaOH concentration and 94% of water. This combination will result in a solution with a 100% concentration (Nafis et al., 2023). Table 3.3 displays the weight ratio of water and the NaOH solution needed for the treatment. The solution will be agitated with H₂O and NaOH until it dissolves. As shown in Figure 3.9, a combination of 6% NaOH and 96% water is used to dissolve the NaOH solution. The equation is shown below:

$$\text{Mass of NaOH} = 1000\text{ml} \times \frac{6\%}{100} = 60\text{g}$$

Table 3.3: Weight ratio of water and NaOH

No	Material Used	Amount (g)	Amount (%)
1)	NaOH	60	6%
2)	Water	940	94%
3)	Total	1000	100%

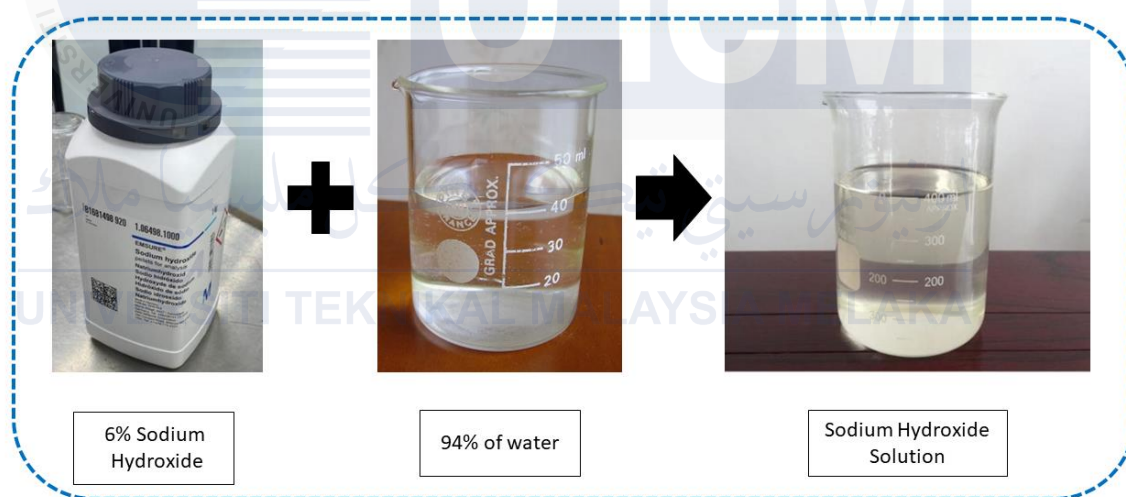


Figure 3.9: Preparation of NaoH solution

3.5.2 Treatment of fiber with NaOH solution

Chemical analysis known as alkaline treatment using NaOH is frequently used to enhance the qualities of fibers, including their thermal properties to enhance the addition between the fiber and matrix and their ability to remove contaminants from the fiber interface (Fiore et al., 2015). This wood fiber will be used in this process together with a sodium

hydroxide (NaOH) solution. The wood fiber filler will be submerged in the NaOH solution that has been made in the beaker. Hence, Figure 3.10 shows the process of doing the wood fiber treatment with NaOH solution.

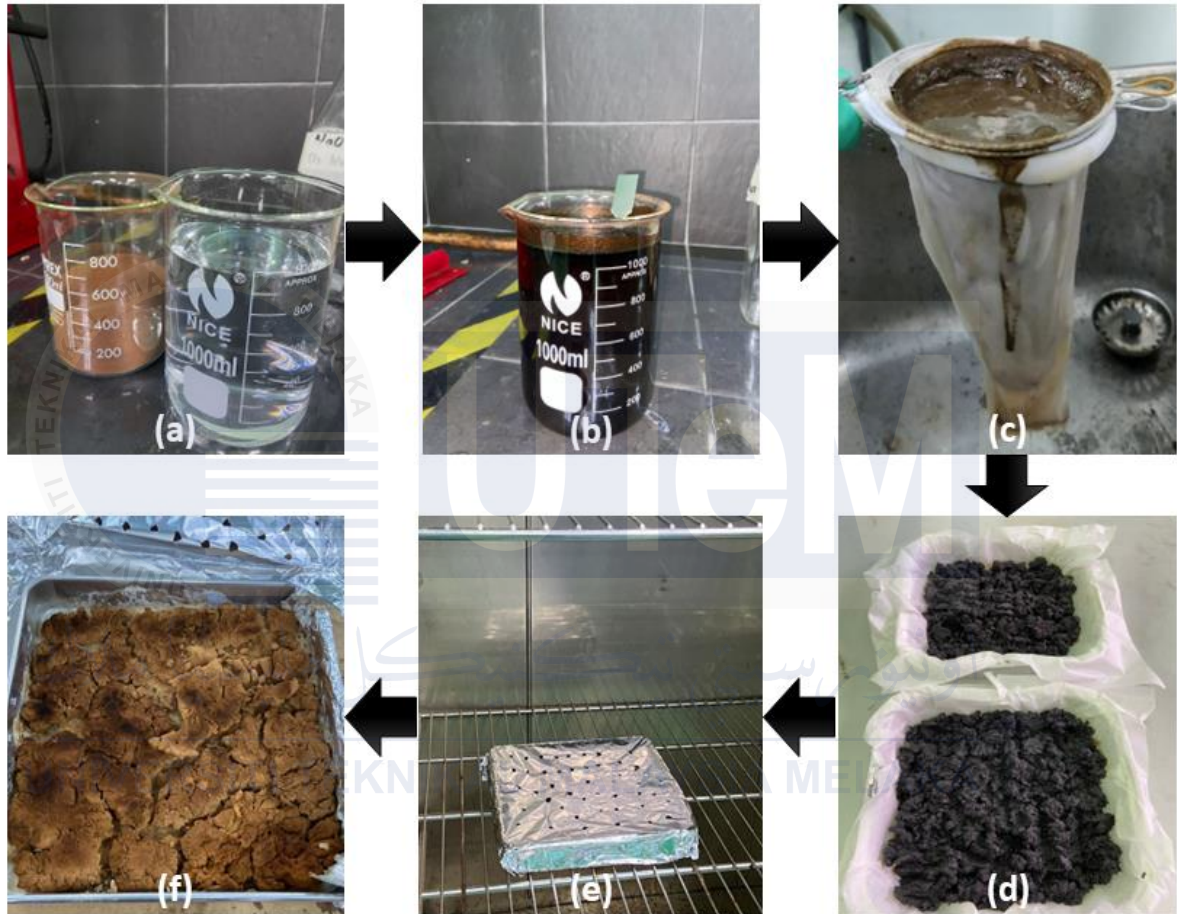


Figure 3.10: Wood fiber treatment with NaOH solution; (a) Wood fiber and NaOH solution, (b) The solution of sodium hydroxide (NaOH) dissolves the wood fiber, (c) Distilled water used to rinse treated wood fiber, (d) Tray with treated wood fiber, (e) The tray is placed inside the oven, (f) Wood fiber after 24 hours in the oven

From Figure 3.10, the wood fiber was added into the NaOH solution by using 1000ml beakers. Then, let it dissolved completely for three hours and make sure the solution is stirred from time to time. After dissolving the wood fiber, the wood fiber must be rinse with distilled water using filter. Put the treated wood fiber in the tray and let it dry for a while. Cover the tray with aluminium foil to avoid it from overflowing or spoiled before entering the oven. Make sure to make some holes on the aluminium foil. After that, put the wood fiber inside oven. Set the temperature to 80°C and let it dry for 24 hours. After 24 hours, take out the tray from the oven and let it cool for a while.

3.6 Preparation of recycled polypropylene/ wood fiber/ MAPP composites

The composites are mixed in plastic bag and distribute evenly in molding plate. These composites will be put into mold in the hot-press machine. Additionally, this machine is used so that the composites can be mix perfectly.



Figure 3.11: Hot-press machine

The amount of wood fiber and recycled polypropylene used are fixed. The amount of wood fiber used is 3% wt while recycled polypropylene used is 97% wt for every sample. Then, the composites are ready to be mixed with MAPP such as in Figure 3.12. The amount of MAPP is based on Table 3.6 for every specimen.

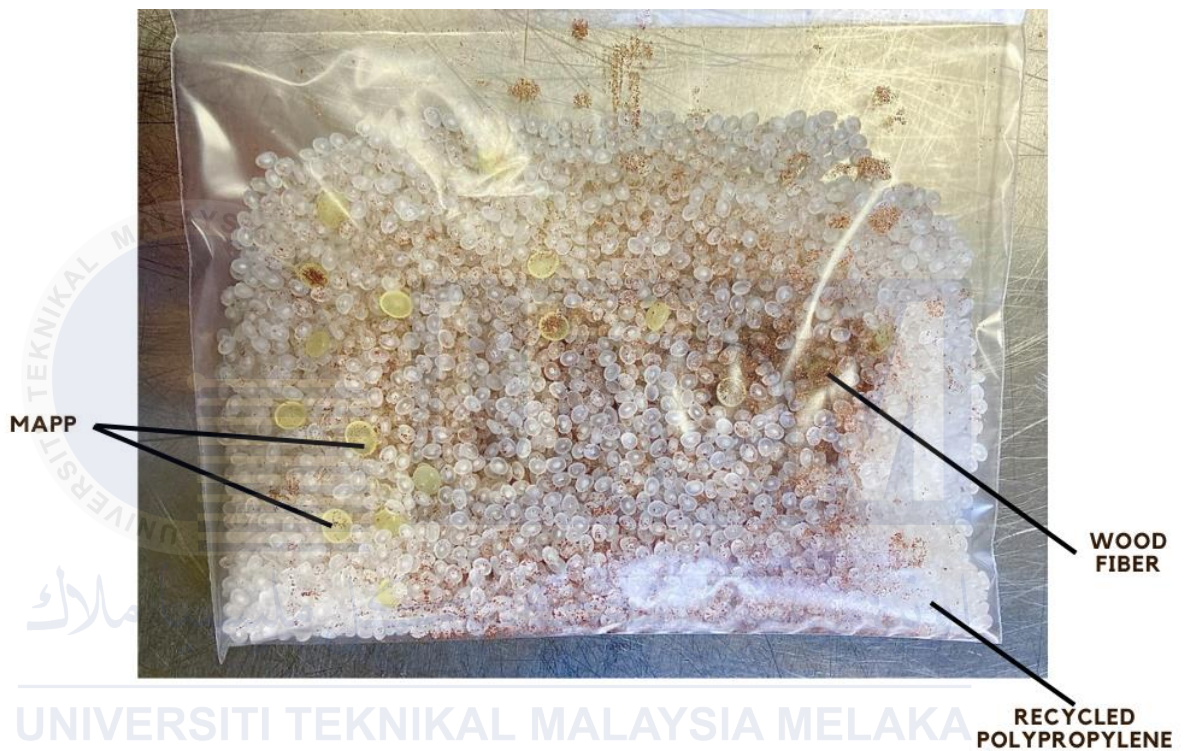


Figure 3.12: The recycled polypropylene, wood fiber and MAPP are mixed together

Table 3.4: Composition of wood fiber, polypropylene and MAPP (wt%).

No	Sample	wood fiber	PP	MAPP
1.	WF + PP	3	97	0
2.	WF + PP + 1% MAPP	3	97	1
3.	WF + PP + 3% MAPP	3	97	3
4.	WF + PP + 5% MAPP	3	97	5

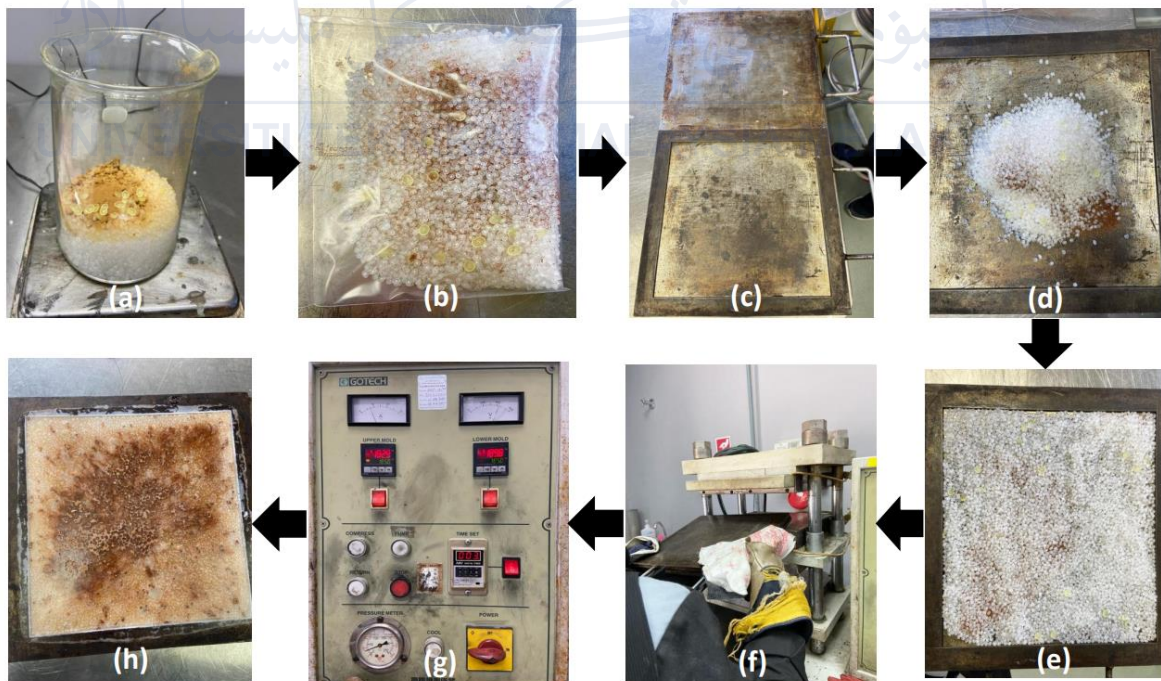


Figure 3.13: Hot-press process; (a) weighing MAPP, PP and wood fiber, (b) combine the composites into the plastic bag, (c) get the moulds ready, (d) place the composites within

the mould, (e) uniformly distribute the composites, (f) insert the mould into the machine, (g) configure the parameter, (h) composites upon completion of hot-pressing

Based on Figure 3.13, the wood fiber, recycled polypropylene and MAPP are weighed in the required amount. Then, combine MAPP, rPP, and WF in a single packaging bag and shake it for a few minutes in all directions before placing it in the hot-press machine. Refer to Table 3.6 for the weight ratio. Prepare the mould and two stainless steel plates for the hot-press procedures. Insert the composites into the mould and distribute the composite evenly throughout the mould. Closed both the top and bottom sides with plates to prevent the composite from escaping. Set the mould in the hotpress and wear a glove to protect hands when putting the mould. Set the parameter of the hot-press such as pressure, temperature and time. Then, proceed to the cooling press so that it can harden the combine composites. After finished the hot-press, remove the mould carefully.

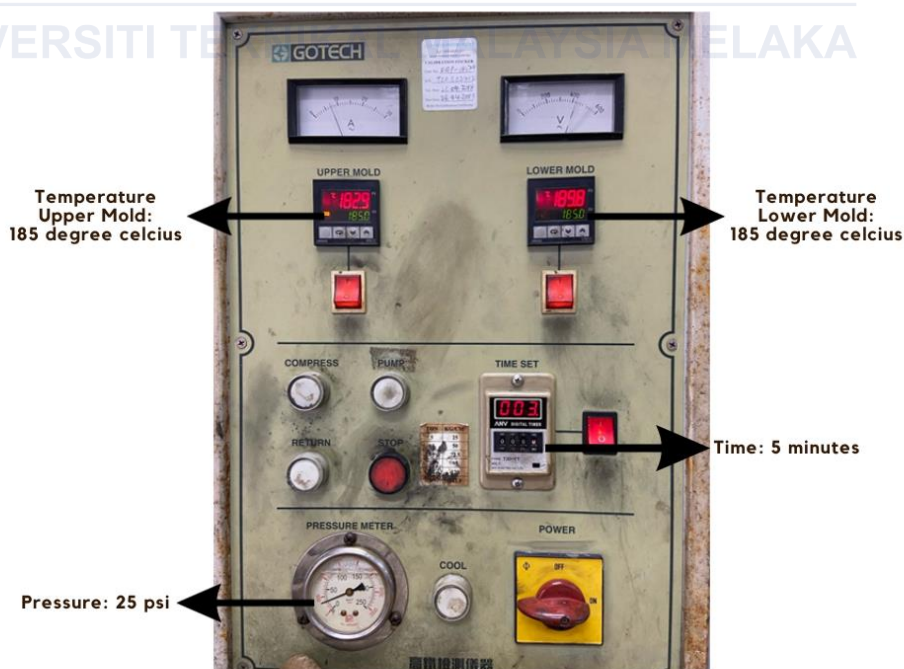


Figure 3.14: Hot-press parameter

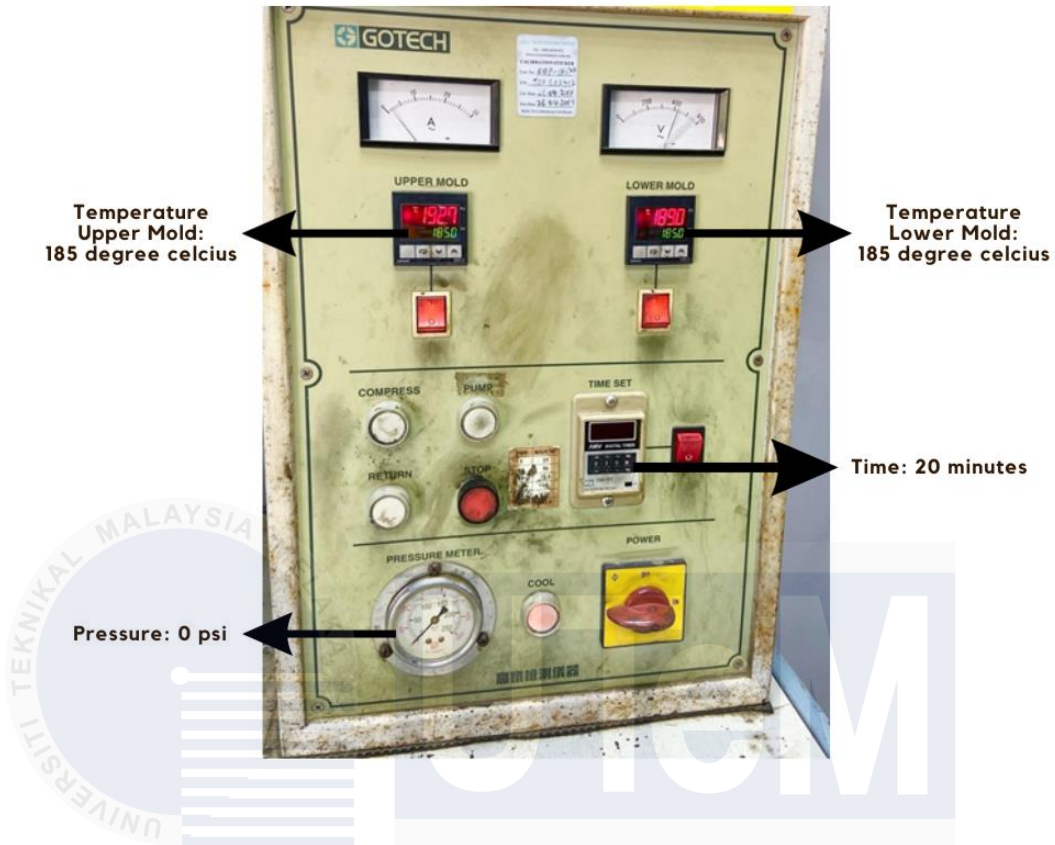


Figure 3.15: Cooling press parameter

3.7 Pellet Fabrication

The mixed composite will next go through a crushing process to become a pellet. This process will be performed two times to ensure that the pellet size is within the acceptable range for extrude process. But before crushing the composite, it must be cut into two parts to fit in the crusher machine. With that, Figure 3.17 shows the process of pellet fabrication.



Figure 3.16: Cheso crusher machine

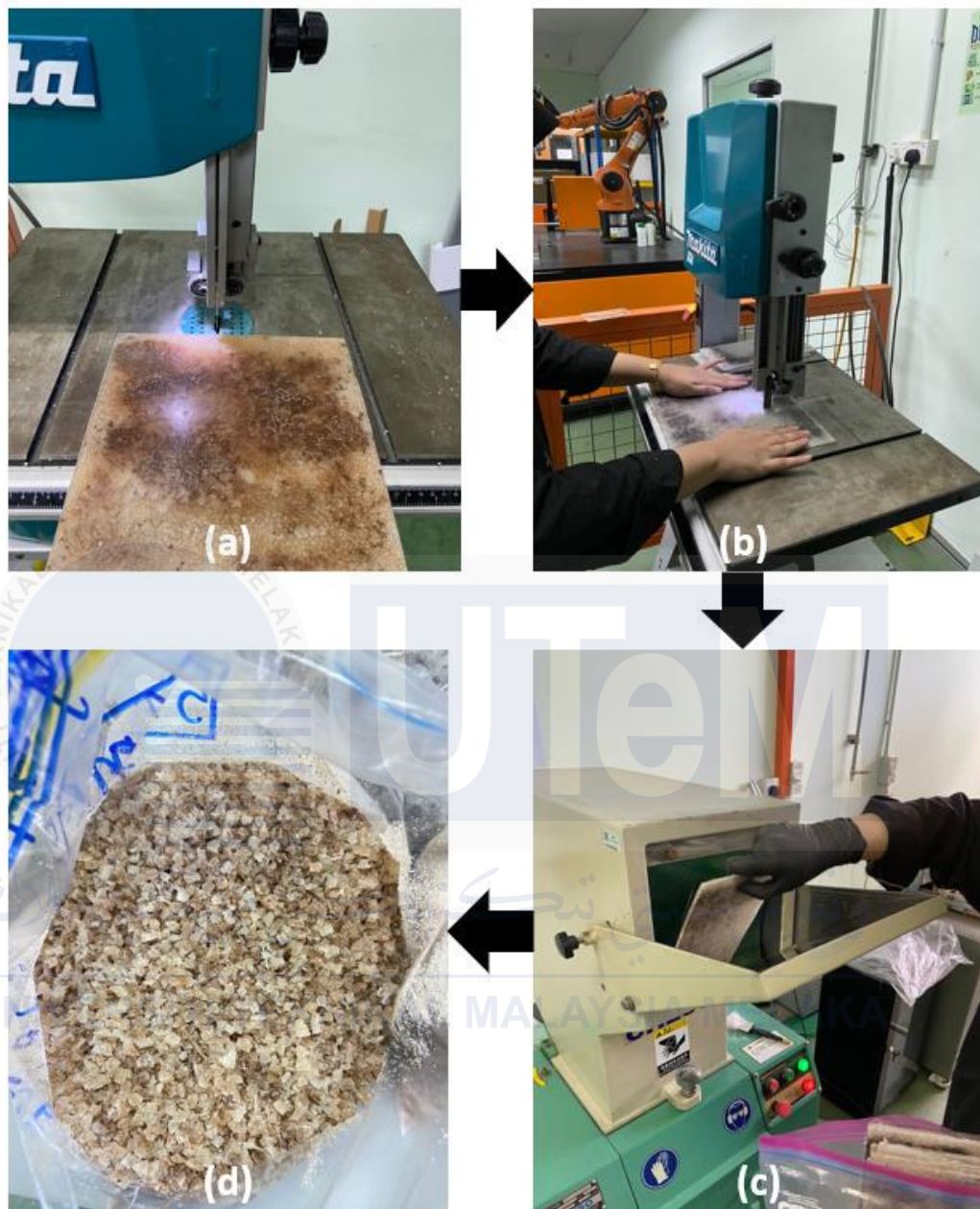


Figure 3.17: Pellet fabrication; (a) composite on the cutting machine, (b) cutting process, (c) insert composite into crusher machine, (d) required size of pellet

The composite is placed on the cutting machine as shown in Figure 3.17. The purpose of cutting the composite is to make sure that it fixed the crusher machine. To prevent harm, gently cut the composite. In order to create pellet, insert the smaller size of the composite into the crusher machine. Figure 3.17(d) illustrates the precise pellet size required to proceed with the extrusion procedure.

3.8 Preparation of Filament

3.8.1 Extrusion Process

The filament was created using a single extruder, as seen in figure 3.18 below.



Figure 3.18: Single Extruder

In Figure 3.19, a single screw extruder with a 1.75 mm die nozzle that fed the material into three heating zones was used to extrude the composite material filament. The temperatures for the barrel and die nozzle zones were preheated to 196-198°C, respectively. The composite material must be heated before it can be placed in the hopper. Furthermore, forward movement of the barrel screw (10-15 rpm) drove molten material upwards to its die nozzle. The feed cooling zone was also adjusted at a cold temperature to pre-heat the pellets/mixture. When the composite filament production temperatures were reached, a certain weight of composite material was fed into the barrel at each feeding interval. The

filament reducer rollers were adjusted to transport the hot extruded filament at 10-20 rpm through a water-cooled bath. Several cooling devices, such as a cooling water bath, were also tested during the extrusion process. The extruded filament was then coiled onto the spooler and placed on the filament storage rollers before being spooled at 300 mm/s. The modifications made to the filament extrusion processing parameters to maintain acceptable filament diameters are summarised in Table 3.5 (Altinkaynak, 2010).

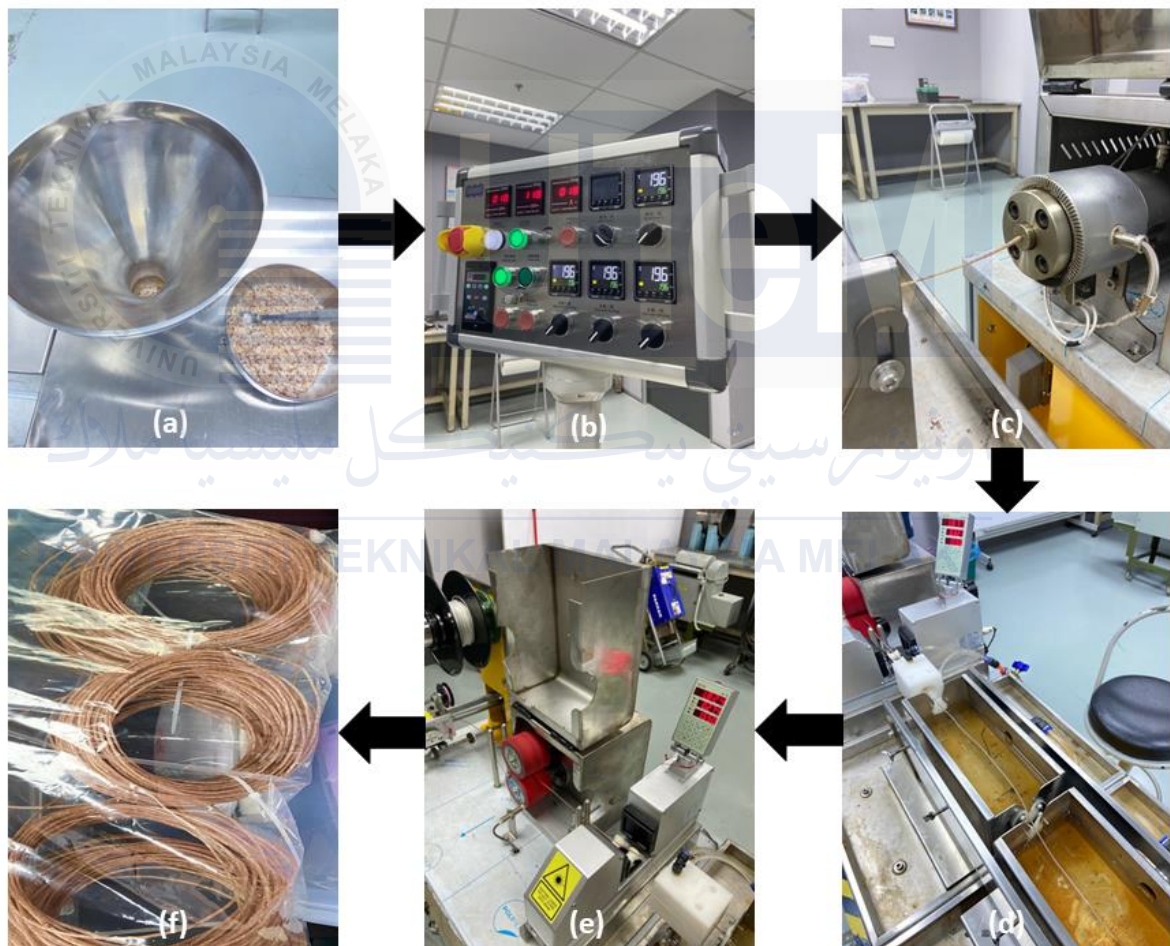


Figure 3.19: Extrusion process of filament; (a) pellets are put into the funnel, (b) parameter is set up, (c) pellet melted and transformed into filament, (d) filament travels through tubs of cooling water, (e) the roller pulls the filament while the sensors measures the filament's size, (f) precise filament size required

Table 3.5: The filament extrusion processing parameters

Categories	(r-WoPPc) Filament
	Value
Barrel Temp (°C)	196-198
Die/nozzle Temp (°C)	196-198
Screw extrusion speed (rpm)	10-15
Filament pulling roller speed (mm/s)	300
Filament winding roller speed (mm/s)	200

3.8.2 Characterization of filament

The test method for evaluating the density of the filament was carried out in accordance with ASTM D792-91. Filament with a diameter of $1.75\text{mm} \pm 0.55\text{mm}$ and a length of 90mm was cut, and densities were calculated using the equation;

$$\text{Density } (\rho) = \frac{\text{Mass of filament composite } (g)}{\text{Volume of filament composites } (m^3)}$$

A digital microscope (Dino-Lite AM4113/AD4113), on the other hand, is being used to characterise the filament surface of various loadings of MAPP. The purpose of this is to examine the morphology and the surface quality of the r-WoPPc filament, which might have

an even or uneven surface. Furthermore, the filament diameter is being defined. It is computed using a vernier caliper to achieve a diameter of 1.75mm for the filament.

3.9 Preparation of specimen

The r-WoPPc filament was 3D printed using an FDM 3D printing equipment (Fig 3.20). Ultimaker Cura 4.8.0 open-source software was used to create (.stl) files for printing. The CAD model of the typical tensile test specimen (Type 1, ASTM D638) (ASTM D790) was created using Solidworks 2021. Three tensile and flexural test samples were created using the composite filaments. Printing nozzle sizes of 0.4 mm and 0.6 mm were used for (r-WoPPc) filaments. Table 3.6 includes the printing parameters [0, 90] degrees printing strategy and 100% infill. To print filament, a nozzle temperature of 180-220 °C and a bed temperature of 85 °C are utilised. When the filament reaches melting point, it is fed through the 1 mm needle at 20m/min, resulting in a 0.30mm thick layer. The 3D-printed specimen's initial layer had trouble sticking to the printer build plate. To prevent warpage, commercially available PP filaments are frequently constructed of a mix or composite. The first print layer failed not stick to the printer bed when using Pritt adhesive and Kapton tape, resulting in the printing process being terminated prematurely (Kristiawan et al., 2022).

Table 3.6: Printing Settings.

Parameters	Values
	(r-WoPPc) Filament
Temperature of printing (°C)	198
Initial layer temperature (°C)	198
Build plate temperature (°C)	98
Build plate temperature, initial layer (°C)	98
Infill pattern	Line
Infill flow (%)	110
The height of the layer (mm)	0.3
Line width (mm)	0.38
Top and bottom layers (layers)	2
The print speed (mm/s)	100
The speed of initial layer (mm/s)	15
Build plate adhesion type	Brim

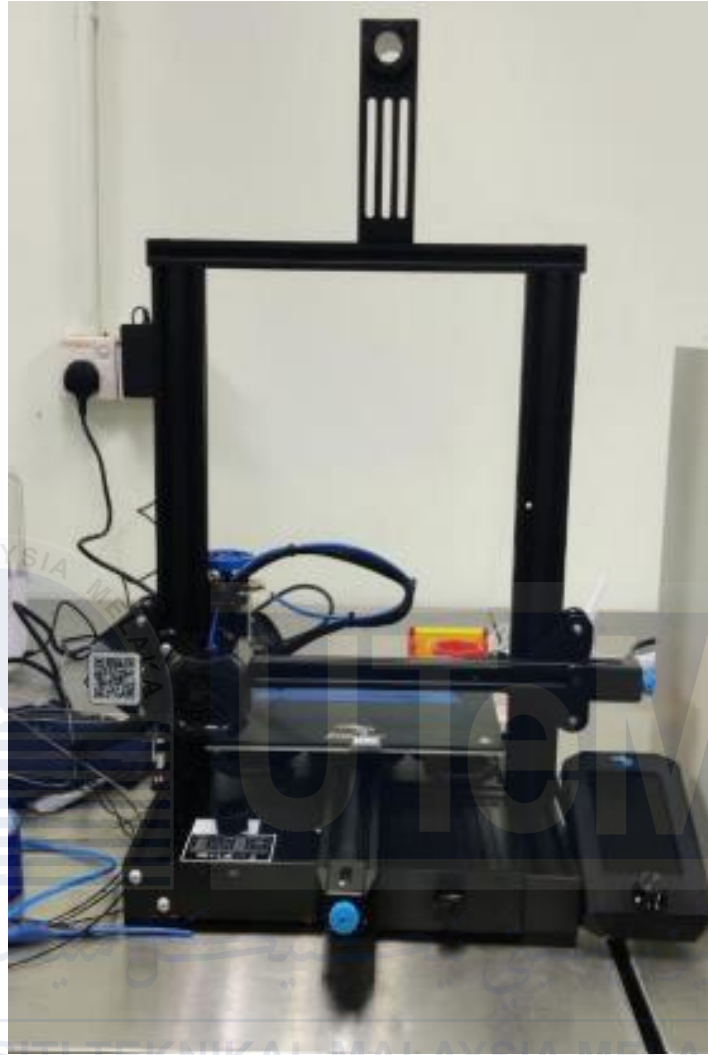


Figure 3.20: FDM 3D printing

3.10 Testing of specimens

3.10.1 Tensile test

The tensile testing was carried out using a universal machine. Tensile tests were performed to measure the tensile strength, Young's (elastic) modulus, and elongation at break of the product. The following conditions were employed: The displacement is 5 mm/s. Three samples were used to be tested (Pérez et al., 2012). ASTM D638 tensile properties were evaluated using Instron Model 8872 with a crosshead speed of 30mm/min. The Type I specimens, which are shaped like dumbbells and size 165 mm in length, 13 mm in breadth

and 70 mm in gauge length, were prepared for testing by conditioning them at room temperature and 30% relative humidity (Saad, 2018).



Figure 3.21: Instron Model 8872

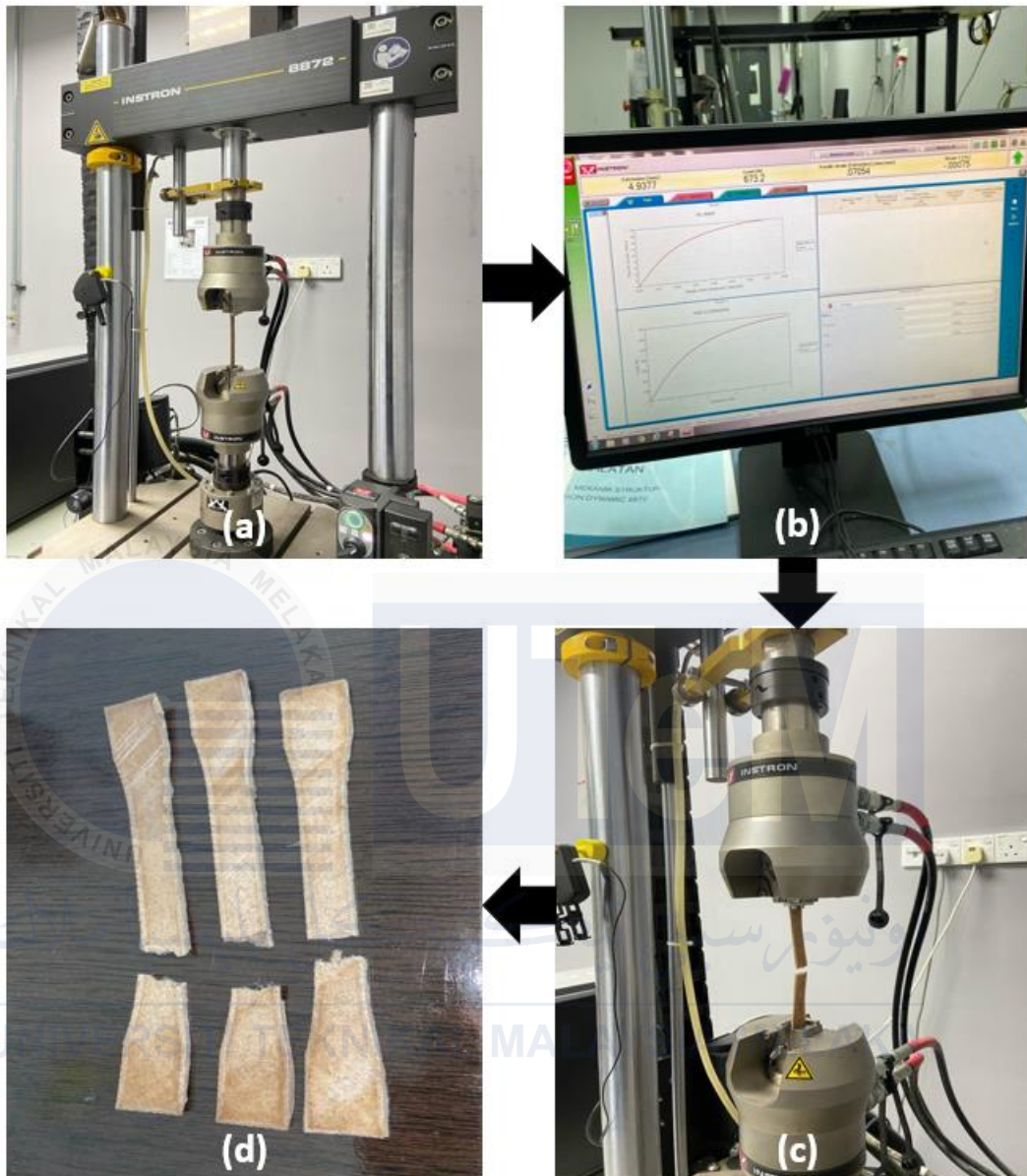


Figure 3.22: Tensile test; (a) Place the specimen to the machine, (b) See the tensile data in the computer, (c) The specimen is break into two, (d) Specimens after the testing



Figure 3.23: Tensile test specimens



Figure 3.24: Tensile test specimens after testing

3.10.2 Flexural test

According to ASTM D790, a three-point bending test with specimens of 125 x 12.7 x 4 mm (length x breadth x thickness) was performed at a speed of 5 mm/min. Three specimens were evaluated for each composition (0%, 1%, 3%, and 5% MAPP). The specimens' support span is determined to be 64 mm. Machine in Figure 3.25, Instron Floor Mounted Material Testing System Model 5585 was used to perform the flexural testing.



Figure 3.25: Instron Floor Mounted Material Testing System Model 5585

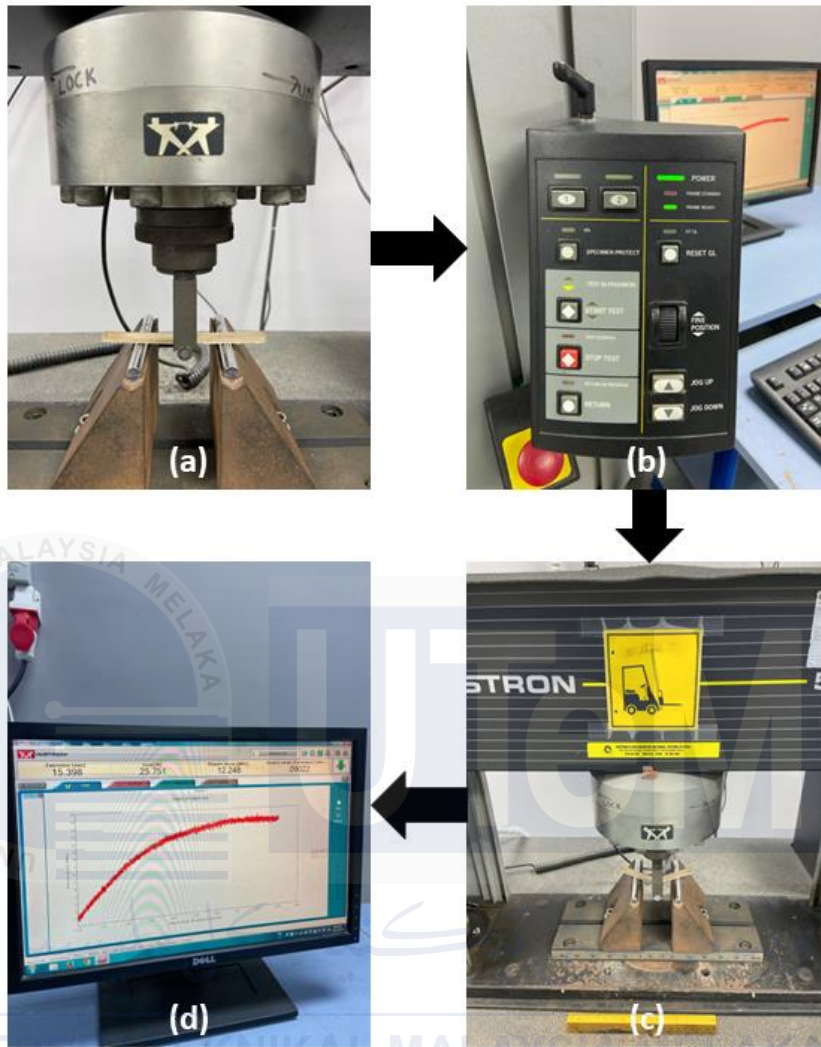


Figure 3.26: Flexural testing; (a) The specimen is placed on the machine, (b) The controller is used to adjust the machine's up and down operation, (c) Three-point bending test , (d) Data obtained from the testing.



Figure 3.27: Flexural specimens for testing



Figure 3.28: Flexural specimens after testing

3.10.3 Water absorption test

Testing for water absorption was done in compliance with ASTM standard D570-98. For a whole day (24 hours), the specimens (r-WoPPc filament) were submerged completely in distilled water. It was computed to find the % increase in weight during immersion. Each % of MAPP was evaluated on three 4 cm specimens. The water intake (percentage) was estimated by dividing the absorbed water weight by the dry weight of the specimen. As illustrated by the following equation:

$$WA (\%) = \frac{W_t - W_o}{W_o} \times 100\%$$

where W_t and W_o were the sample weights at a certain time and the initial time, respectively (Hao et al., 2021).

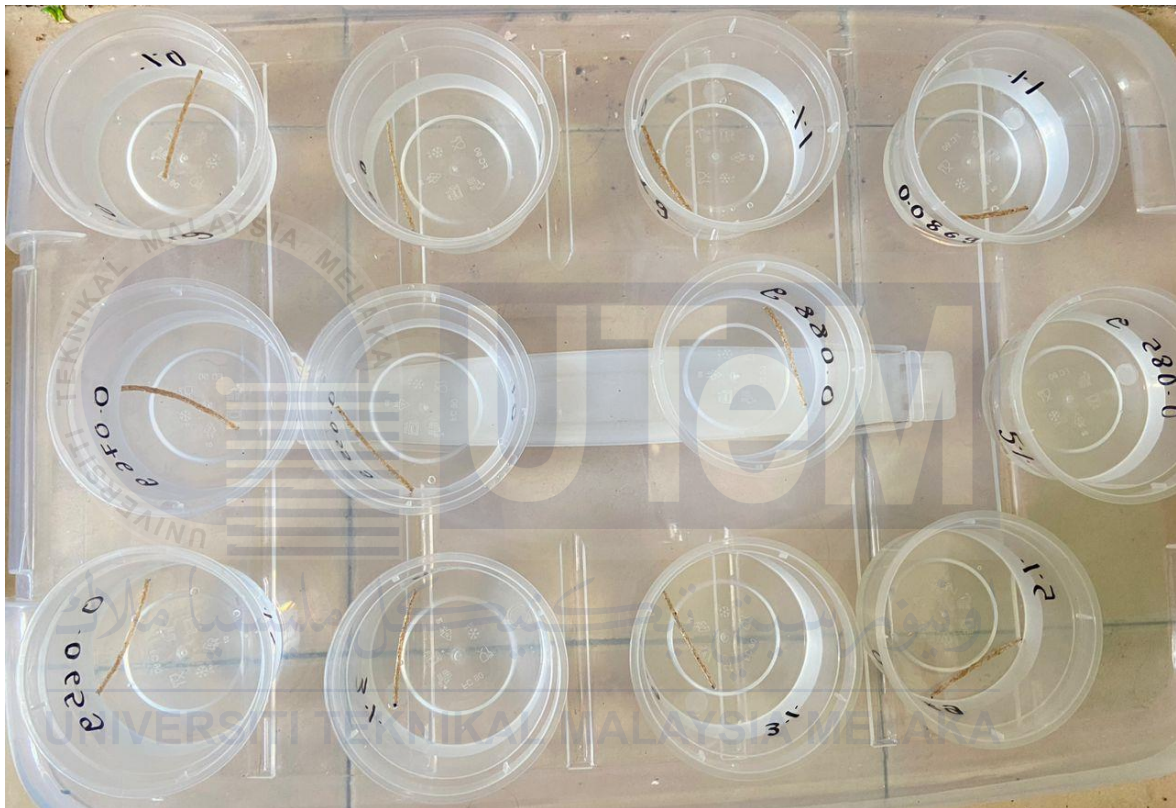


Figure 3.29: Water absorption test

3.10.4 Soil burial test

Soil burial tests were used in laboratory-scale biodegradation studies of composite materials. Figure 3.30 demonstrates the test procedure. The filament was mixed with garden soil. 50g of soil were placed into plastic containers. Three 4 cm long samples of each r-WoPPc filament (0%, 1%, 3% and 5% MAPP) were weighed, distributed out on the soil, and then covered with 50g more of soil. Each sample was wrapped in mesh cloths to make it easier to remove the degraded sample. Over the course of seven days, three milliliters of

water were applied to each treatment. The 21-day experimentation was conducted. At 7, 14, and 21 days, the r-WoPPc filaments were removed from the plastic container (Shahrim et al., 2022). The mesh cloths were gently removed and filament is washed with distilled water to remove the contaminants. The following formula was used to assess the filament's biodegradability by weight loss:

$$\% \text{ weight loss} = \frac{W_i - W_t}{W_i} \times 100$$

Where W_i represents the initial weight and W_t is the weight after the established time.

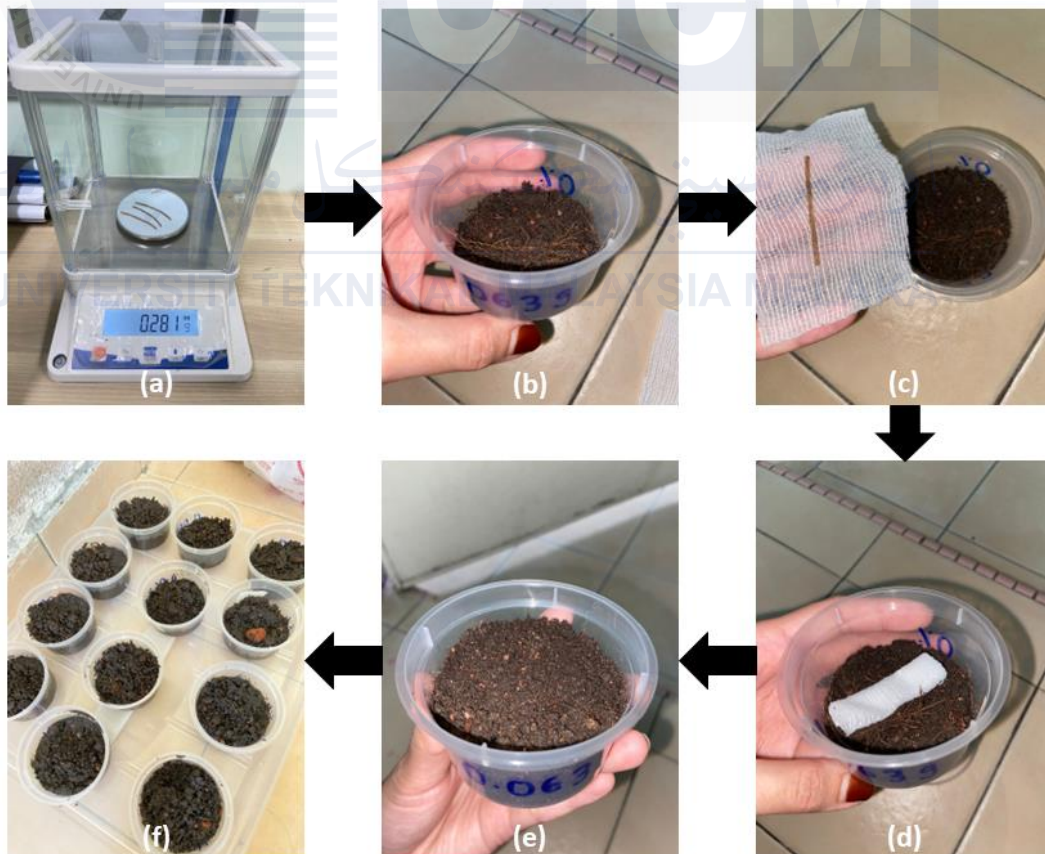


Figure 3.30: Soil burial testing process; (a) An electronic balance is being utilised for weighing the filament, (b) 50g of soil are added to the plastic container at first, (c) Wrap

the filament with a mesh cloth, (d) Place the wrapped filament on the soil, (e) Buried the wrapped filament in an additional 100g of soil, (f) Repeat the steps to all % of MAPP.

3.10.5 Surface morphology

Surface morphology was carried out to evaluate the state of dispersion and adhesion of poplar and WFs into the PP matrix (Kada et al., 2016). The morphological microstructure of the tensile test specimens, filament surface morphology and filament surface are photographed using a digital microscope. Figure 3.31 depicts the sort of digital microscope used for this experiment.



Figure 3.31: Digital Microscope Dino-Lite AM4114 / AD4113

3.11 Summary

This chapter demonstrates how to perform the study. The research focuses on the production of wood fiber/recycled polypropylene composites with varying percentages of MAPP. Some content was well prepared, while others required more time to prepare. The proportion of MAPP in the composite will affect its tensile strength. Furthermore, the physical test on water absorption and soil burial would vary based on the proportion of MAPP. This method was created from prior research and is currently being applied to new samples. To attain the greatest results, the research made use of every available resource.

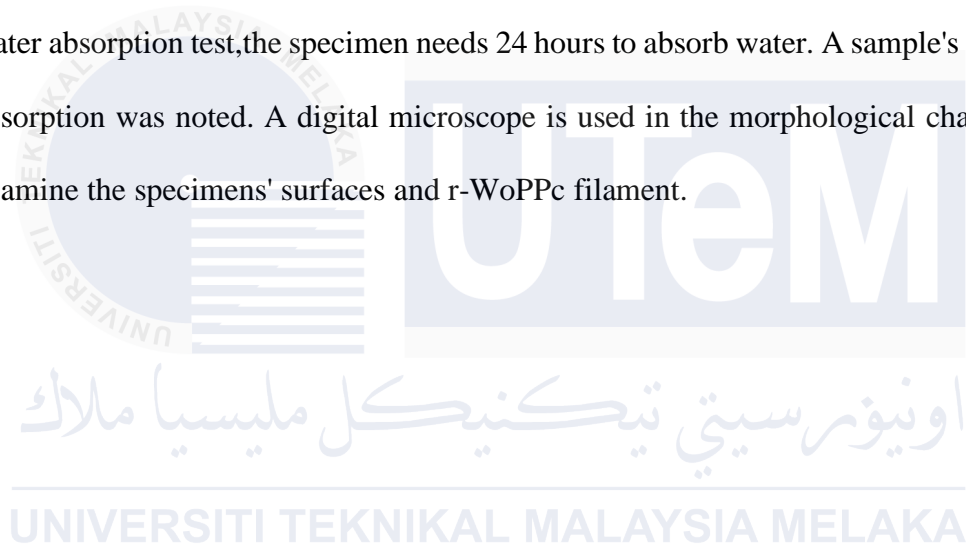


CHAPTER 4

RESULTS AND DISCUSSION

4.1 Introduction

The outcomes of this investigation were determined using a surface morphology, tensile and flexural testing, water absorption characteristics, and soil burial test. Three samples were taken for each specimen, and the average of the results is reported. For the water absorption test, the specimen needs 24 hours to absorb water. A sample's average water absorption was noted. A digital microscope is used in the morphological characteristics to examine the specimens' surfaces and r-WoPPc filament.



4.2 Fabrication of r-WoPPc filament

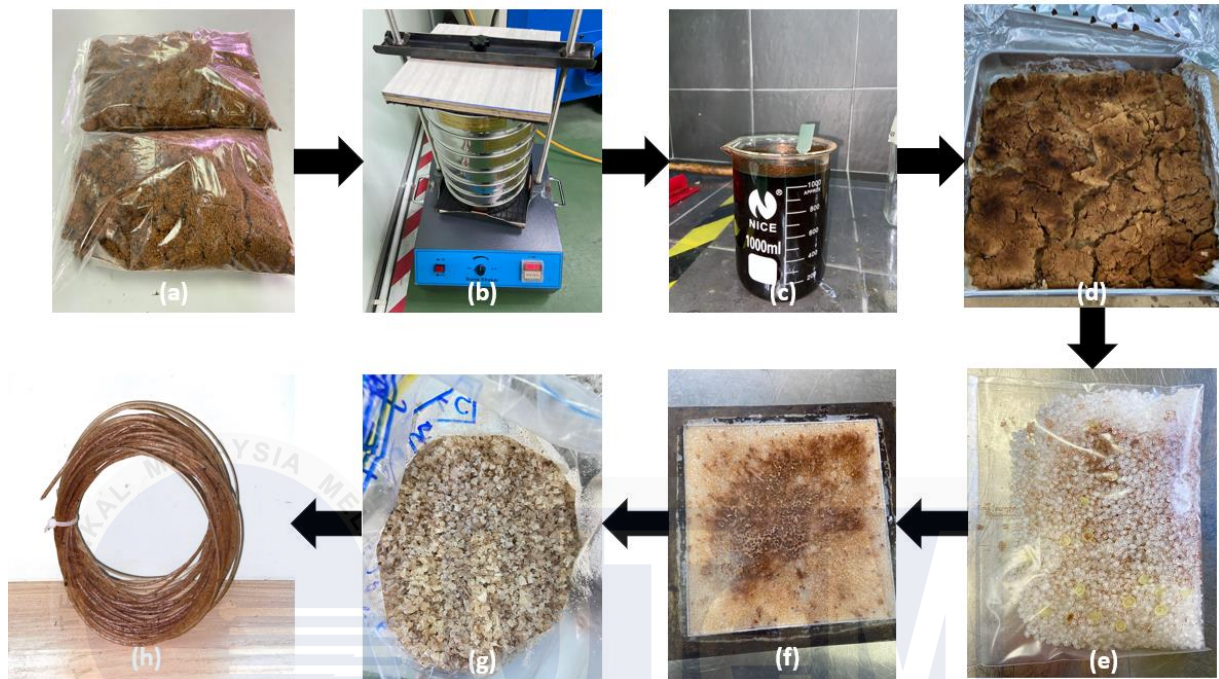


Figure 4.1: Fabrication of r-WoPPc filament; (a) Wood fiber is prepared, (b) A sieving machine is used to sieve wood fiber, (c) NaOH solution is used to treat wood fiber, (d) Post-oven treatment of wood fiber, (e) The recycled polypropylene, wood fiber and MAPP composite is blended within a plastic bag, (f) The r-WoPPc after being hot-pressed, (g) The composite is crushed to pellet, (h) Filament obtained after extrusion process

The production of filament begins by meticulously sieving wood fibers to achieve a size of $125\mu\text{m}$, reaching the desired weight of 500g. Subsequently, the wood fibers undergo treatment with a NaOH solution, enhancing their qualities, including thermal properties for improved interaction with the matrix and the ability to eliminate contaminants from the fiber interface. Following treatment, the weighted mixture of treated wood fibers, recycled polypropylene and various MAPP is introduced into a mould for hot-press method. Once pressed, the resulting r-WoPPc is crushed using a crusher machine, transforming it into pellet size. These pellets are then employed in the extrusion process to create filament. Figure 4.1

depicts the process flow of this project's fabrication of r-WoPPc filament and Figure 4.2 shows the filament of r-WoPPc with different percentage of MAPP.

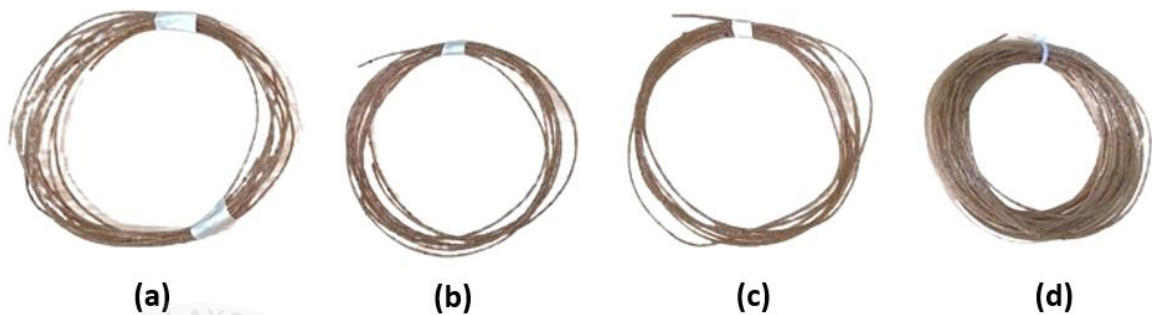


Figure 4.2: Filament of r-WoPPc; (a) Without MAPP, (b) 1% MAPP, (c) 3% MAPP, (d) 5% MAPP

4.3 Fabrication of 3D printed r-WoPPc

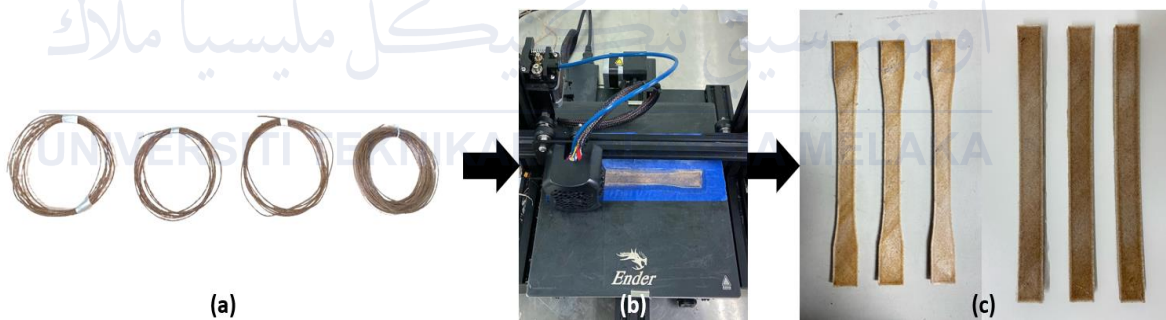


Figure 4.3: Fabrication of 3D printed r-WoPPc

From Figure 4.3, to produce the 3D printed specimens, varying proportions of MAPP filaments (0%, 1%, 3% and 5% MAPP) are employed. The parameters of a 3D printing machine are under scrutiny, encompassing its infill pattern as lines and its infill percentage is 50%, the build plate adhesion type configured as brim, the nozzle temperature at 198°C, bed temperature at 98° and a printing speed of 100 mm/s.

To ensure accurate testing results, the fabricated specimens are then subjected to tensile and flexural testing using appropriate testing equipment. Tensile testing assesses the material's strength under axial forces, while flexural testing evaluates its resistance to bending. The results obtained from these tests provide valuable insights into the mechanical performance of the 3D printed specimens and help validate the efficacy of the r-WoPPc composite achieving the desired properties for structural applications.

4.4 Characterization of the r-WoPPc filament

4.4.1 r-WoPPc filament dimension

The precision of the 1.75mm filament dimension is crucial for maintaining a controlled and uniform extrusion of the specialized composite material through the printing nozzles. This precision results in consistent layer deposition and optimal bonding between the r-WoPPc composite. To ensure the filament consistently adheres to the 1.75mm diameter, the extrusion machines undergo meticulous calibration, ensuring the production of filaments with the specified dimensions. Continuous monitoring throughout the extrusion process further guarantees uniformity (Hachimi et al., 2021). Adjustments in nozzle temperature and pulley speed are made to achieve the desired filament diameter, as indicated by the labeled dimension in Figure 4.4. Observations indicate that a filament diameter of 1.75mm can be consistently achieved at nozzle extrusion temperatures ranging 198-200°C (Nafis et al., 2023).



Figure 4.4: r-WoPPc filament dimension (mm)

4.4.2 r-WoPPc filament density

MAPP-created layers on the fiber surface stimulated an increase in fiber density, as seen in Figure 4.5, where density of 5% has the greatest density values of 6.06 g/mm^3 correspondingly. The MAPP layer that formed on the wood fiber surface improved adhesion with the recycled PP, resulting in higher filament strength. Furthermore, the 5.60 g/mm^3 r-PP filament, which is as a neat filament, does not contain any fiber mixing, making it one of the lowest compared to others, where it also exhibits a close likeness to the commercial value of PP. The lowest density filament is 0% of MAPP at 5.77 g/mm^3 . This might be owing to the absence of the coupling agent, which makes it lighter. Due to the existence of holes and voids in the sample, the density of the filament is reduced. Air trapping during extrusion and moisture absorption during storage are the main causes of formation. The existence of voids and gaps caused poor interfacial adhesion between the fiber and the matrix, resulting in low

strength. It is also important to note that the density results may have been influenced in part by the coupling agent, which might result in a minor decrease in the density of the r-WoPPc, according to (Brites et al., 2019).

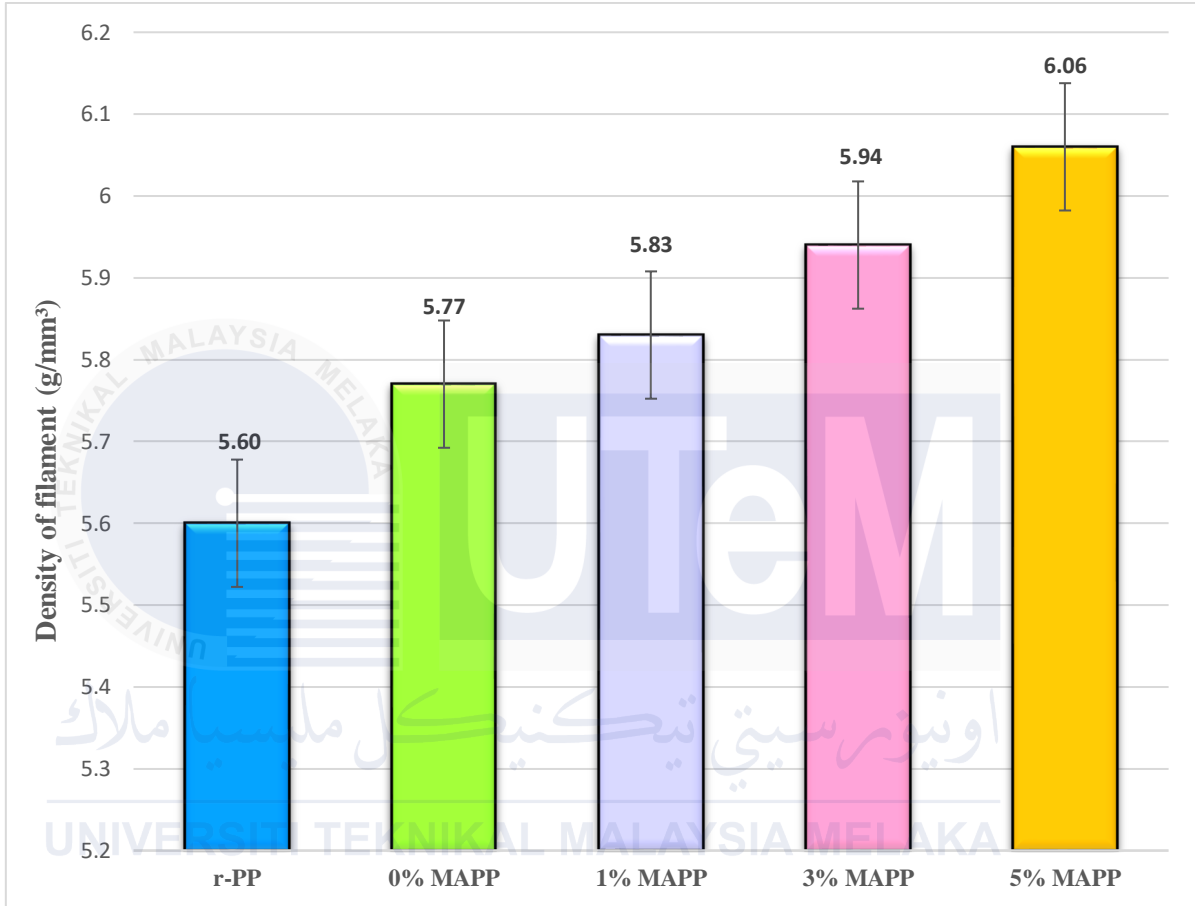


Figure 4.5: Density of filament (g/mm³)

4.4.3 r-WoPPc filament surface morphology

Images of the filament composite with various MAPP loading types captured with a digital microscope are displayed in Figure 4.6. It is commonly recognized that the polymer matrix, reinforcing filler, surface chemistry between components, and processing circumstances all affect the mechanical characteristics of polymer composites. The r-WoPPc filaments with and without MAPP have variable morphologies and surface conditions due to variations in MAPP loading. Referring to Figure 4.6, the 5% MAPP shows the wood fiber

is adequately adhered to the matrix PP and the other percentages (0%, 1% and 3%) shows that the r-WoPPc filament of wood fiber is not adequately adhered to the matrix PP. The reason for this is that the compatibilizer MAPP's anhydride group interacts with the hydroxyl group of alcohol in the wood fiber to decrease the fiber's polarity and hydrophilicity, hence improving the compatibility of the wood fiber with recycled polypropylene (Sanadi et al., 2023). Additionally, it improves the fibers' and polymers' compatibility with the surface simultaneously.

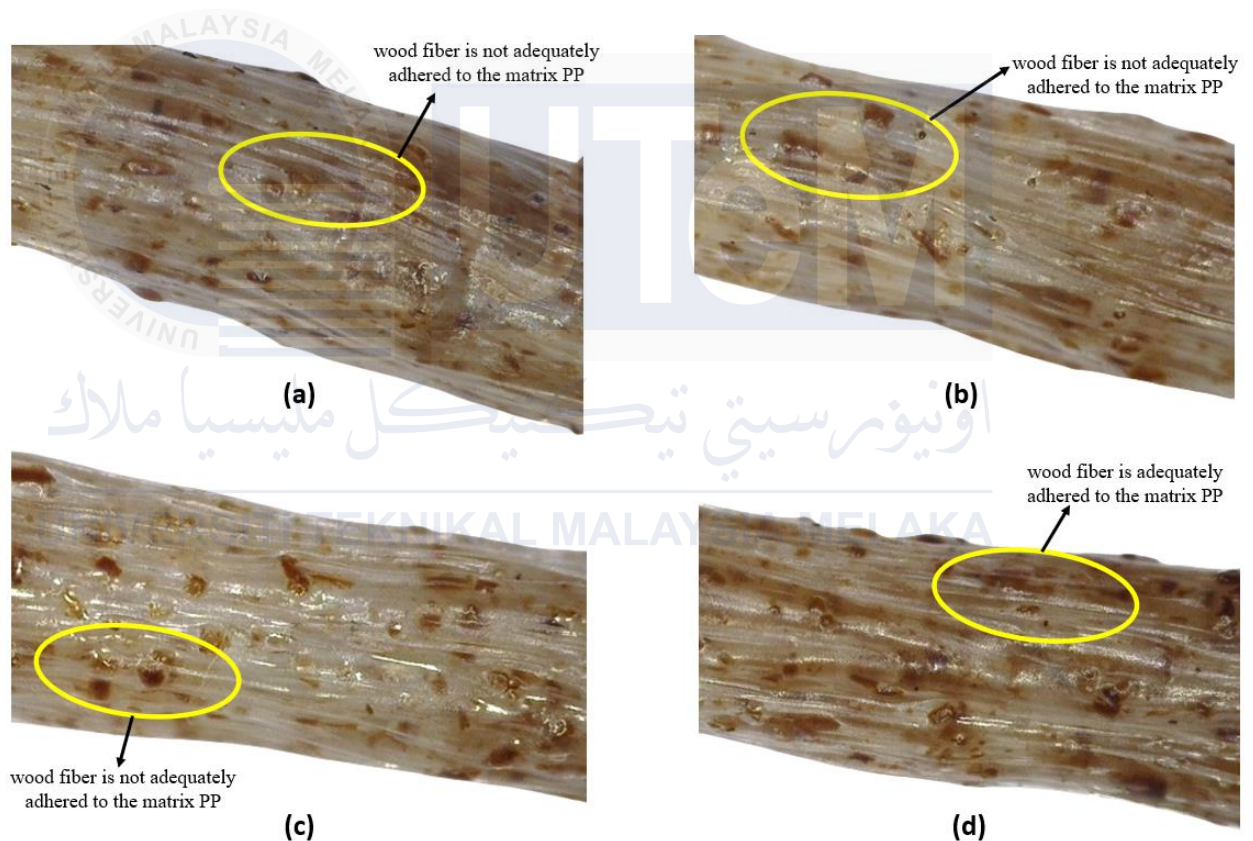


Figure 4.6: High precision micrograph with 250x magnification of r-WoPPc filament surface morphology; (a) without MAPP, (b) 1% MAPP, (c) 3% MAPP, (d) 5% MAPP

4.5 Mechanical properties

4.5.1 Tensile strength

Considering that polypropylene is hydrophobic and wood fibers are hydrophilic, there is a potential opportunity to enhance the composites' characteristics by introducing a compatibilizer. Notably, the inclusion of the compatibilizer led to substantial improvements in both strength and modulus, with extent of enhancement varying based on the quantity of the compatibilizer (Saad, 2020). Figure 4.7 and Figure 4.8 illustrate the influence of MAPP percentage on the tensile characteristics of r-WoPPc with and without MAPP. It can be seen from the figure below that r-WoPPc has the lowest tensile strength and modulus without MAPP. This finding suggests that MAPP improved fiber-matrix interfacial adhesion (Kada et al., 2016).

There was almost little improvement in r-WoPPc tensile strength without the application of MAPP. Tensile strength is only 7.306 MPa. The lack of chemical interaction between the polar wood and non-polar PP matrix caused this outcome. This is also relevant to tensile modulus with the 0% MAPP, as its modulus is just 297.79 MPa. As shown in Figure 4.7, the tensile strength improved by 84.12% at 1% MAPP. Increasing the MAPP content to 3% further boosted the strength by 6.82%, and at 5% MAPP, the strength increased by 6.91%. Remarkably, a larger percentage of PP in the r-WoPPc led to a greater degree of property enhancement (Yang & Yeh, 2020). Although modulus increased with MAPP as well, it did so to a considerably smaller proportion. When the MAPP content was raised from 1 to 5% in comparison to r-WoPPc without any MAPP, a gradual rise of 77.66%, 2.74% and 3.13% was observed. The tensile strength of r-WoPPc improved due to the formation of ester linkages between the carbonyl groups of the MAPP and the hydroxyl groups of the wood fiber when MAPP was used (Nam et al., 2014a).

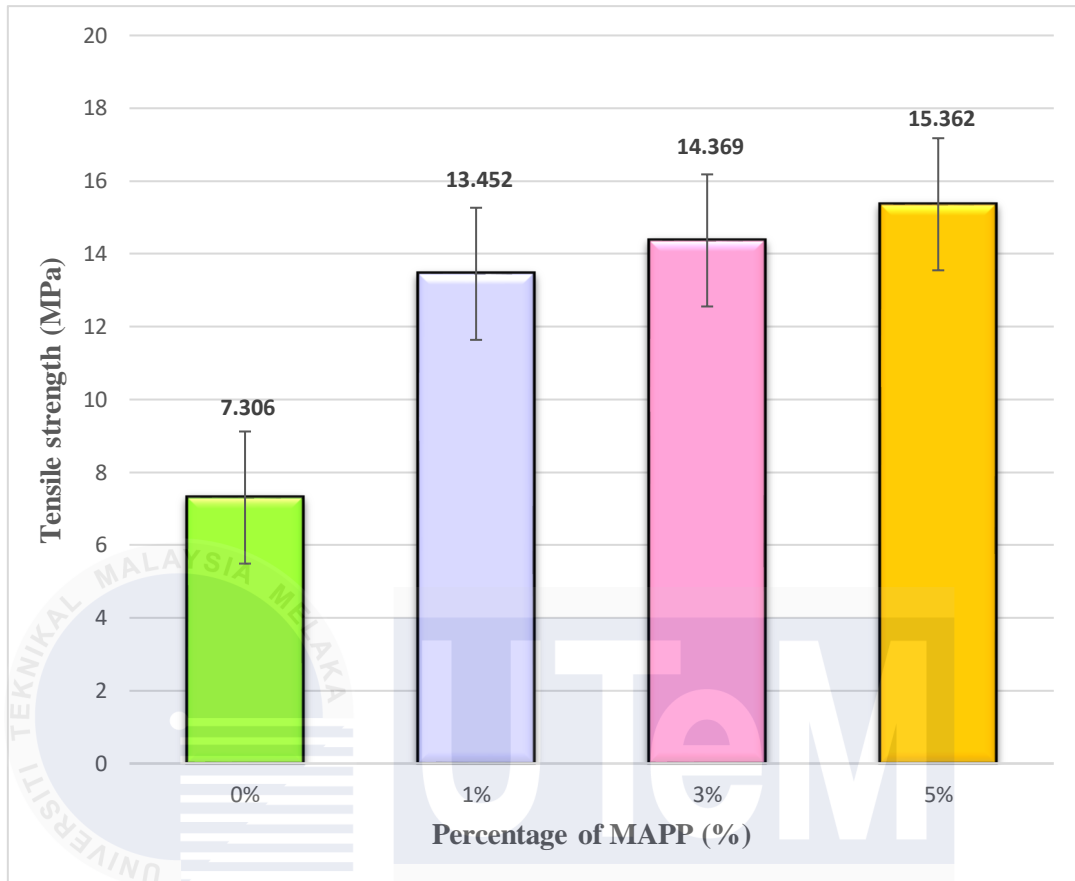


Figure 4.7: Effect of MAPP content on tensile strength of r-WoPPc.

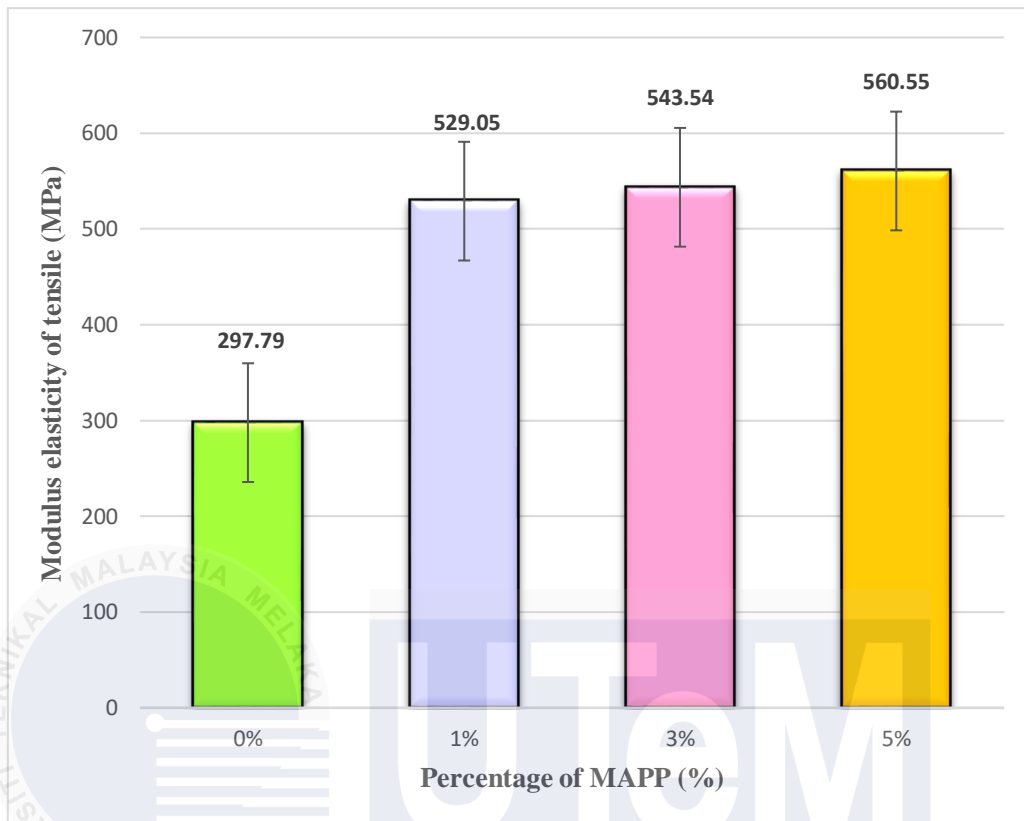


Figure 4.8: Effect of MAPP content on modulus elasticity of tensile of r-WoPPc.

The MAPP reaction mechanism with the lignocellulosic surface hydroxyl groups of r-WoPPc in a tensile test involves a complex interplay of chemical interactions aimed at enhancing the interfacial adhesion between the polymeric matrix and the wood fibers as shows in Figure 4.8. MAPP are reactive moieties that seek to form covalent bonds with the hydroxyl groups present on the surface of lignocellulosic materials such as wood fiber. The reaction typically begins with the nucleophilic attack of the hydroxyl groups on the anhydride ring of MAPP, leading to the formation of ester linkages (Sabri et al., 2013). This esterification process contributes to establishment of a chemical bridge between the MAPP and the lignocellulosic surface (Rowell, 2006).

The increase in the content of 5% MAPP further strengthens the r-WoPPc's performance in a tensile test by enhancing both tensile strength and modulus. The covalent

bonds formed between MAPP and the lignocellulosic surface exhibit a direct correlation with the load transfer capabilities at the interface (Figure 4.9). As the MAPP content to 5%, more covalent bonds are established, significantly enhancing the efficiency of stress transfer between the polymeric matrix and wood fibers. This heightened load transfer capability plays a pivotal role in reducing the likelihood of interfacial failure during tensile loading (Dikobe & Luyt, 2017). The improved adhesion resulting from the increased MAPP content plays a vital role in mitigating the inherent differences in the mechanical properties of the polymeric matrix and wood fiber. The addition of 5% MAPP contributes to a more homogenous composite material, where the covalent bonds act as reinforcing bridges across the interface (Sanadi & Stelte, 2023a). This homogeneity leads to a more uniform distribution of stress and strain across the r-WoPPc, resulting in a robust r-WoPPc that exhibits higher tensile strength and modulus.

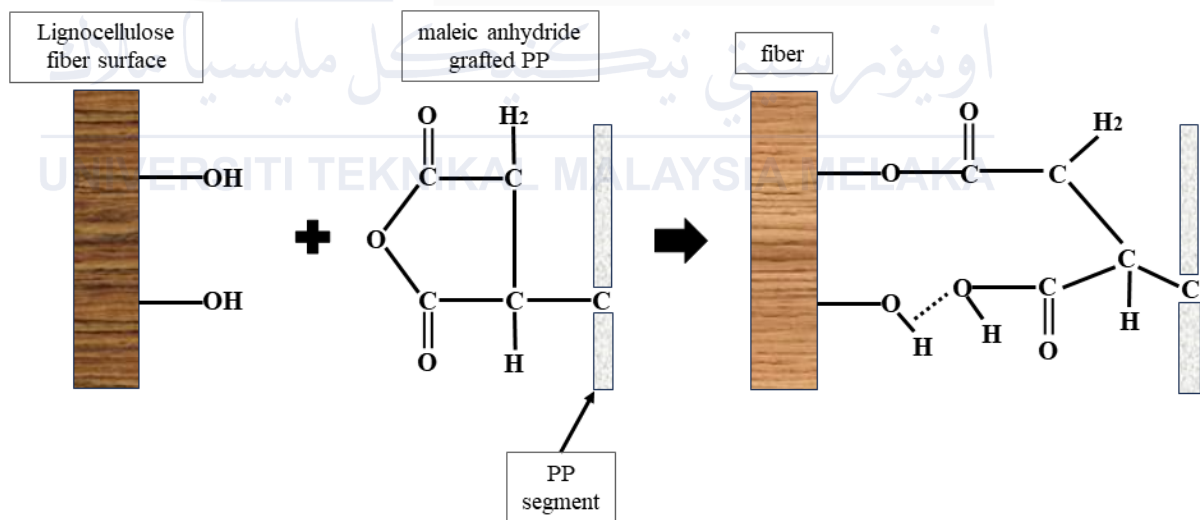


Figure 4.9: MAPP reaction mechanism with a lignocellulosic surface hydroxyl

4.5.2 Tensile fracture surface morphology

Digital microscope was used to look at the fracture surface of the filament tensile test and r-WoPPc filament. This observation was made in order to look at the adherence bonding between recycled polypropylene and wood fiber in all of the composite filaments. The digital

micrographs of the r-WoPPc filament at 250x magnification for MAPP concentrations of 0%, 1%, 3%, and 5% are displayed in Figure 4.10 and 4.11.

Among all the four different tensile test specimens, the r-WoPPc with 5% of MAPP shows the greatest tensile test strength. This greatest strength is associated with the even fracture of tensile as seen in Figure 4.10(d). Moreover, upon scrutinizing Figure 4.10(a), (b), and (c) in comparison to Figure 4.10(d), it is evident that the former exhibits uneven fracture surfaces, indicating matrix failure without effective stress transfer along entire length of the fibers. In stark contrast, the inclusion of MAPP facilitates not only the dispersion of fibers but also enhances their ability to withstand both tensile strength and modulus (Vallejos et al., 2023a).

One key contributing factor 5% MAPP has even surface is that the formation of covalent bonds between the maleic anhydride groups in MAPP and the hydroxyl groups present on the surface of lignocellulosic fibers. This chemical bonding significantly improves the interfacial adhesion, creating a robust connection between the matrix and the reinforcing fibers (Saad, 2020). The improved interfacial adhesion is crucial in promoting effective stress transfer across the r-WoPPc. Unlike uneven fracture surfaces that may result from weak bonding or insufficient load transfer, the inclusion of 5% MAPP ensures that stress is distributed more uniformly along the fibers (Kada et al., 2016). This uniform stress distribution prevents localized concentrations of stress, reducing the likelihood of interfacial failure and promoting a more even fracture surface during mechanical testing, such as in tensile test.

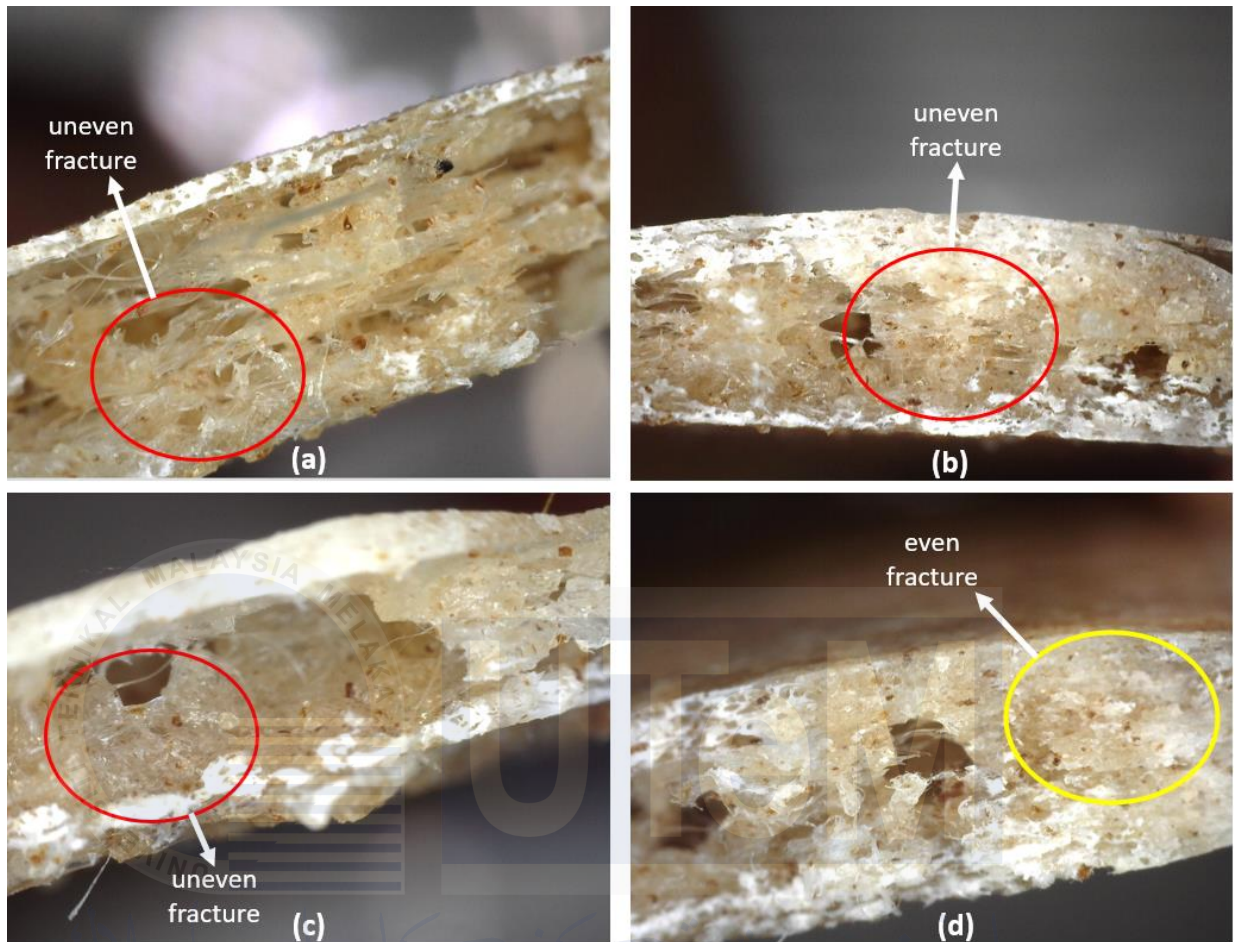
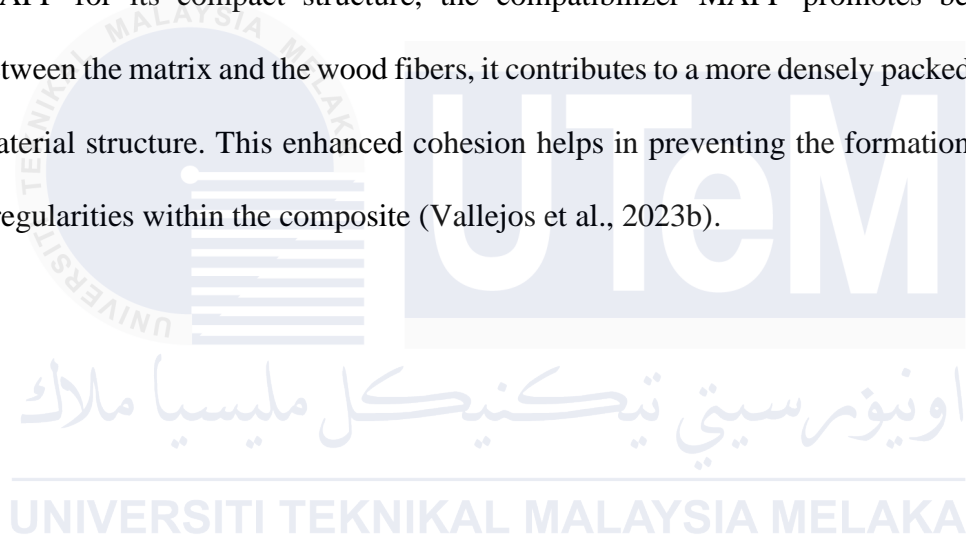


Figure 4.10: High precision micrograph with 250x magnification of r-WoPPc tensile fracture specimens; (a) without MAPP, (b) 1% MAPP, (c) 3% MAPP, (d) 5% MAPP

A noticeable distinction is seen in Figure 4.11, where the 0% MAPP has more voids and hollow structure area. This might be the result of the fiber coming loose from the recycled polypropylene or not adhering completely. Additionally, it illustrates the impact of the fiber tensile test, which extracts fiber during the tensile test to give the 0% MAPP the lowest strength. For the 1% MAPP r-WoPPc in Figure 4.11(b) displays an uneven surface with voids. The presence of voids occurs when the incomplete dispersion or inadequate mixing of MAPP within the r-WoPPc matrix. If MAPP is not uniformly distributed, it may result in localized regions with higher concentrations of MAPP, leading to irregularities in the r-WoPPc structure (Serra-Parareda et al., 2020). Similarly, in the case of the 3% MAPP

r-WoPPc depicted in Figure 4.11(c), although voids are absent, the surface remains uneven. Then, the optimum smooth surface is for 5% MAPP and no voids at all. This shows that 5% has the highest tensile strength and modulus. The formulation is designed to create a well-distributed mix of MAPP with the other components at 5% MAPP content, ensuring that MAPP works repeatedly across the material. This uniform distribution reduces the possibility of localized concentrations or irregularities resulting in a void-free and structurally robust composite (Mijiyawa et al., 2015). As for the compact structure of 5% MAPP for its compact structure, the compatibilizer MAPP promotes better adhesion between the matrix and the wood fibers, it contributes to a more densely packed and cohesive material structure. This enhanced cohesion helps in preventing the formation of voids and irregularities within the composite (Vallejos et al., 2023b).



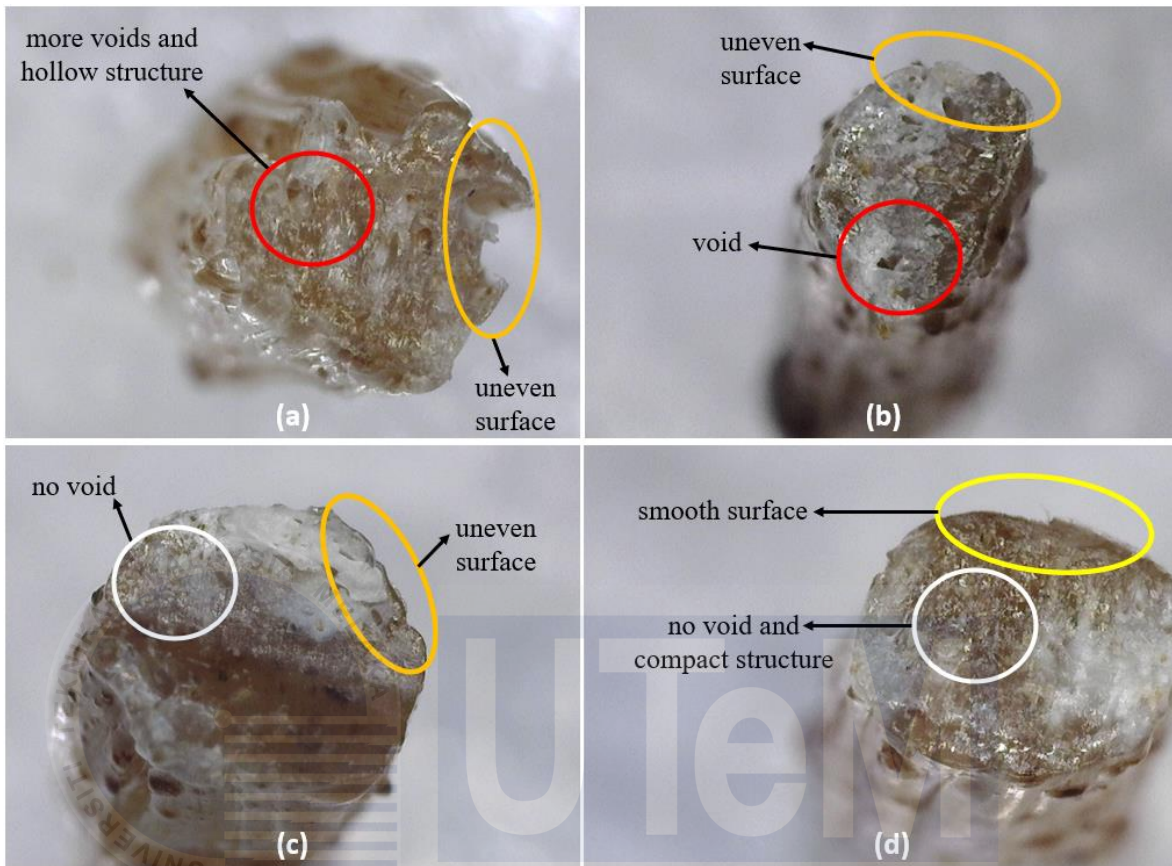


Figure 4.11: High precision micrograph with 250x magnification of r-WoPPc filament; (a) without MAPP, (b) 1% MAPP, (c) 3% MAPP, (d) 5% MAPP

4.5.3 Flexural strength

Figure 4.12 and 4.13 depicts the change in flexural strength and modulus of r-WoPPc with and without a coupling agent. The modulus increased with increasing poplar fiber content, both with and without MAPP. The rigidity and homogeneous dispersion of wood fibers are responsible for this rise. Regardless of the bonding action of MAPP, r-WoPPc with coupling agent have greater flexural strength than those without coupling agent.

The amount of MAPP utilized determined the extent of improvement in flexural characteristics of the r-WoPPc. As shown in Figure 4.12, the flexural strength is the lowest at 0% of MAPP, with a value of 11.95, and the flexural modulus is likewise the lowest, with

a value of 355.73 (Figure 4.13). Flexural strength with 1% of MAPP rose by 2.6%, reaching 12.26 MPa, while the modulus exhibited a more substantial increase of approximately 16.71%, climbing from 355.73 to 415.17 MPa. As MAPP content was raised to 3% in the r-WoPPc, strength increased from 12.26 to 16.10 MPa (31.32% increase) and modulus raised from 415.17 to 530.74 MPa (27.84% increase). The amount of MAPP directly effects the improvement in r-WoPPc characteristics. Several studies have found that adding MAPP improves interfacial adhesion and binding between the matrix and reinforcement (Sanadi et al., 2023). When 5% of MAPP was employed as a compatibilizer for r-WoPPc, it resulted the highest percentage of strength and modulus from all the other percentages of MAPP. It increased the strength r-WoPPc by 40.37% from 16.10 to 22.60 MPa and the modulus by 52.79% from 530.74 to 810.90 MPa. R-WoPPc containing MAPP proved less breaking than pullouts, indicating an effective interaction between matrix and reinforcement. The OH groups in wood fiber establish ester bond with MAPP, resulting in improved interactions (Kada et al., 2016).

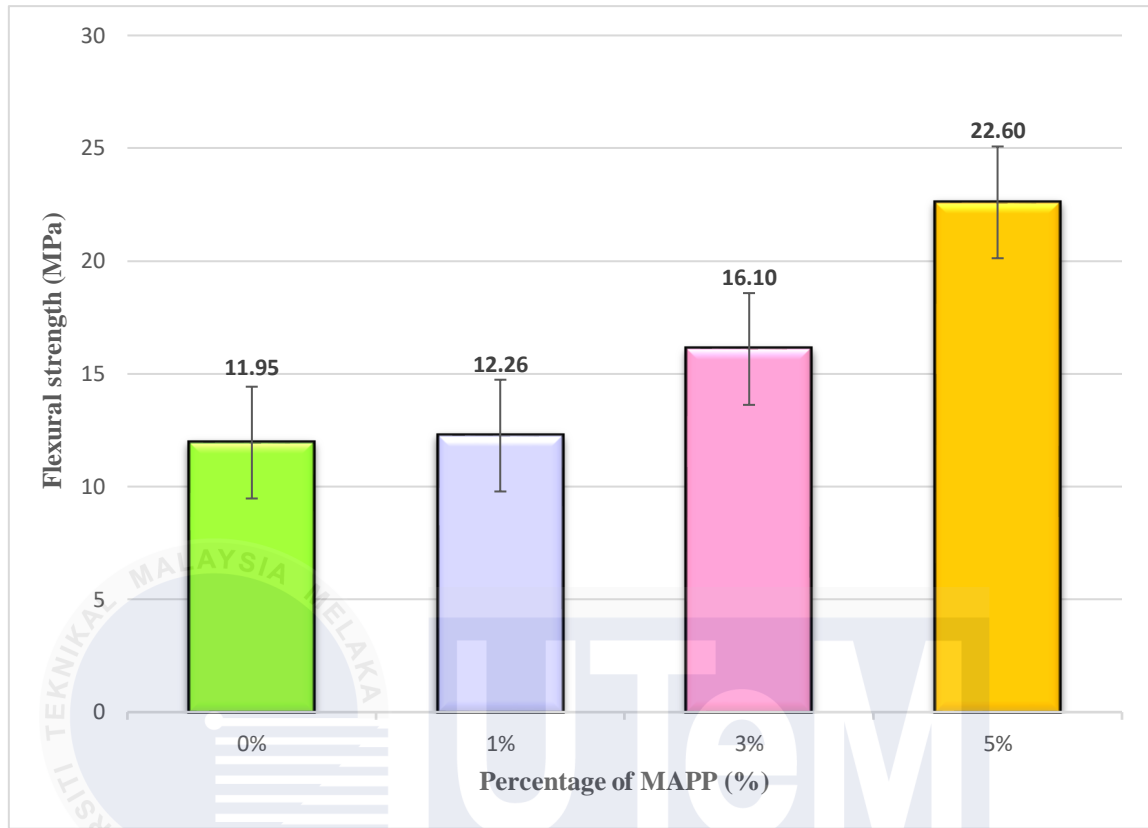


Figure 4.12: Effect of MAPP content on flexural strength of r-WoPPc.

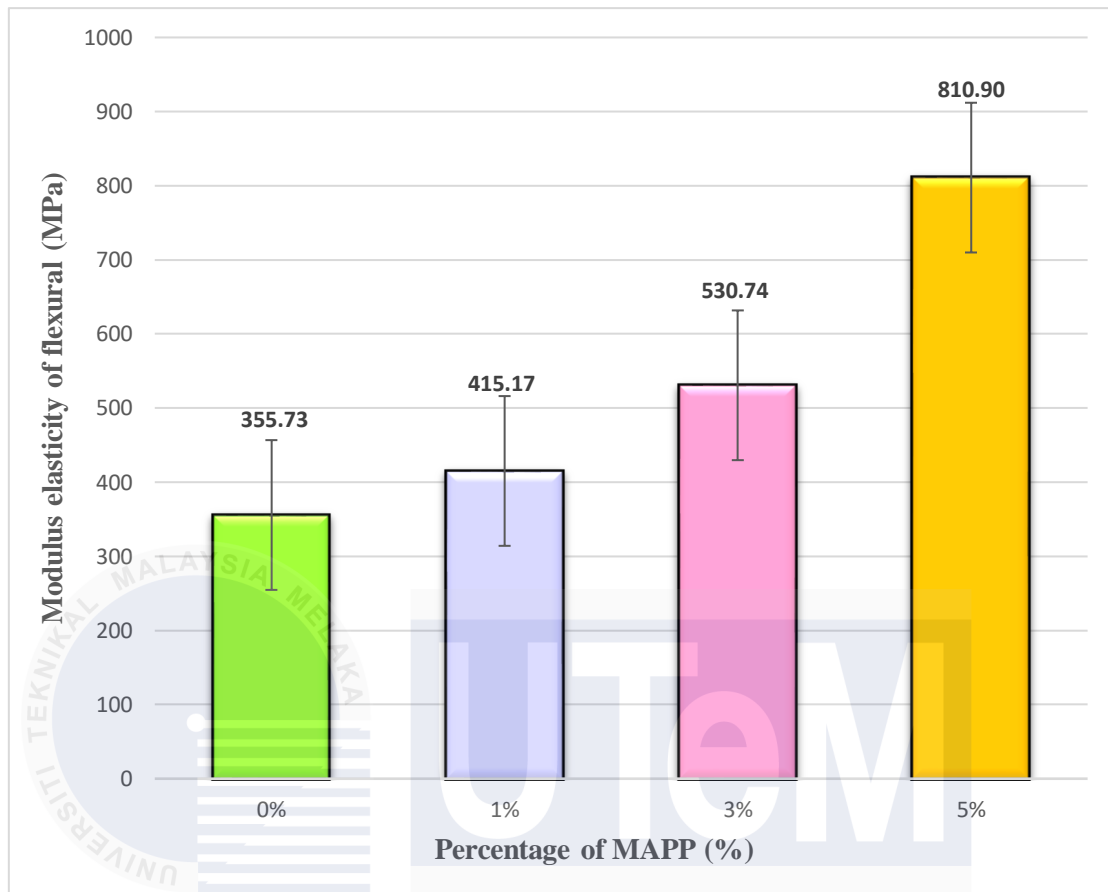


Figure 4.13: Effect of MAPP content on modulus elasticity of flexural of r-WoPPc.

The presence of 5% MAPP that gives the highest flexural strength and modulus is likely optimizing the dispersion of wood fibers within the polymer matrix. Uniform distribution of the reinforcing material is crucial for achieving a balanced load distribution during flexural loading, leading to increased strength and modulus. The effect of 5% MAPP on the crystallinity and structure of the polypropylene matrix further comes into play, influencing the material's resistance to deformation and enhancing its mechanical properties (Saad, 2018). The observed synergy between the wood fibers and MAPP, fostering effective load transfer between the matrix and reinforcement, also contributes to the r-WoPPc's superior flexural characteristics (Sanadi et al., 2023). Not like lower percentage of MAPP (0%, 1% and 3%) concentrations, the effectiveness of the coupling agent in

promoting interfacial adhesion between the recycled polypropylene matrix and wood fiber may be compromised. The lower percentage of MAPP might lead to weaker bonding at the interface, increasing the susceptibility to delamination and decreasing the overall flexural strength (Che Ismail & Akil, 2018). Additionally, lower concentrations of MAPP may result in suboptimal dispersion of wood fibers within the polymer matrix. Inadequate dispersion can lead to uneven load distribution during flexural loading, creating stress concentrations and diminishing the material's strength and modulus. Furthermore, the impact of MAPP on the crystallinity and polymer chain structure of the polypropylene matrix may be less pronounced at lower concentration, limiting its ability to enhance the material's resistance to deformation (Kim et al., 2007).

4.6 Physical properties

4.6.1 Water absorption test

The addition of emulsion (MAPP) significantly reduced water absorption, as seen in Figure 4.14 and Table 4.1. Upon increasing MAPP and immersion time, the amount of water absorbed decrease gradually (Nam et al., 2014b). R-WoPPc without a compatibilizer absorb up to 5.56% of their weight in water within 24 hours, affecting their strength and stability. MAPP containing composites exhibit much reduced absorption in comparison. Even the addition of 1% MAPP reduced water absorption to 2.24%, compared to 5.56% without any compatibilizer. Despite being immersed in water for 24 hours, raising the MAPP level to 3% and 5% decreased water absorption to 1.6% and 1.25%, respectively. MAPP forms a hydrophobic layer on the wood fiber that restricts movement of water. There are also fewer voids which reduces water movement and consequently, the overall water absorption.

Table 4.1: Weight of r-WoPPc absorption test

Percentage of MAPP (%)	Weight (g)	
	before	after
0	0.0540	0.0570
1	0.0670	0.0685
3	0.0810	0.0823
5	0.0800	0.0810

اونيورسيتي تيكنيكل مليسيا ملاك

UNIVERSITI TEKNIKAL MALAYSIA MELAKA

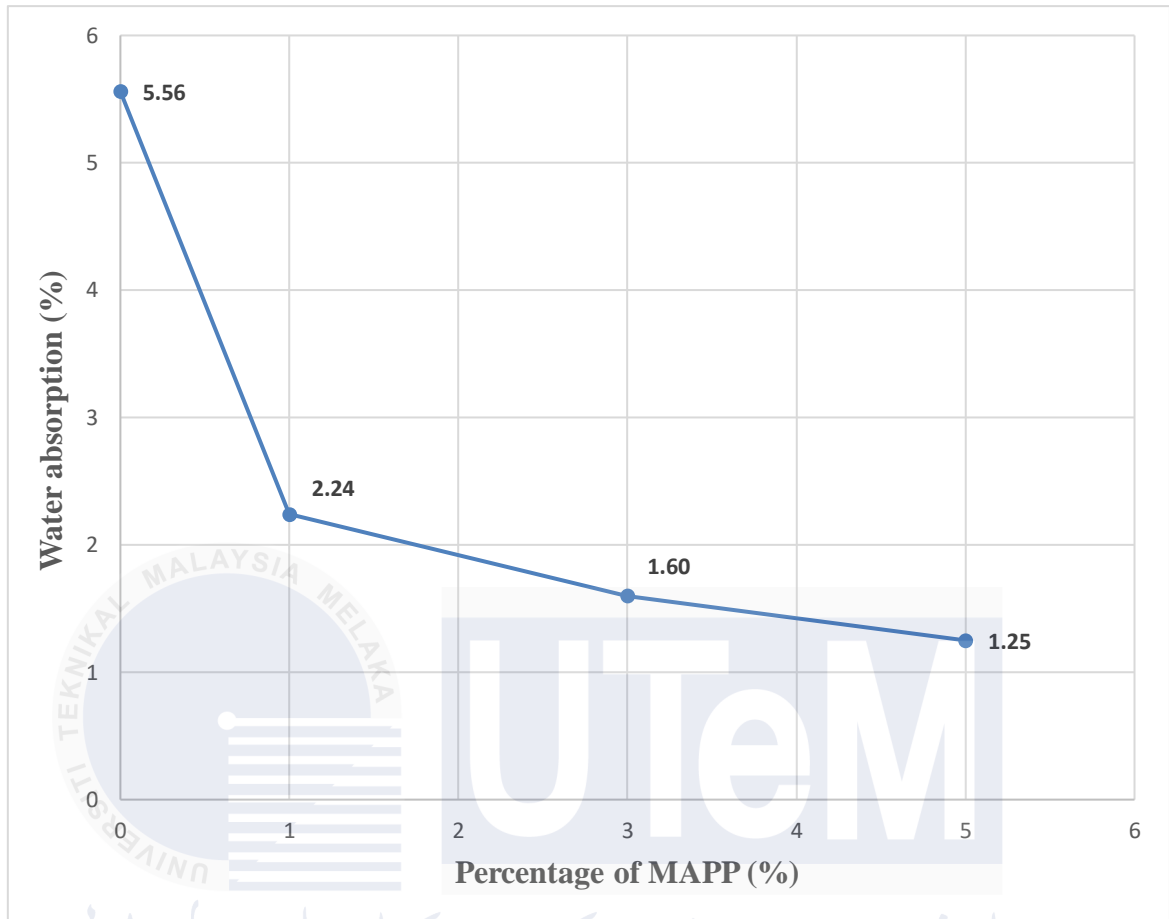


Figure 4.14: Water absorption rate of r-WoPPc (%)

When 5% of MAPP is used, it enhanced stickiness limits the r-WoPPc's capacity to absorb water. MAPP's functional groups may create chemical connections with the polymer matrix as well as the wood fibers, resulting in a more homogenous and water-resistant substance. Water absorption must be reduced in order for the r-WoPPc's mechanical properties to be maintained over time. Excessive water absorption can cause swelling, dimensional instability and composite material breakdown (Brites et al., 2019). Therefore, increasing the amount of MAPP is expected to improve the water resistance of the r-WoPPc by improving interfacial adhesion and minimizing the absorption of water into the material.

Figure 4.15 represent the compatibilization mechanism of MAPP on the r-WoPPc composite filament. First, the MAPP's anhydride end combines with a hydroxyl group on the surface of the wood substance to generate an ester bond. The PP tail on the grafted MAPP then becomes entangled with the melted thermoplastic, forming a mechanical contact between the hydrophilic lignocellulosic and the hydrophobic thermoplastic. This improved compatibility reduces the tendency of composite material to absorb water. As a result, the overall water absorption decreases with an increasing amount of MAPP (Rowell, 2006).

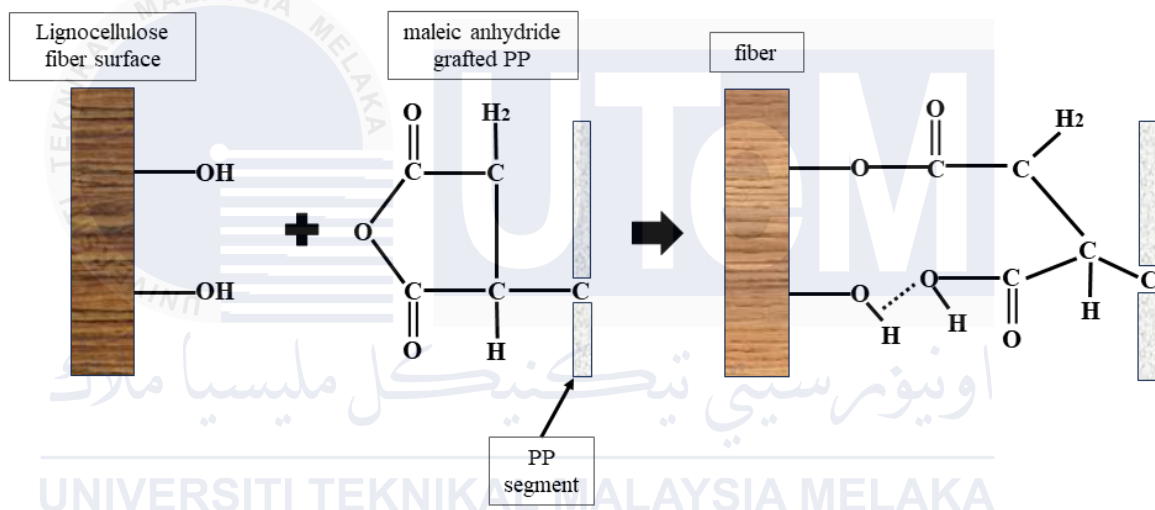


Figure 4.15: MAPP reaction mechanism with a lignocellulosic surface hydroxyl

4.6.2 Soil burial test

One technique used to track the biodegradation rate of composites is weight loss measurement. The filaments were buried and monitored every seven days until day 21 in order to assess the biodegradability rate of the four distinct MAPP formulation variants (0%, 1%, 3%, and 5%), as indicated in Table 4.2 and Figure 4.16. The incorporation of compatibilizing agent marginally reduced bioactivity by stabilizing the interface (Brebu, 2020). Soil burial testing determines the biodegradability of materials embedded in soil. Weight loss in this context often reflects material degradation or breakdown over time as a

result of microbial activity in the soil. Living things are responsible for achieving biodegradability. The breakdown of organic materials and the release of nutrients into forms that plants may use are processes that soil microbes are essential for (Chaisuwan et al., 2022).

Table 4.2: Weight loss of r-WoPPc (g)

Sample/Days	Day 0	Day 7	Day 14	Day 21
0% MAPP	0.063	0.063	0.063	0.062
1% MAPP	0.075	0.075	0.074	0.074
3% MAPP	0.086	0.085	0.083	0.082
5% MAPP	0.075	0.073	0.069	0.067

Maleic anhydride polypropylene (MAPP) percentage has a significant impact on the behavior of r-WoPPc during soil burial tests. MAPP is a popular coupling agent used to increase the compatibility of hydrophobic polypropylene matrix with the hydrophilic wood fibers. In the context of soil burial testing, the concentration of MAPP in the composite can have significant effects on both polypropylene and wood fiber components. Higher levels of MAPP generally enhance compatibility, reducing the risk of phase separation between polypropylene and wood fiber (Trombetta et al., 2010). This improved compatibility results in a stronger interfacial adhesion, potentially leading to better stability of the composite in the soil conditions. Additionally, MAPP acts as a water repellent, reducing the water absorption of the r-WoPPc. This is crucial in soil burial testing, as excessive water absorption could lead to swelling and degradation of the material (Shahrim et al., 2022). The introduction of reactive sites on the polypropylene matrix by MAPP can also make the r-WoPPc more susceptible to microbial attack, potentially accelerating the degradation

process. The enhanced compatibility provided by MAPP exposes a larger surface area of wood fibers to microbial activity, further contributing to the degradation of r-WoPPc.

The water absorption of r-WoPPc demonstrates a decrease in water intake percentage with the increasing content of MAPP. Consequently, in soil burial testing the rise of MAPP content is observed to enhance the degradability of r-WoPPc due to its reduced water uptake. Table 4.2 shows that the 5% with MAPP had the largest weight reduction. The second goes to 3% MAPP, then 1% MAPP and finally 0% MAPP. The highest weight loss, recorded at 10.67% after 21 days of soil burial, was observed in the sample containing 5% MAPP, corresponding to a weight loss of 0.067g. Additionally, the percentages of weight loss for this r-WoPPc were 8% at day 14 and 2.67% at day 7, as illustrated in Figure 4.16. This is due to the introduction of reactive sites on the polypropylene matrix by increased MAPP addition can also make the r-WoPPc more susceptible to microbial attack, thus speeding up the breakdown process (Shahrim et al., 2022).

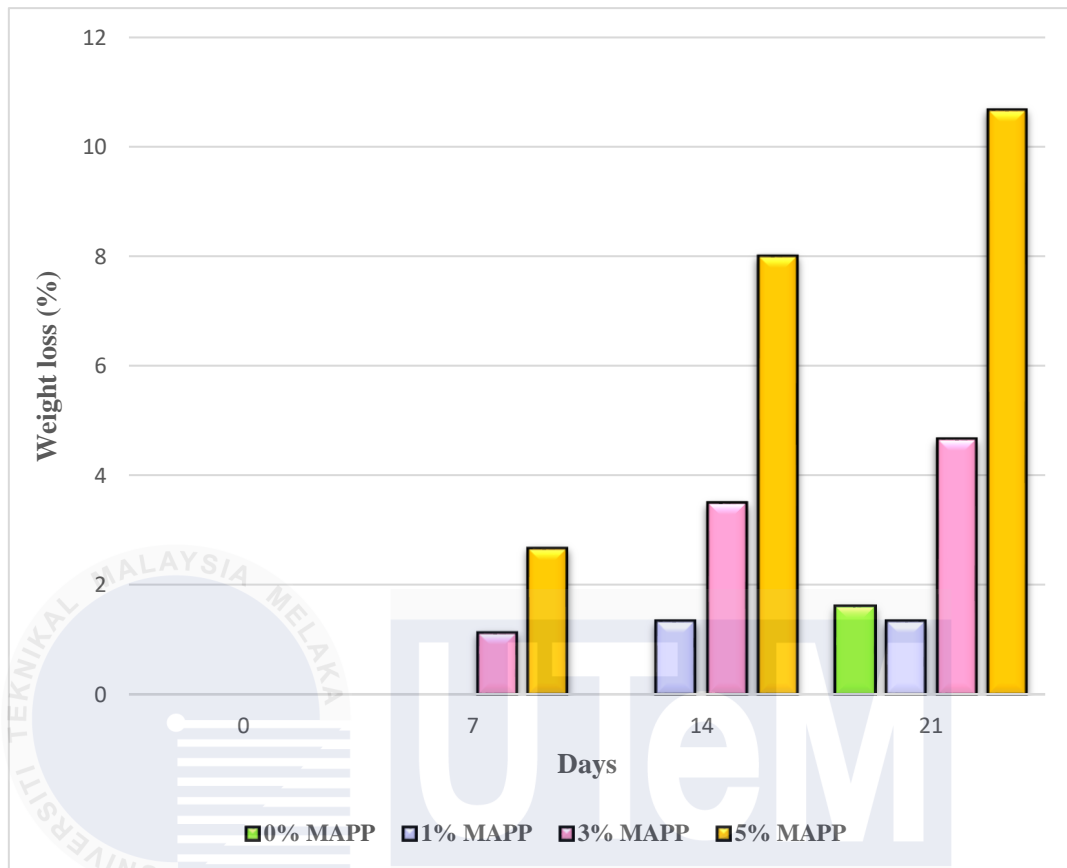


Figure 4.16: Weight loss of r-WoPPc after buried in soil for 21 days.

Currently, the lowest weight loss is observed in the r-WoPPc without the presence of a coupling agent (0% MAPP). As indicated in Figure 4.16, only by day 21 does the r-WoPPc exhibit a percentage weight loss of 1.59%. The absence of a coupling agent on days 7 and 14 results in a consistent percentage weight loss, attributed to the lack of strong interfacial adhesion, which leads to a less homogeneous structure, rendering the material more resistant to microbial attack (Shahrim et al., 2022). Furthermore, the absence of MAPP eliminates its water-repellent effect, allowing the composite to absorb more water, potentially impeding degradation. The lack of MAPP may also restrict the formation of reactive sites, diminishing the r-WoPPc's susceptibility to microbial breakdown (Siakeng et al., 2020).

CHAPTER 5

CONCLUSION AND RECOMMENDATIONS

5.1 Conclusion

Several studies have been conducted to achieve the research objective of (1) to produce 3D-printing filament with the material made of wood fiber, recycled polypropylene with the different ratios of MAPP, (2) to investigate mechanical properties of the 3D printed samples from filament made of wood fiber, and recycled polypropylene with and without the use of MAPP coupling agent. Therefore, from all the analysis, there are few important conclusions were draw as follow:

- (1) To conclude, the MAPP loading of 0%, 1% and 3% MAPP shows that wood fiber is not adequately adhered to the matrix PP. Possibility there is a lack of chemical bonding between the above group which is rPP and r-wood dust. With adding 5% MAPP, the wood fiber is adequately adhered to the matrix PP. This is because after the addition of the compatibilizer MAPP, its anhydride group reacts with the alcohol hydroxyl group in the wood fiber to reduce the polarity and hydrophilicity of the fiber, which further enhances the compatibility between the wood fiber and polypropylene.
- (2) The tensile and flexural strength increased by 110.27% and 89.12% compared to without MAPP. The tensile and flexural strength of r-WoPPc improved due to the formation of ester linkages between the carbonyl groups of the MAPP and the hydroxyl groups of the wood fiber when MAPP was used. Better adhesion between wood fiber and PP can be observed from of 5% r-WoPPc morphology

of the tensile fracture surface shown an even fracture for the specimen with 5% MAPP while the specimens with 0%, 1% and 3% MAPP showed uneven fracture.

- (3) The water absorption rate (WAR) of all the filament noticeably increased upon increasing the MAPP loading, due to the association of hydrophilic groups of wood fiber with water. The water absorption shows that 5% MAPP adhesion has the lowest percentage of water absorbed for 42.1%. The soil burial result has proven that with the presence of 5% MAPP in the composite makes the soil burial degradation of filament with the highest weight loss of 8.06%. This is because the introduction of reactive sites on the polypropylene matrix by 5% MAPP make the r-WoPPc more susceptible to microbial attack, potentially accelerating the degradation process.

At the end of this study of “THE INFLUENCE OF MAPP COUPLING AGENT ON 3D PRINTING FILAMENT MADE OF WOOD FIBER AND RECYCLED POLYPROPYLENE COMPOSITES” there are a few conclusions that can be made. The addition of a coupling agent was shown to improve bonding conditions and increase the surface condition of the filament. The increase in tensile and flexural, and the decrease in water absorption properties and void fraction of the r-WoPPc with the MAPP as compatibilizer indicate the enhancement of the interfacial adhesion between wood fiber (WF) and recycle polypropylene (rPP) in WPC. The sample of r-WoPPc show variant result because of the different type of MAPP loading. This indicated that these compatibilizer have a positive effect on the interfacial adhesion between the filler and the matrix.

5.2 Recommendations

To enhance the precision and reliability of the testing methodologies, it is necessary to argue for an increase in the number of samples utilised during the stage of testing. While informative, the current dataset may not fully capture the diversity and unpredictability inherent in the phenomenon under investigation. Increasing the sample size allows the project to obtain a more full and representative range of data points, minimising biases and contributing to a more accurate picture of the underlying trends and patterns. The statistical robustness of the findings is intimately tied to the size of the sample, and a bigger dataset would not only increase the findings' credibility but also their generalizability to a broader population. Besides, to optimise printing results and improve the overall quality of testing specimens, it is critical to conduct a thorough investigation of additional 3D printing properties and procedures. The present understanding of 3D printing parameters may provide useful insights, but further research into a broader range of printing factors, such as layer thickness, infill density, print speed, and temperature settings, is required. Each of these parameters is critical in assessing the structural integrity, dimensional correctness, and surface polish of 3D-printed items, all of which have a substantial influence on the dependability of testing specimens.

5.3 Project Potential

The study of the effects of MAPP (Maleic Anhydride Polypropylene) coupling agent on the mechanical characteristics of wood fiber and recycled polypropylene composites has enormous project potential with far-reaching ramifications. This research project not only addresses the urgent demand for sustainable materials, but it also advances composite material science. By delving into the complexities of how MAPP, a commonly used coupling agent, affects the mechanical properties of wood fiber and recycled polypropylene

composites, the project hopes to gain valuable insights that will revolutionize the development of eco-friendly and high-performance materials. Potential applications include building (beams, panels), automotive (side panels, fenders, bumpers) and consumer products (chair, tables, cabinets), where such composites might replace existing materials, providing a more sustainable alternative without sacrificing mechanical strength and durability. Furthermore, the project's discoveries have the potential to inform future material design techniques, creating the path for innovative approaches in the larger field of polymer composites. As society increasingly embraces sustainable practices, the project on the effects of MAPP coupling agents is poised to make significant contributions to both academia and industry, fostering advancements that align with contemporary environmental and technological needs. Then, the research of this study has a strong potential for being commercialization in industry as a commercial bio composite filament. This filament also potentially can be used in any type of FDM 3D print machine and also their pellet can be extruded through any kind of extruder.

REFERENCES

- Abedi, M., Hassanshahi, O., Rashiddel, A., Ashtari, H., Seddik Meddah, M., Dias, D., Arjomand, M. A., & Keong Choong, K. (2023). A sustainable cementitious composite reinforced with natural fibers: An experimental and numerical study. *Construction and Building Materials*, 378, 131093. <https://doi.org/10.1016/J.CONBUILDMAT.2023.131093>
- Aguirre-Cortés, J. M., Moral-Rodríguez, A. I., Bailón-García, E., Davó-Quiñonero, A., Pérez-Cadenas, A. F., & Carrasco-Marín, F. (2023). 3D printing in photocatalysis: Methods and capabilities for the improved performance. In *Applied Materials Today* (Vol. 32). Elsevier Ltd. <https://doi.org/10.1016/j.apmt.2023.101831>
- Akhoundi, B., & Sousani, F. (2023). An experimental investigation of screw-based material extrusion 3D printing of metallic parts. *Journal of Engineering Research*, 100102. <https://doi.org/10.1016/J.JER.2023.100102>
- Almeshari, B., Junaedi, H., Baig, M., & Almajid, A. (2023a). Development of 3D printing short carbon fiber reinforced polypropylene composite filaments. *Journal of Materials Research and Technology*, 24, 16–26. <https://doi.org/10.1016/J.JMRT.2023.02.198>
- Almeshari, B., Junaedi, H., Baig, M., & Almajid, A. (2023b). Development of 3D Printing Short Carbon Fiber Reinforced Polypropylene Composite Filaments. *Journal of Materials Research and Technology*. <https://doi.org/10.1016/j.jmrt.2023.02.198>
- Altinkaynak, A. (2010). *Three dimensional finite element simulation of polymer melting and flow in a single-screw extruder : optimization of screw channel geometry*. <http://digitalcommons.mtu.edu/etdshttp://digitalcommons.mtu.edu/etds/346>
- Ansari, R., Rouhi, S., Ahmadi, M., Ansari, R., Rouhi, S., & Ahmadi, M. (2018). On the thermal conductivity of carbon nanotube/polypropylene nanocomposites by finite element method Structural Analysis of CF-CNT-Composite using Finite Element-Based Multi-Scale Modeling Approach View project nanocomposites View project On the Thermal Conductivity of Carbon Nanotube/Polypropylene Nanocomposites by Finite Element Method. *JCAMECH*, 49(1), 70–85. <https://doi.org/10.22059/jcamech.2017.243530.195>
- Ardente, F., Cellura, M., Lo Brano, V., & Mistretta, M. (2007). Multidiscipline LCA application to an experience of industrial symbiosis in South of Italy. *Integrated Environmental Assessment and Management*, preprint(2009), 1. https://doi.org/10.1897/ieam_2008-065.1
- Awogbemi, O., & Kallon, D. V. Von. (2023). Achieving affordable and clean energy through conversion of waste plastic to liquid fuel. *Journal of the Energy Institute*, 106, 101154. <https://doi.org/10.1016/J.JOEL.2022.101154>
- Behera, S., Prasad, N., & Kumar, S. (2018). Study of Mechanical Properties of Bamboo fibers before and after Alkali Treatment. In *International Journal of Applied Engineering Research* (Vol. 13, Issue 7). <http://www.ripublication.com>
- BG, P. K., Mehrotra, S., Marques, S. M., Kumar, L., & Verma, R. (2023). 3D printing in personalized medicines: A focus on applications of the technology. *Materials Today Communications*, 35, 105875. <https://doi.org/10.1016/J.MTCOMM.2023.105875>
- Bobo, E. (2013). *Development of a controllable polymer system using interpenetrating networks*. <https://www.researchgate.net/publication/280662230>
- Brebu, M. (2020). Environmental Degradation of Plastic Composites with Natural Fillers—A Review. *Polymers*, 12(1), 166. <https://doi.org/10.3390/polym12010166>

- Brites, F., Malça, C., Gaspar, F., Horta, J. F., Franco, M. C., Biscaia, S., & Mateus, A. (2019). The Use of Polypropylene and High-Density Polyethylene on Cork Plastic Composites for Large Scale 3D Printing. *Applied Mechanics and Materials*, 890, 205–225. <https://doi.org/10.4028/www.scientific.net/amm.890.205>
- Chaisuwan, K., Anurakumphan, D., Hemmanee, S., Ruamcharoen, J., & Leelakriangsak, M. (2022). SOIL BURIAL DEGRADATION OF STARCH-BASED FILMS ON MICROBIAL LOAD AND PLANT GROWTH. *Journal of Sustainability Science and Management*, 18(3), 110–124. <https://doi.org/10.46754/jssm.2023.03.008>
- Che Ismail, N. H., & Akil, H. M. (2018). Improving the Flexural Properties of Abs/Muscovite Composites by Introducing Modified Muscovite. *Journal of Physics: Conference Series*, 1082(1). <https://doi.org/10.1088/1742-6596/1082/1/012016>
- Cheewawuttipong, W., Fuoka, D., Tanoue, S., Uematsu, H., & Iemoto, Y. (2013). Thermal and mechanical properties of polypropylene/boron nitride composites. *Energy Procedia*, 34, 808–817. <https://doi.org/10.1016/j.egypro.2013.06.817>
- Črešnar, K. P., Bek, M., Luxbacher, T., Brunčko, M., & Zemljič, L. F. (2021). Insight into the surface properties of wood fiber-polymer composites. *Polymers*, 13(10). <https://doi.org/10.3390/polym13101535>
- Crowley, M. M., Zhang, F., Repka, M. A., Thumma, S., Upadhye, S. B., Battu, S. K., McGinity, J. W., & Martin, C. (2007). Pharmaceutical applications of hot-melt extrusion: Part I. In *Drug Development and Industrial Pharmacy* (Vol. 33, Issue 9, pp. 909–926). <https://doi.org/10.1080/03639040701498759>
- Das, A. K., Agar, D. A., Rudolfsson, M., & Larsson, S. H. (2021). A review on wood powders in 3D printing: processes, properties and potential applications. In *Journal of Materials Research and Technology* (Vol. 15, pp. 241–255). Elsevier Editora Ltda. <https://doi.org/10.1016/j.jmrt.2021.07.110>
- Dikobe, D. G., & Luyt, A. S. (2017). Thermal and mechanical properties of PP/HDPE/wood powder and MAPP/HDPE/wood powder polymer blend composites. *Thermochimica Acta*, 654, 40–50. <https://doi.org/10.1016/J.TCA.2017.05.002>
- Dimple, Singh, G. P., & Mangal, R. (2023). A comprehensive review of natural fiber reinforced composite and their modern application. *Materials Today: Proceedings*. <https://doi.org/10.1016/J.MATPR.2023.03.745>
- Elsheikh, A. H., Panchal, H., Shanmugan, S., Muthuramalingam, T., El-Kassas, A. M., & Ramesh, B. (2022). Recent progresses in wood-plastic composites: Pre-processing treatments, manufacturing techniques, recyclability and eco-friendly assessment. *Cleaner Engineering and Technology*, 8, 100450. <https://doi.org/10.1016/J.CLET.2022.100450>
- Faruk, O., Bledzki, A. K., Fink, H. P., & Sain, M. (2012). Biocomposites reinforced with natural fibers: 2000–2010. *Progress in Polymer Science*, 37(11), 1552–1596. <https://doi.org/10.1016/J.PROGPOLYMSCI.2012.04.003>
- Fiore, V., Di Bella, G., & Valenza, A. (2015). The effect of alkaline treatment on mechanical properties of kenaf fibers and their epoxy composites. *Composites Part B: Engineering*, 68, 14–21. <https://doi.org/10.1016/J.COMPOSITESB.2014.08.025>
- Gao, J. S., Wang, X., Xu, Q., Kuai, B. Bin, Wang, Z. H., Cai, L., Ge, S., Zhang, Y. L., & Li, G. (2023). Efficient preparation and properties of wood fiber transparent materials with powdered wood. *Industrial Crops and Products*, 193, 116291. <https://doi.org/10.1016/J.INDCROP.2023.116291>
- Geng, S., Luo, Q., Liu, K., Li, Y., Hou, Y., & Long, W. (2023). Research status and prospect of machine learning in construction 3D printing. *Case Studies in Construction Materials*, 18, e01952. <https://doi.org/10.1016/J.CSCM.2023.E01952>

- Hachimi, T., Naboulsi, N., Majid, F., Rhanim, R., Mrani, I., & Rhanim, H. (2021). Design and Manufacturing of a 3D printer filaments extruder. *Procedia Structural Integrity*, 33(C), 907–916. <https://doi.org/10.1016/j.prostr.2021.10.101>
- Hao, X., Xu, J., Zhou, H., Tang, W., Li, W., Wang, Q., & Ou, R. (2021). Interfacial adhesion mechanisms of ultra-highly filled wood fiber/polyethylene composites using maleic anhydride grafted polyethylene as a compatibilizer. *Materials & Design*, 212, 110182. <https://doi.org/10.1016/J.MATDES.2021.110182>
- Izzati Zulkifli, N., Samat, N., Anuar, H., & Zainuddin, N. (2015a). Mechanical properties and failure modes of recycled polypropylene/microcrystalline cellulose composites. *Materials & Design*, 69, 114–123. <https://doi.org/10.1016/J.MATDES.2014.12.053>
- Izzati Zulkifli, N., Samat, N., Anuar, H., & Zainuddin, N. (2015b). Mechanical properties and failure modes of recycled polypropylene/microcrystalline cellulose composites. *Materials and Design*, 69, 114–123. <https://doi.org/10.1016/j.matdes.2014.12.053>
- Jin, Y., Lei, Z., Taynton, P., Huang, S., & Zhang, W. (2019). Malleable and Recyclable Thermosets: The Next Generation of Plastics. *Matter*, 1(6), 1456–1493. <https://doi.org/10.1016/J.MATT.2019.09.004>
- Kada, D., Migneault, S., Tabak, G., & Koubaa, A. (2016). Physical and mechanical properties of polypropylene-wood-carbon fiber hybrid composites. *BioResources*, 11(1), 1393–1406. <https://doi.org/10.15376/biores.11.1.1393-1406>
- Karthikeyan, A., Balamurugan, K., & Kalpana, A. (2014). The effect of sodium hydroxide treatment and fiber length on the tensile property of coir fiber-reinforced epoxy composites. *Science and Engineering of Composite Materials*, 21(3), 315–321. <https://doi.org/10.1515/secm-2013-0130>
- Kazemi, M., Faisal Kabir, S., & Fini, E. H. (2021). State of the art in recycling waste thermoplastics and thermosets and their applications in construction. In *Resources, Conservation and Recycling* (Vol. 174). Elsevier B.V. <https://doi.org/10.1016/j.resconrec.2021.105776>
- Kim, H. S., Lee, B. H., Choi, S. W., Kim, S., & Kim, H. J. (2007). The effect of types of maleic anhydride-grafted polypropylene (MAPP) on the interfacial adhesion properties of bio-flour-filled polypropylene composites. *Composites Part A: Applied Science and Manufacturing*, 38(6), 1473–1482. <https://doi.org/10.1016/j.compositesa.2007.01.004>
- Kostic, M. M., & Reifschneider, L. G. (2006). *Design of Extrusion Dies*. <https://doi.org/10.1081/E-ECHP-120039324>
- Kristiawan, R. B., Imaduddin, F., Ariawan, D., Ubaidillah, & Arifin, Z. (2021). A review on the fused deposition modeling (FDM) 3D printing: Filament processing, materials, and printing parameters. In *Open Engineering* (Vol. 11, Issue 1, pp. 639–649). De Gruyter Open Ltd. <https://doi.org/10.1515/eng-2021-0063>
- Kristiawan, R. B., Rusdyanto, B., Imaduddin, F., & Ariawan, D. (2022). Glass powder additive on recycled polypropylene filaments: A sustainable material in 3d printing. *Polymers*, 14(1). <https://doi.org/10.3390/polym14010005>
- Le Duigou, A., Castro, M., Bevan, R., & Martin, N. (2016). 3D printing of wood fibre biocomposites: From mechanical to actuation functionality. *Materials and Design*, 96, 106–114. <https://doi.org/10.1016/j.matdes.2016.02.018>
- Li, W., Bai, Z., Zhang, T., Jia, Y., Hou, Y., Chen, J., Guo, Z., Kong, L., Bai, J., & Li, W. (2023). Comparative study on pyrolysis behaviors and chlorine release of pure PVC polymer and commercial PVC plastics. *Fuel*, 340. <https://doi.org/10.1016/j.fuel.2023.127555>
- Lin, T. A., Lin, J. H., & Bao, L. (2020). Effect of melting-recycling cycles and mechanical fracture on the thermoplastic materials composed of thermoplastic polyurethane and

- polypropylene waste blends. *Applied Sciences (Switzerland)*, 10(17).
<https://doi.org/10.3390/app10175810>
- Liu, Y., Chen, F., Ni, X., & Xia, X. (2022). The effect of reinforcement on the mechanical properties of veneered wood fiber/polypropylene composites assembled with chlorinated polypropylene. *Scientific Reports*, 12(1). <https://doi.org/10.1038/s41598-022-17777-w>
- Loganathan, T. M., Sultan, M. T. H., Ahsan, Q., Jawaid, M., Naveen, J., Md Shah, A. U., & Hua, L. S. (2020). Characterization of alkali treated new cellulosic fibre from *Cyrtostachys renda*. *Journal of Materials Research and Technology*, 9(3), 3537–3546.
<https://doi.org/10.1016/J.JMRT.2020.01.091>
- Maddah, H. A. (2016a). Polypropylene as a Promising Plastic: A Review. *American Journal of Polymer Science*, 6(1), 1–11. <https://doi.org/10.5923/j.ajps.20160601.01>
- Maddah, H. A. (2016b). Polypropylene as a Promising Plastic: A Review. *American Journal of Polymer Science*, 6(1), 1–11. <https://doi.org/10.5923/j.ajps.20160601.01>
- Mijiyawa, F., Koffi, D., Kokta, B. V., & Erchiqui, F. (2015). Formulation and tensile characterization of wood-plastic composites: Polypropylene reinforced by birch and aspen fibers for gear applications. *Journal of Thermoplastic Composite Materials*, 28(12), 1675–1692. <https://doi.org/10.1177/0892705714563120>
- Mohammed, M., Rahman, R., Mohammed, A. M., Adam, T., Betar, B. O., Osman, A. F., & Dahham, O. S. (2022). Surface treatment to improve water repellence and compatibility of natural fiber with polymer matrix: Recent advancement. *Polymer Testing*, 115, 107707. <https://doi.org/10.1016/J.POLYMERTESTING.2022.107707>
- Mohebbi, B., & Kazemi, S. (2011). Influence of Maleic-Anhydride-Polypropylene (MAPP) on Wettability of Polypropylene/Wood Flour/Glass Fiber Hybrid Composites Production of energy and activated carbon from agriculture feedstocks View project An Innovative Biological Approach for Wood Protection Industry View project. In *Article in Journal of Agricultural Science and Technology*.
<https://www.researchgate.net/publication/267555059>
- Mpofu, T. P., Mawere, C., & Mukosera, M. (2014). The Impact and Application of 3D Printing Technology Article in. In *International Journal of Science and Research*.
<https://www.researchgate.net/publication/291975129>
- Musa, L., Krishna Kumar, N., Abd Rahim, S. Z., Mohamad Rasidi, M. S., Watson Rennie, A. E., Rahman, R., Yousefi Kanani, A., & Azmi, A. A. (2022). A review on the potential of polylactic acid based thermoplastic elastomer as filament material for fused deposition modelling. *Journal of Materials Research and Technology*, 20, 2841–2858. <https://doi.org/10.1016/J.JMRT.2022.08.057>
- Nafis, Z. A. S., Nuzaimah, M., Kudus, S. I. A., Yusuf, Y., Ilyas, R. A., Knight, V. F., & Norrrahim, M. N. F. (2023). Effect of Wood Dust Fibre Treatments Reinforcement on the Properties of Recycled Polypropylene Composite (r-WoPPC) Filament for Fused Deposition Modelling (FDM). *Materials*, 16(2). <https://doi.org/10.3390/ma16020479>
- Nam, G., Wakamoto, N., Okubo, K., & Fujii, T. (2014a). Study of Maleic Anhydride Grafted Polypropylene Effect on Resin Impregnated Bamboo Fiber Polypropylene Composit. *Agricultural Sciences*, 05(13), 1322–1328.
<https://doi.org/10.4236/as.2014.513141>
- Nam, G., Wakamoto, N., Okubo, K., & Fujii, T. (2014b). Study of Maleic Anhydride Grafted Polypropylene Effect on Resin Impregnated Bamboo Fiber Polypropylene Composit. *Agricultural Sciences*, 05(13), 1322–1328.
<https://doi.org/10.4236/as.2014.513141>
- Nur Hamzah, H., Mustafa Al Bakri Abdullah, M., Cheng Yong, H., Remy Rozainy Mohd Arif Zainol, M., Mahmad Nor, A., & Wazien, W. A. (2016). *Correlation of the Na 2*

- SiO 3 to NaOH Ratios and Solid to Liquid Ratios to the Kedah's Soil Strength.*
<https://doi.org/10.1051/01071>
- Oyinlola, M., Okoya, S. A., Whitehead, T., Evans, M., & Lowe, A. S. (2023). The potential of converting plastic waste to 3D printed products in Sub-Saharan Africa. *Resources, Conservation and Recycling Advances*, 17.
<https://doi.org/10.1016/j.rcradv.2023.200129>
- Parre, A., Karthikeyan, B., Balaji, A., & Udhayasankar, R. (2020). Investigation of chemical, thermal and morphological properties of untreated and NaOH treated banana fiber. *Materials Today: Proceedings*, 22, 347–352.
<https://doi.org/10.1016/j.matpr.2019.06.655>
- Patil, H., Tiwari, R. V., & Repka, M. A. (2016). Hot-Melt Extrusion: from Theory to Application in Pharmaceutical Formulation. *AAPS PharmSciTech*, 17(1), 20–42.
<https://doi.org/10.1208/s12249-015-0360-7>
- Pavan Kalyan, B., & Kumar, L. (2022). 3D Printing: Applications in Tissue Engineering, Medical Devices, and Drug Delivery. In *AAPS PharmSciTech* (Vol. 23, Issue 4). Springer Science and Business Media Deutschland GmbH.
<https://doi.org/10.1208/s12249-022-02242-8>
- Pérez, E., Famá, L., Pardo, S. G., Abad, M. J., & Bernal, C. (2012). Tensile and fracture behaviour of PP/wood flour composites. *Composites Part B: Engineering*, 43(7), 2795–2800. <https://doi.org/10.1016/J.COMPOSITESB.2012.04.041>
- Rais, M. H., Ahsan, M., & Ahmed, I. (2023). FRoMEPP: Digital forensic readiness framework for material extrusion based 3D printing process. *Forensic Science International: Digital Investigation*, 44. <https://doi.org/10.1016/j.fsidi.2023.301510>
- Rajendran Royan, N. R., Leong, J. S., Chan, W. N., Tan, J. R., & Shamsuddin, Z. S. B. (2021). Current state and challenges of natural fibre-reinforced polymer composites as feeder in fdm-based 3d printing. In *Polymers* (Vol. 13, Issue 14). MDPI AG.
<https://doi.org/10.3390/polym13142289>
- Ramanadha reddy, S., & Venkatachalapathi, Dr. N. (2023). A review on characteristic variation in PLA material with a combination of various nano composites. *Materials Today: Proceedings*. <https://doi.org/10.1016/J.MATPR.2023.04.616>
- Ramli, R., Yunus, R. M., Beg, M. D. H., & Prasad, D. M. R. (2012). Oil palm fiber reinforced polypropylene composites: Effects of fiber loading and coupling agents on mechanical, thermal, and interfacial properties. *Journal of Composite Materials*, 46(11), 1275–1284. <https://doi.org/10.1177/0021998311417647>
- Ravinder kumar, S. S. (2019). *Different method of Fabrication of composite material-A review*. <https://doi.org/10.6084/m9.jetir.JETIREL06080>
- Reddy, C. P., Ksc, C., & Rao, M. Y. (2011). *A review on bioadhesive buccal drug delivery systems: current status of formulation and evaluation methods 1,2* (Vol. 19, Issue 6). <http://journals.tums.ac.ir/>
- Rezaeian, P., Ayatollahi, M. R., Nabavi-Kivi, A., & Mohammad Javad Razavi, S. (2022). Effect of printing speed on tensile and fracture behavior of ABS specimens produced by fused deposition modeling. *Engineering Fracture Mechanics*, 266, 108393.
<https://doi.org/10.1016/J.ENGFRACMECH.2022.108393>
- Rocha, D. B., & Rosa, D. dos S. (2019). Coupling effect of starch coated fibers for recycled polymer/wood composites. *Composites Part B: Engineering*, 172, 1–8.
<https://doi.org/10.1016/J.COMPOSITESB.2019.05.052>
- Rowell, R. M. (2006). *Proceedings of the 8 th Pacific Rim Bio-Based Composites Symposium*. <https://www.researchgate.net/publication/239769722>

- Saad, M. J. (2018). Effect of Maleated Polypropylene (MAPP) on the Tensile, Impact and Thickness Swelling Properties of Kenaf Core-Polypropylene Composites. In *Journal of Science and Technology*.
- Saad, M. J. (2020). Effect of Maleated Polypropylene (MAPP) on the Tensile, Impact and Thickness Swelling Properties of Kenaf Core-Polypropylene Composites. In *Journal of Science and Technology*.
- Sabri, M., Mukhtar, A., Shahril, K., Rohana, A. S., & Salmah, H. (2013). Effect of compatibilizer on mechanical properties and water absorption behaviour of coconut fiber filled polypropylene composite. *Advanced Materials Research*, 795, 313–317. <https://doi.org/10.4028/www.scientific.net/AMR.795.313>
- Sahu, M., Patnaik, A., Kishor Sharma, Y., & Dalai, A. (2023). Physico-mechanical and tribological behaviour of natural fiber reinforced polymer composites: A short review. *Materials Today: Proceedings*. <https://doi.org/10.1016/J.MATPR.2023.03.822>
- Sanadi, A. R., Guna, V., Hoysal, R. V., Krishna, A., Deepika, S., Mohan, C. B., & Reddy, N. (2023). MAPP Compatibilized Recycled Woodchips Reinforced Polypropylene Composites with Exceptionally High Strength and Stability. *Waste and Biomass Valorization*. <https://doi.org/10.1007/s12649-023-02150-3>
- Sanadi, A. R., & Stelte, W. (2023a). Effect of the Characteristics of Maleic Anhydride-Grafted Polypropylene (MAPP) Compatibilizer on the Properties of Highly Filled (85%) Kenaf-Polypropylene Composites. *Materials Research*, 26. <https://doi.org/10.1590/1980-5373-mr-2022-0428>
- Sanadi, A. R., & Stelte, W. (2023b). Effect of the Characteristics of Maleic Anhydride-Grafted Polypropylene (MAPP) Compatibilizer on the Properties of Highly Filled (85%) Kenaf-Polypropylene Composites. *Materials Research*, 26. <https://doi.org/10.1590/1980-5373-mr-2022-0428>
- Sarioğlu, E., Turhan, E. A., Karaz, S., Bengü, B., Biçer, A., Yarıcı, T., Erkey, C., & Senses, E. (2023). A facile method for cross-linking of methacrylated wood fibers for engineered wood composites. *Industrial Crops and Products*, 193, 116296. <https://doi.org/10.1016/J.INDCROP.2023.116296>
- Serra-Parareda, F., Espinach, F. X., Pelach, M. À., Méndez, J. A., Vilaseca, F., & Tarrés, Q. (2020). Effect of NaOH treatment on the flexural modulus of hemp core reinforced composites and on the intrinsic flexural moduli of the fibers. *Polymers*, 12(6). <https://doi.org/10.3390/polym12061428>
- Shahrim, N. A., Sarifuddin, N., Azhar, A. Z. A., & Zaki, H. H. M. (2022). BIODEGRADATION OF MANGO SEED STARCH FILMS IN SOIL. *IJUM Engineering Journal*, 23(1), 258–267. <https://doi.org/10.31436/IJUM.EJ.V23I1.1620>
- Shahrubudin, N., Lee, T. C., & Ramlan, R. (2019). An Overview on 3D Printing Technology: Technological, Materials, and Applications. *Procedia Manufacturing*, 35, 1286–1296. <https://doi.org/10.1016/J.PROMFG.2019.06.089>
- Sharma, P., Vaid, H., Vajpeyi, R., Shubham, P., Agarwal, K. M., & Bhatia, D. (2022). Predicting the dimensional variation of geometries produced through FDM 3D printing employing supervised machine learning. *Sensors International*, 3, 100194. <https://doi.org/10.1016/J.SINTL.2022.100194>
- Shinde, A. A., Dandekar, A., Dhawale, N., Shinde, M. A. A., Patil, M. R. D., Dandekar, M. A. R., & Dhawale, N. M. (2020). 3D Printing Technology, Material Used For Printing and its Applications Mosquito killing drone View project Development of butter spreader using generic product development process View project 3D Printing Technology, Material Used For Printing and its Applications. <http://www.ijser.org>

- Shubhra, Q. T. H., Alam, A. K. M. M., & Quaiyyum, M. A. (2013). Mechanical properties of polypropylene composites: A review. In *Journal of Thermoplastic Composite Materials* (Vol. 26, Issue 3, pp. 362–391). <https://doi.org/10.1177/0892705711428659>
- Siakeng, R., Jawaid, M., Asim, M., & Siengchin, S. (2020). Accelerated weathering and soil burial effect on biodegradability, colour and texture of coir/pineapple leaf fibres/PLA biocomposites. *Polymers*, *12*(2). <https://doi.org/10.3390/polym12020458>
- Sigdel, D. D., & Giri, R. (2016). *Study on Pinewood/Recycled Polypropylene Composite* (Vol. 2). www.ijariie.com
- Singh, P., Katiyar, P., & Singh, H. (2023). Impact of compatibilization on polypropylene (PP) and acrylonitrile butadiene styrene (ABS) blend: A review. *Materials Today: Proceedings*. <https://doi.org/10.1016/j.matpr.2023.01.350>
- Siregar, A. N., Mahmud, W. M. F. W., Ghani, J. A., Haron, C. H. C., & Riza, M. (2014). Design and analysis of single screw extruder for jatropha seeds using finite element method. *Research Journal of Applied Sciences, Engineering and Technology*, *7*(10), 2098–2105. <https://doi.org/10.19026/rjaset.7.503>
- Trombetta, E., Flores-Sahagun, T., & Satyanarayana, K. G. (2010). Evaluation of polypropylene/saw dust composites prepared with maleated polypropylene (MAPP) produced by reactive extrusion. *Revista Materia*, *15*(2), 345–355. <https://doi.org/10.1590/s1517-70762010000200032>
- Truong, T. T., Hsu, Q. C., & Tong, V. C. (2020). Effects of solid die types in complex and large-scale aluminum profile extrusion. *Applied Sciences (Switzerland)*, *10*(1). <https://doi.org/10.3390/app10010263>
- Tsuchikura, N., Faudree, M. C., & Nishi, Y. (2013). Charpy impact value of sandwich structural (CFRP/ABS/CFRP) composites constructed with carbon fiber reinforced epoxy polymer (CFRP) and acrylonitrile butadiene styrene (ABS) sheets separately irradiated by electron beam prior to lamination. *Materials Transactions*, *54*(3), 371–379. <https://doi.org/10.2320/matertrans.MBW201209>
- Vallejos, M. E., Aguado, R. J., Morcillo-Martín, R., Méndez, J. A., Vilaseca, F., Tarrés, Q., & Mutjé, P. (2023a). Behavior of the Flexural Strength of Hemp/Polypropylene Composites: Evaluation of the Intrinsic Flexural Strength of Untreated Hemp Strands. *Polymers*, *15*(2). <https://doi.org/10.3390/polym15020371>
- Vallejos, M. E., Aguado, R. J., Morcillo-Martín, R., Méndez, J. A., Vilaseca, F., Tarrés, Q., & Mutjé, P. (2023b). Behavior of the Flexural Strength of Hemp/Polypropylene Composites: Evaluation of the Intrinsic Flexural Strength of Untreated Hemp Strands. *Polymers*, *15*(2). <https://doi.org/10.3390/polym15020371>
- Vidakis, N., Petousis, M., Tzounis, L., Grammatikos, S. A., Porfyrakis, E., Maniadi, A., & Mountakis, N. (2021). Sustainable additive manufacturing: Mechanical response of polyethylene terephthalate glycol over multiple recycling processes. *Materials*, *14*(5), 1–16. <https://doi.org/10.3390/ma14051162>
- Weidenfeller, B., Höfer, M., & Schilling, F. R. (2004). Thermal conductivity, thermal diffusivity, and specific heat capacity of particle filled polypropylene. *Composites Part A: Applied Science and Manufacturing*, *35*(4), 423–429. <https://doi.org/10.1016/j.compositesa.2003.11.005>
- Yağci, Ö., Eker Gümüş, B., & Taşdemir, M. (2021). Thermal, structural and dynamical mechanical properties of hollow glass sphere-reinforced polypropylene composites. *Polymer Bulletin*, *78*(6), 3089–3101. <https://doi.org/10.1007/s00289-020-03257-6>
- Yang, T. C., & Yeh, C. H. (2020). Morphology and mechanical properties of 3D printed wood fiber/polylactic acid composite parts using Fused Deposition Modeling (FDM): The effects of printing speed. *Polymers*, *12*(6), 1334. <https://doi.org/10.3390/POLYM12061334>

- Yuan, Q., Wu, D., Gotama, J., & Bateman, S. (2008a). Wood fiber reinforced polyethylene and polypropylene composites with high modulus and impact strength. *Journal of Thermoplastic Composite Materials*, 21(3), 195–208.
<https://doi.org/10.1177/0892705708089472>
- Yuan, Q., Wu, D., Gotama, J., & Bateman, S. (2008b). Wood fiber reinforced polyethylene and polypropylene composites with high modulus and impact strength. *Journal of Thermoplastic Composite Materials*, 21(3), 195–208.
<https://doi.org/10.1177/0892705708089472>
- Zaferani, S. H. (2018). Introduction of polymer-based nanocomposites. *Polymer-Based Nanocomposites for Energy and Environmental Applications: A Volume in Woodhead Publishing Series in Composites Science and Engineering*, 1–25.
<https://doi.org/10.1016/B978-0-08-102262-7.00001-5>
- Zulkifli, N. I., & Noorasikin, S. (2013). Mechanical properties of green recycled polypropylene composites: Effect of maleic anhydride grafted polypropylene (MAPP) coupling agent. *Advanced Materials Research*, 812, 187–191.
<https://doi.org/10.4028/www.scientific.net/AMR.812.187>
- Zuo, Q., Wang, C., Pei, X., Lin, L., Li, Y., & Sun, W. (2023). Analysis and prediction of tensile properties based on rule of mixtures model for multi-scale ramie plain woven fabric reinforced composite. *Composite Structures*, 311, 116785.
<https://doi.org/10.1016/J.COMPSTRUCT.2023.116785>
- Zuo, Y., Feng, J., Soyol-Erdene, T.-O., Wei, Z., Hu, T., Zhang, Y., & Tang, W. (2023). Recent advances in wood-derived monolithic carbon materials: Synthesis approaches, modification methods and environmental applications. *Chemical Engineering Journal*, 463, 142332. <https://doi.org/10.1016/J.CEJ.2023.142332>

APPENDICES

APPENDIX A Gantt Chart for PSM 1 & 2



No.	Project Activities	Plan VS Actual Plan	March			April				May				Jun			
			1	2	3	4	5	6	7	8	9	10	11	12	13	14	15
1.	PSM Briefing	Plan	■														
		Actual	■														
2.	Report Briefing with Supervisor	Plan		■													
		Actual		■													
3.	Report writing: Chapter 2 (Literature Review)	Plan			■	■	■	■									
		Actual			■	■	■	■									
4.	Report writing: Chapter 3 (Methodology)	Plan						■	■	■							
		Actual									■	■	■	■			
5.	Report writing: Chapter 4 (Preliminary Results)	Plan									■	■					
		Actual										■	■	■			
6.	Report writing: Chapter 1 (Introduction)	Plan												■			
		Actual												■			
7.	Report Finalization	Plan												■	■		
		Actual													■		
8.	Report Submission	Plan													■		
		Actual													■		
9.	Slide Preparation	Plan													■	■	
		Actual													■	■	
10.	Final Improvement	Plan													■		
		Actual													■		
11.	Final Presentation	Plan															■
		Actual															■

Plan	■
Actual	■

Table 5.2: Gantt Chart PSM 2

No.	Project Activities	Plan VS Actual Plan	August			September				October				January			
			Week	1	2	3	4	5	6	7	8	9	10	11	12	13	14
1.	Data Collection	Plan	■	■	■	■											
		Actual															
2.	Development	Plan			■	■	■	■	■								
		Actual															
3.	Testing	Plan						■	■	■	■						
		Actual															
4.	Analysis	Plan								■	■						
		Actual															
5.	Discussion	Plan									■	■					
		Actual															
6.	Conclusion	Plan									■	■					
		Actual															
7.	Report Finalization	Plan										■	■	■			
		Actual															
8.	Report Submission	Plan													■		
		Actual															
9.	Final Presentation	Plan															■
		Actual															

Plan

